UNIVERSITÀ DEGLI STUDI DI MILANO

CORSO DI DOTTORATO in MEDICINA TRASLAZIONALE

35° ciclo

DIPARTIMENTO DI SCIENZE BIOMEDICHE PER LA SALUTE

BIO/10

Lipid composition of microglial cells and effects of a remyelination-promoting antibody on the sphingolipid patterns

DOTTORANDO: CHIARA D'APRILE

TUTOR: Professor Alessandro Prinetti

COORDINATORE DEL DOTTORATO: Professoressa Chiarella Sforza

A.A. 2021-2022

ABBREVIATIONS

HC: 24(S)-hydroxycholesterol

α-Syn: Alpha-Synuclein

Acetyl-CoA: Acetyl-coenzyme A

AD: Alzheimer disease

Ad. Cells: adherent cells

ABC: ATP binding cassette transporters

ACAT1/SOAT1: cholesterol acyltransferase 1

APCs: Antigen presenting cells

ASA: Arylsulfatase A

ATM: Axon tract-associated microglia

ATP: adenosine triphosphate

BBB: Blood brain barrier

BMP: Bone morphogenic protein

Cav-1: Caveolin 1

Cav-3: Caveolin 3

CDP-DAG: Cytidine diphosphate diacylglycerol

Cer: Ceramide

Cer (Sphingosine 18:2): Ceramide with sphingosine back bone 18 carbon atoms long and two double bonds

Cer (Sphingosine 18:1): Ceramide with sphingosine back bone 18 carbon atoms long and one double bond. Of this molecular specie different fatty acid chain length, with a single double bond are shown: 24:1, 23:2, 22:1. But also different fatty acid chain length, with no double bond are shown 24:0, 23:0, 22:0, 18:0, 17:0, 16:0, 15:0,14:0

Cer (Sphingosine 17:1): Ceramide with sphingosine back bone 17 carbon atoms long and one double bond

Cer (Sphinganine 18:0): Ceramide with sphingosine back bone 18 carbon atoms long with no double bond

Cer (Sphinganine 16:0): Ceramide with sphingosine back bone 16 carbon atoms long with no double bond

Cer (Sphinganine 14:0): Ceramide with sphingosine back bone 14 carbon atoms long. Of this molecular specie different fatty acid chain length, with a multiple double bond are shown: 24:5, 21:2, 20:5, 20:2

CERT: Ceramide transporter

CGT UDP-galactose: Ceramide galactosyltransferase

Chol: cholesterol

CL: Cardiolipin

CNS: Central nervous system

CNTF: Ciliary neurotrophic factor

CSF: Cerebral spinal fluid

CSF-1: Colony stimulator factor 1

CST: Cerebroside sulfotransferase

CTP: Cytidine 5'-triphosphate

DAG: Diacylglycerol

DAM: Disease associated microglia

DE: desmosterol

DES: Dihydroceramide desaturase

DRM: Detergent resistant membrane

dHCer: dihydroceramide

Dhcr24: 24-dehydrocholesterol reductase

EAE: Experimental autoimmune encephalomyelitis

ECM: Extracellular matrix

EGFR: Epidermal growth factor receptor

ER: Endoplasmic reticulum

ERK: Extracellular signal-Regulated Kinase

ESI-MS: Electrospray ionisation mass spectrometry

FAK: Focal adhesion kinases

FGF: Fibroblast growth factor

Fl. Cells: floating cells

FPP: Farnesyl pyrophosphate

G3P: Glycerol three phosphate

GalCer: Galactosylceramide

GalCers: Galactosylceramide synthase

GCS: Glucosylceramide synthase

GFAP: Glial fibrillary acidic protein

GlcCer: Glucosylceramide

GlcCer (Sphingosine 18:1): Glucosylceramide with sphingosine back bone 18 carbon atoms long and one double bond

GPAT: Glycerol three phosphate acyltransferase

GPI-anchored proteins: Glycosylphosphatidylinositol anchored proteins

GSLs: Glycosphingolipids

HAM: Human AD microglia

HMG-CoA:3-hydroxy-3-methylglutaryl-coenzyme A

HMGCR: 3-hydroxy-3-methyl-glutaryl-coenzyme A reductase

ICS: isolated clinical syndrome

IFN-γ: Interferon gamma

IL- : interleukin

IPP: isopentenyl pyrophosphate

IR: insulin receptor

IRM: Injury responsive microglia

LacCer: Lactosylceramide

LacCer (Sphingosine 18:1): Lactosylceramide with sphingosine back bone 18 carbon atoms long and one double bond

LDAM: Lipid-droplet-accumulating microglia

LysoPC: Lysophosphatidylcholine

LN: Lanosterol

LT: Lathosterol

LXR: Liver X receptor

LPS: Lipopolysaccharides

MAG: Myelin associated glycoprotein

MAPK: Mitogen-Activated Protein Kinase

Met. Ad. Cells: methanolized adherent cells

Met. Fl. Cells: methanolized floating cells

MBP: myelin basic protein

MIMS: microglia inflamed in multiple sclerosis

MHCII: Major histocompatibility complex

MOG: Myelin oligodendrocyte glycoprotein

MRI: magnetic resonance imaging

MS: Multiple sclerosis

MRI: Magnetic resonance imaging

Neu5Ac: *N*-Acetylneuraminic acid or sialic acid

NF-kB: Nuclear factor kB

NG2: nerve/glial antigen 2

NOS: Nitric oxide synthase (NOS)

OLs: Oligodendrocytes

OPCs: Oligodendrocyte progenitor cells

PA: Phosphatidic acid

PAGE: Polyacrylamide gel electrophoresis

PC: Phosphatidylcholine

PD: Parkinson disease

PDGFαR: Platelet-derived growth factor receptor alpha

PE: Phosphatidylethanolamine

PG: Phosphatidylglycerol

PI: Phosphatidylinositol

PI-4-P: Phosphatidylinositol 4-phosphate

PI-4,5-P2: Phosphatidylinositol 4,5-bisphosphate

PI-3-P: Phosphatidylinositol 3-phosphate

PI-3,4-P2: Phosphatidylinositol 3,4-bisphosphate

PI-3,4,5-P3: Phosphatidylinositol 3,4,5-Trisphosphate

PLP: Proteolipid protein

PPMS: Primary progressive multiple sclerosis

PS: Phosphatidylserine

PVDF: Polyvinylidene fluoride

rHIgM22: Recombinant human Immunoglobulin M22

RGCs: Radial glial cells

ROS: Reactive oxygen species

RRMS: Relapsing remitting multiple sclerosis

S1P: Sphingosine-1-phosphate

S1P lyase: Sphingosine -1-posphate lyase

SDS: Sodium dodecyl sulphate

SHH: Sonic hedgehog

SK1: Sphingosine kinase 1

SK2: Sphingosine kinase 2

SLs: Sphingolipids

SM: Sphingomyelin

SM (Sphingosine 19:2): Sphingomyelin with sphingosine back bone 19 carbon atoms long and two double bonds

SM (Sphingosine 18:2): Sphingomyelin with sphingosine back bone 18 carbon atoms long and two double bonds

SM (Sphingosine 18:1): Sphingomyelin with sphingosine back bone 18 carbon atoms long and one double bond. Of this molecular specie different fatty acid chain length, with a single bond are shown: 24:1, 23:1, 22:1. But also different fatty acid chain length, with no double bond are shown 24:0, 23:0, 22:0, 18:0, 17:0,14:0

SM (Sphingosine 17:1): Sphingomyelin with sphingosine back bone 17 carbon atoms long and one double bond

SM (Sphinganine 18:0): Sphingomyelin with sphingosine back bone 18 carbon atoms long and no double bond. Of this molecular specie different fatty acid chain length, with a single bond are shown: 24:1, 23:1. But also different fatty acid chain length, with no double bond are shown 22:0, 20:0, 17:0, 16:0,14:0

SM (Sphinganine 16:0): Sphingomyelin with sphingosine back bone 16 carbon atoms long and no double bond

SM-1: Sphingomyelin synthase 1

SM-2: Sphingomyelin synthase 2

SREBP2: Sterol regulatory element-binding protein 2

SPMS: secondary progressive multiple sclerosis

SPT: serine-palmitoyl-transferase

Sulfatide: 3-O-sulfogalactosylceramide

TLC: Thin layer chromatography

Th-1/17: Lymphocyte T helper 1/17

TMEV: Theiler's murine encephalomyelitis virus

TNF-α: Tumor necrosis factor alpha

TrihexosylCer (Sphingosine 18:1): Trihexosylceramide with sphingosine back bone 18 carbon atoms long and one double bond

TrihexosylCer (Sphinganine 18:0): Trihexosylceramide with sphinganine back bone 18 carbon atoms long and no double bond

VDR: Retinoid receptor for vitamin D

ABSTRACT

Multiple sclerosis (MS) is one of the most prevalent demyelinating diseases among young adults (Lemus et al., 2018). Myelin damage and oligodendrocyte death are caused by the autoimmune attack of T cells that cross the blood-brain barrier resulting in the formation of sclerotic plaques (Pearce, 2005, Lubetzki and Stankoff, 2014). In the early stages of the disease, damaged myelin is to some extent repaired, however the process is inefficient due to several factors, including impairment in OPCs recruitment and/or OLs differentiation likely due to the inflamed environment, and the inhibitory effect of myelin debris present at the lesion sites (Barres, 2008, Lassmann, 2014, Domingues et al., 2016). There are currently no cures for multiple sclerosis, only treatments that aim at alleviating its symptoms or slow down its progression. Therefore, interventions that stimulate and promote endogenous myelin repair mechanisms may be a feasible treatment option (Lemus et al., 2018).

In animal models of demyelination, the ability of certain monoclonal antibodies to stimulate myelin sheath synthesis has been proven. In this regard, the rHIgM22 monoclonal antibody has showed particularly promising results. This antibody seems to act mainly on cells of the oligodendrocyte lineage, in particular on oligodendrocyte precursor cells promoting their proliferation and inhibiting their apoptosis (Warrington et al., 2000). However, experimental evidence suggests that not only OPCs and OLs are targeted by rHIgM22, but also other glial cells*, e.g.,* astrocytes and microglia, In particular, it has been shown that rHIgM22 stimulates an increase in the phagocytic activity in microglia (Zorina et al., 2018). The phagocytosis of myelin debris by microglia is one of the most delicate and limiting steps in the myelin repair mechanism (Neumann et al., 2009, Domingues et al., 2016, Napoli and Neumann, 2009, Lloyd and Miron, 2019).

The protective effects exerted by rHIgM22, at least towards the primary targeted glial cells, appear to be mediated by the reorganisation of membrane lipids leading to the recruitment of a multimolecular complex that results in the development of numerous signalling mechanisms (Watzlawik et al., 2010, Watzlawik et al., 2013a). Indeed, data obtained in our laboratory showed that different glycosphingolipids were involved in rHIgM22 binding at the cell surface but also that rHIgM22 treatment induced changes in the sphingolipid pattern of oligodendroglial cells (Grassi et al., 2015, S. Grassi et al. , 2021).

Since microglia seem to be a crucial player in the processes that are at the centre of myelin repair, they have been the focus of this thesis. We used as an experimental model the BV-2 microglial cell line. The BV-2 cell line is widely used because it retains the morphological,

phenotypical, and functional characteristics described for freshly isolated primary microglia and has functional markers of macrophages (Blasi et al., 1990). BV-2 is a semi adherent cell line, where adherent and floating cells may represent two different sub-populations.

Due to the paucity of information in the literature regarding the lipid composition of microglia, as the first step, we analysed the lipid composition of BV-2 cells using a combination of traditional chemical analysis and lipidomic using ESI-mass spectrometry. We analysed lipids in different culture conditions since it is well known that culture conditions affect the composition of certain lipid classes (Frechin et al., 2015). We identified differences in the lipid pattern depending on cell culture conditions but also some differences in the lipid composition among adherent and floating cells. Specifically, we observed key differences between adherent and floating cells at 80-90% confluence. In this experimental condition, ceramide was present at higher levels in the floating cells while sphingomyelin was more enriched in the adherent cells; in the cells collected at over confluence, these distinctions were absent. In addition, we identified the absence of specific lipids, including galactosylceramide and sulfatide, and a generally low amount of gangliosides in both sub-populations, irrespective of confluence.

Then, we studied more in detail the sphingolipid turnover using a metabolic labelling approach. Our results showed that BV-2 cells are characterised by a rapid sphingolipid turnover rate.

Finally, based on our previous findings indicating that rHIgM22 was able to modify sphingolipid patterns in OPCs and OLs, we evaluated the effects of rHIgM22 on the sphingolipid pattern of BV-2 cells using different experimental settings and culture conditions. Our findings showed that rHIgM22 could influence sphingolipid patterns in microglia as well.

Comparing different experimental approach, the effects of the two antibodies, rHIgM22 and the human IgM used as the negative control, are distinct. Specifically, rHIgM22 decreases GlcCer, SM, GM1, and PE in adherent cells relative to control IgM, whereas increases GlcCer and GD1a in floating cells. Moreover, in another experimental approach, rHIgM22 decreases GlcCer, SM, GM1, and PE in adherent cells relative to control IgM, whereas GlcCer and GD1a increase in floating cells.

Therefore, it is plausible to hypothesise that also in microglia the effects of the treatment with rHIgM22 might be due to the reorganisation of the membrane lipid microenvironment, possibly affecting the function of membrane-associated signalling complexes.

INTRODUCTIONS

1. Overview of plasma membrane structure

Cell membranes perform several functions, including separating inner cell structures by acting as barriers and supplying platforms for cellular signalling (Merrill, 2011, Paukner et al., 2022). Indeed, the bilayers are formed mostly by lipids that are not only structural components but also act as signalling molecules (Harayama and Riezman, 2018). The cell membranes are composed of a double layer of lipids and proteins that are distributed in different ways; actually indeed, the two bilayers are asymmetric. Phospholipids and cholesterol are the most abundant lipid class; together, these two classes form most of membrane lipids. Minor plasma membrane constituents also include sphingolipids with a sphingosine or sphinganine backbone (Vance, 2015). However, membrane lipid composition varies significantly between different biological organisms, cell types, and tissues, as well as depending on the stage of the cell cycle and the surrounding environment (Ingolfsson et al., 2014). For example, gangliosides are particularly enriched in brain cells, *e.g.,* neurons (Sonnino and Prinetti, 2010). Moreover, in most cellular membranes the molar ratio of cholesterol, phospholipids and glycosphingolipids (GSLs) is 25:65:10, whereas in brain, and particularly in myelin these ratios change to 40:40:20 (O'Brien, 1965).

Even within a single cell, the composition of the bilayer varies greatly between the various organelles and the plasma membrane; for example, cardiolipin is a phospholipid present only in the mitochondrial membranes, cholesterol is scarcely present in the endoplasmic reticulum (ER) with respect to the plasma membrane, and phosphatidylethanolamine is particularly enriched in the mitochondria with respect to the plasma membrane (Farooqui et al., 2000, Harayama and Riezman, 2018). In other cells such as polarized cells a different composition between their basolateral and apical membranes is found. In the apical membrane, there is a deficiency of phosphatidylcholine, one of the most abundant phospholipids in plasma membranes, accompanied by an enrichment of glycolipids, whereas in the basolateral membrane, the composition is similar to that of non-polarized cells (Simons and van Meer, 1988b).

According to the fluid mosaic membrane model proposed by Nicolson and Singer in 1972, globular heads of amphipathic integral membrane proteins are interconnected with the phospholipid bilayer, where the intrinsic properties of the lipids and proteins drive their non-

covalent bonds, generating a unique organisation in each bilayer and determining the asymmetry and positive or negative curvature of both bilayers (Singer and Nicolson, 1972).

This model is still accepted on a nano-scale basis after 50 years. However, new sub compartmentalisations of the membrane have been found, in which lipids-lipids or lipids-proteins communicate in a more complex and organised manner with one another and with other cell structures. Consequently, the increasing complexity of membrane component interactions identifies a reduced possibility for membrane components to easily move between the bilayer (Nicolson, 2013).

Lipids, indeed, as the major membrane's components, handle the primary organisation of membrane itself. The organisation of the membrane is attributable to the asymmetry of location of different phospholipids, as well as the natural curvature that results due to different saturation of their acyl chain, and that leads to a different segregation of all the membrane components into the two bilayers (McMahon and Boucrot, 2015, Harayama and Riezman, 2018). In neural cells the specific presence of phospholipids, for example, drive membrane fluidity, permeability and local curvature (Farooqui et al., 2000).

Cholesterol is the most prevalent and unique sterol present in membrane, although other sterols are found in organelles and lipid droplets (Zhang and Liu, 2015). Cholesterol stabilises the membrane and its constituents, enriching the transient microdomains that are resistant to detergents, also known as lipid rafts. Cholesterol inserts itself between the hydrophobic gap of other lipids to stabilise the membrane by lining up other lipids into a liquid-ordered state in which their acyl chains are more ordered and stretched (Sonnino and Prinetti, 2010, Nicolson, 2013). Sphingolipids also have structural properties in membranes, and glycosphingolipids have a strong tendency to form segregated domains within the phospholipid bilayer due to their unique structure of the head group, which is quite different from that of glycerophospholipids. These domains are highly enriched in cholesterol and sphingolipids, especially sphingomyelin, and in addition to a glycerophospholipid base, they also contain a small number of proteins. These lipid and protein aggregates are referred to as lipid rafts or detergent resistant membrane domains (DRM) and serve as platforms for a variety of cell signalling processes (Sonnino et al., 2006).

2.4 ***Phospholipids***

Phospholipids and cholesterol are the most abundant lipids in the plasma membrane, and their ratio is 0.75, with phospholipids being more abundant than cholesterol (Vance, 2015).

Phospholipids, known as glycerophospholipids, comprise four class of lipids: 1,2-diacyl glycerophospholipid, 1-alk-1-enyl-2-acyl glycerophospholipid (namely plasmalogen), 1-alkyl-2-acyl glycerophospholipid and sphingomyelin (SM), all are found in the brain and other mammalian tissue (Farooqui et al., 2000). The first three classes define amphipathic lipids with a glycerol backbone connected to a polar head group and a nonpolar acyl tail substituent in sn-1 e sn-2 (Harayama and Riezman, 2018). The sn-1 fatty acid substituent is frequently saturated or monounsaturated, while the sn-2 fatty acid is more frequently monounsaturated or polyunsaturated (Harayama and Riezman, 2018). In plasmalogens the sn-1 substituent is a fatty aldehyde instead of an acid, determining the vinyl-ether linkage in place of the ester bond of other phospholipid (Farooqui et al., 2000).

The most represented phospholipids in membrane are phosphatidylcholine (PC) approximately 40-50% of total, phosphatidylethanolamine (PE), phosphatidylserine (PS) and phosphatidylinositol (PI). Sphingomyelin (SM) is a phospho-sphingolipid formed by a sphingoid base, phosphocholine, and a fatty acid and is one of the major components of the plasma membrane, along with cholesterol and PC (Vance, 2015).

In plasma membranes, and particularly in myelin, plasmalogens of ethanolamine are abundant in the inner leaflet, where they form a very strong hydrogen bond with adjacent lipids, thereby increasing the membrane's density and stability (Aggarwal et al., 2011b, Schmitt et al., 2015).

1.1.1 Phospholipids metabolism

Phospholipids are synthesised on the cytoplasmatic leaflet of the ER, in the Golgi apparatus in the case of the sphingomyelin (SM), and in the mitochondria in the case of cardiolipin (CL) (Vance, 2015).

Phospholipid biosynthesis begins from glycerol three phosphate (G3P) which by action of G3P acyltransferase (GPAT) forms lysophosphatidic acid and then an acylation performed by Lyso-PA acyltransferase leads to the formation of the phosphatidic acid (PA). PA from the ER is

transformed in diacylglycerol (DAG) or cytidine diphosphate diacylglycerol (CDP-DAG), by the cytosolic enzyme phosphatidic acid phosphatase-1 or CDP-diacylglycerol synthase in the ER, respectively (Vance, 2015).

DAG is utilised in the formation of PE, PC, PS, and SM, while CDP- diacylglycerol is utilised in the formation of PI, CL the proper mitochondrial phospholipids, and phosphatidylglycerol (PG) (Farooqui et al., 2000). PS is produced through the substitution of phosphate groups from PE and PC by PS synthases 2 and 1, respectively; also PS can be decarboxylated back to PE, however this activity mediated by PS decarboxylase is restricted to the mitochondria (Vance, 2015).

PC, together with ceramide, are the precursors of SM, one of the main phosphosphingolipids. Ceramide and PC are transferred to the Golgi apparatus where the phosphocholine of PC is joined to 1-OH of ceramide by Sphingomyelin synthase 1 (SM-1 synthase) in the Golgi apparatus producing SM e DAG. SM can also be synthesised at plasma membrane level by SM-2 synthase (Merrill, 2011).

The biosynthetic pathways for phospholipids in cell membranes, which are the most abundant and significantly important for cellular functionality, are described below.

PC and PE are formed through the Kennedy pathway (Vance, 2015). Extracellular choline and ethanolamine are transferred into the cytosol and phosphorylated by choline kinase and ethanolamine kinase, respectively. Subsequently, choline or ethanolamine cytidyl transferase merge the cytidine 5'-triphosphate (CTP) to 20P-choline or 20P-ethanolamine leading to the formation of CDP-choline o CDP-ethanolamine, respectively.

DAG is eventually combined in the ER with CTD-Choline or CTD-ethanolamine by two distinct enzymes, CDP-Choline:1,2-diacylglycerol-choline-phosphotransferase and CDP-ethanolamine: 1,2-diacylglycerol-ethanolamine-phosphotransferase, respectively, forming PC and PE (Vance, 2015, Farooqui et al., 2000).

CDP-DAG is utilised, also, for the formation of PI, CL and PG. PI is formed by union of inositol to CDP-DAG via phosphatidylinositol synthase. PI undergoes transient and reversible transformations at this point, forming a large class of phosphatidylinositol derivatives (PI-4-P, PI-4,5-P2 the most abundant, PI-3-P, PI-3,4-P2, and PI-3,4,5-P3) that play crucial roles in signal transduction, autophagy, and membrane trafficking despite being present in a much smaller proportion than other phospholipids (Farooqui et al., 2000, Vance, 2015, Blunsom and Cockcroft, 2020).

1.1.2 Phospholipid's functions

All the above-mentioned lipids are asymmetrically distributed between the two bilayers: PC and SM reside preferentially in the outer leaflet, while PE, PS and PI reside in the inner leaflet (Farooqui et al., 2000). However, some of these lipids can undergo change of position between the two bilayers in response to cellular needs through the translocation operated by specific proteins defined flippase (from inner to outer leaflet) or floppase (from outer to inner leaflet) (Bevers et al., 1999, Vance, 2015). In this regard, the transfer of PS and PE from the inner to the outer leaflet in response to the "eat me" signal during apoptosis or to initiate the clotting cascade in platelet activation is a well-known occurrence (Farooqui et al., 2000, Nicolson, 2013, Vance, 2015, Harayama and Riezman, 2018).

Homeostasis of membrane phospholipids is selectively balanced between biosynthetic pathways, metabolic processes and catabolism via phospholipase A_{1-3},C,D , and re-acylation throughout the remodelling pathway; additionally, some precursors, such as DAG, are quantitatively limiting in the production of new phospholipids and are used also as intracellular messenger (Farooqui et al., 2000, Wakelam, 1998).

Phospholipids allow the modification and maintenance of the membrane's curvature, as for their geometric structure they contain different bulky-head substituents, and saturated or unsaturated and polyunsaturated acyl chains that determine a natural membrane curvature, which is functionally modified by different signalling mechanisms. Overall, unsaturation in acyl chains increases membrane fluidity and accordingly the level of unsaturation of membrane's lipids might affect its organization; in contrast, long, and saturated acyl chains drive to less fluidity and major lipid-lipid interaction (Harayama and Riezman, 2018, McMahon and Boucrot, 2015).

PC and PS, the major and minor phospholipid component of plasma membrane, are a zwitterionic and a ionic ammino phospholipid, respectively; both are cylindrical lipids that form an uniform non curved monolayer, whereas PE, PA, and DAG, due to their less bulky headgroup are more conical driving to a negative curvature (McMahon and Boucrot, 2015, Vance and Steenbergen, 2005, Fernandez-Murray and McMaster, 2007). PI, on the other hand, has an inverted cone structure and when inserted into the membrane, together with all its phosphorylated derivatives determines a positive curvature (Harayama and Riezman, 2018).

Phospholipids are not only a membrane backbone, they exert many function related to autophagy, cell signalling through generation of second messenger, membrane anchor, antioxidant effect (Farooqui et al., 2000). PI-3-P, for example, is present in early endosomes and takes part in endosomal trafficking; when found in the autophagosomal compartment, it is likely involved in autophagy; PI-3-P is also involved in regulating neurotransmitter receptors on the cell surface. PI-4-P, which is predominantly located in the Golgi complex and plasma membrane, plays a role in vesicular trafficking and lipid homeostasis (Raghu et al., 2019).

1.2 Cholesterol

Sterols, including cholesterol, are a prevalent part of cellular membranes. Cholesterol is also a precursor of oxysterols, steroid hormones, and bile acids (Orth and Bellosta, 2012).
Cholesterol, being an amphipathic molecule due to its four hydrocarbon rings and the hydroxyl group (Goluszko and Nowicki, 2005)) can alter the molecular order, permeability, thickness, and microdomain structure of a membrane (Williams et al., 2000). Due to the extremely small size of the polar headgroup in relation to the non-polar portion, cholesterol induces intrinsic negative curvature in lipid bilayers (Yang et al., 2016). Cholesterol, moreover, is asymmetrically distributed in the membranes of numerous cell types, and its trans bilayer distribution is affected by the degree of membrane phospholipid saturation (Williams et al., 2000). Cholesterol is found in both bilayers and has a rapid flip-flop rate between the two leaflets (Ingolfsson et al., 2014). Consequently, there are multiple ways by which cholesterol influences the behaviour of membrane proteins in lipid bilayers (Williams et al., 2000).
As an essential component of the plasma membrane, cholesterol couples with sphingolipid and glycosylphosphatidylinositol (GPI)-anchored proteins to form small, dynamic, and transient domains that are distributed in the outer leaflets. These domains, also known as lipid rafts, regulate numerous cellular processes (Aureli et al., 2015).

1.2.1 Cholesterol synthesis

Cholesterol, in the body, is derived from food or synthesised by nearly all cells, but at least 50% comes primarily from the liver cells, which also control the availability of lipoproteins, the primary cholesterol acceptors, and transporters. In healthy brain, however, because the blood brain barrier (BBB) is strongly impermeable to many molecules, brain cholesterol content depends almost entirely on the local *de novo* cholesterol (Paukner et al., 2022, Moutinho et al., 2016). However, a very small amount of cholesterol has been found to be exchanged through the BBB (Orth and Bellosta, 2012).
Oligodendrocytes are responsible for the majority of cholesterol synthesis during development as their membrane, myelin, is the most cholesterol-rich plasma membrane; however, astrocytes and neurons also produce cholesterol and provide a pool to oligodendrocytes via apolipoprotein E (ApoE)-containing lipoproteins, and ATP binding

cassette (ABC) transporters that transport vehicles of cholesterol and other lipids in the CNS (Orth and Bellosta, 2012, Berghoff et al., 2022).

Brain cholesterol accumulates during early development (Zhang and Liu, 2015), since it has a very high biosynthetic activity during the myelination process (Moutinho et al., 2016). The biosynthesis of cholesterol continues in adulthood, but its turnover is extremely slow; the half-life of cholesterol, in the brain, ranges from half a year to five years, whereas it is days in the rest of the body (Orth and Bellosta, 2012, Qian et al., 2022). Moreover, physiologically, and pathologically, cells afferent to the CNS do not behave identically regarding the synthesis of this lipid and its rate (Nieweg et al., 2009, Berghoff et al., 2021)**.**

The *de novo* synthesis of cholesterol occurs in the ER, where two acetyl coenzyme A are combined to create acetoacetyl-CoA, then HMG-CoA synthase adds a third molecule of acetyl-CoA to form 3-hydroxy-3-methylglutaryl-CoA; subsequently, this newly formed molecule is reduced to mevalonate by HMG-CoA reductase; mevalonate is then phosphorylated and decarboxylated to form isopentenyl pyrophosphate (IPP). Polymerization of IPP results in farnesyl pyrophosphate (FPP), and the union of two FPP results in the formation of squalene (Shi et al., 2022). After squalene is synthetised, to form cholesterol, additional and numerous enzymatic activities are expected; however, two distinct pathways have been identified in brain cells. Neurons and glial cells synthesise cholesterol from different sterol precursors at different rates; neurons use dehydrocholesterol and lathosterol (LT) via the Kandutsch-Russel pathway, while glial cells use desmosterol (DE) via the Bloch pathway (Nieweg et al., 2009).

Astrocytes are the primary producers and suppliers of cholesterol in the adult brain; neurons, oligodendrocytes, and microglia have a slow biosynthesis rate. Astrocytes produce additional cholesterol pools by esterifying and storing it, which they then transfer to neighbouring cells for their support (Nieweg et al., 2009).

There are precise feedback mechanisms and rate-limiting enzymes during biosynthesis, which occurs at the transcriptional, translational, and posttranslational levels. Sterol regulatory element-binding protein 2 (SREBP2), liver X receptor (LXR) transcription factors, 3-hydroxy-3-methylglutaryl-coenzyme A (HMG-CoA) reductase, and squalene monooxygenase, are involved (Berghoff et al., 2022). Similarly, the various precursors of cholesterol appear to have feedback effects on the synthesis of new cholesterol, although the underlying causes are unknown; for instance, desmosterol stimulates cholesterol efflux and the esterification pathway, influencing the LXR; lanosterol and dihydrolanosterol promote the ubiquitination of

HMG-CoA reductase, thereby terminating cholesterol synthesis (Berghoff et al., 2022, Yamauchi et al., 2007, Nieweg et al., 2009).

Additionally, other mechanisms help maintain cholesterol homeostasis, including esterification, cerebral spinal fluid (CSF), and BBB excretion (Qian et al., 2022). Excess in cholesterol content is not beneficial to cellular processing; indeed, cholesterol imbalances are found in many diseases, including Niemann-Pick disease type C, Alzheimer disease (AD), and Multiple Sclerosis (MS) (Zhang and Liu, 2015, Berghoff et al., 2022, Berghoff et al., 2021).

Therefore, this lipid is esterified by acyl coenzyme A: cholesterol acyltransferase 1 (ACAT1/SOAT1) in the ER and stored in lipid droplets, at least 1% of the esterified cholesterol of the whole is stored in lipid droplets (Zhang and Liu, 2015). Other methods of limiting excess cholesterol include the transport of cholesterol complexed with ApoE through the CSF; and the conversion of cholesterol via the neuronal-specific cytochrome P450, CYP46A1, into 24(S)-hydroxycholesterol (24OHC), which crosses the BBB, enters the systemic circulation, and is then eliminated by the liver (Qian et al., 2022, Moutinho et al., 2016, Zhang and Liu, 2015).

1.2.2 Cholesterol alterations in multiple sclerosis

During demyelination in MS, cholesterol metabolism is altered.

The biosynthetic enzyme 3-hydroxy-3-methyl-glutaryl-coenzyme A reductase (HMGCR), which converts acetyl-coenzyme A (acetyl-CoA) into mevalonate, is downregulated at the peak of MOG-induced EAE in rats and in lysolecithin models of demyelination. This suppression seems to be correlated with downregulated transcription of several myelin proteins, such as myelin oligodendrocyte glycoprotein (MOG), myelin basic protein (MBP) and myelin associated glycoprotein (MAG) (Mueller et al., 2008), suggesting a connection between the cholesterol synthesis pathway and myelin gene expression. Moreover, altered HMGCR expression is associated with misdirected OPC migration, leading to hypomyelination (Mathews et al., 2014). Cholesterol concentration has a negative effect on HMGCR expression. Because of this, the lower expression of both the HMGCR transcript and protein at the peak of EAE may be due to a high concentration of cholesterol in demyelinating lesions in the spinal cords of EAE animals, which decreases the need for cholesterol biosynthesis. In contrast, the observed increase in HMGCR expression at the end of the disease is likely attributable to the increased

cholesterol demand required for remyelination during the recovery period (Lavrnja et al., 2017).

In EAE models, cholesterol recycling is also altered. ApoE, which facilitates the recycling and transport of cholesterol from the brain and plays a crucial role in maintaining the integrity of the BBB, was found to be downregulated at the onset of experimental autoimmune encephalomyelitis (EAE) and upregulated at the disease's peak and conclusion (Lavrnja et al., 2017). This increase may be attributable to the increased number of glial cells found in the spinal cords of EAE animals. Consistent with this, ApoE expression was found to be elevated in astrocytes and macrophages in active MS lesions (Carlin et al., 2000), supporting ApoE involvement in lipid trafficking as a need for neuronal repair (Mahley, 2016). In addition, cholesterol released by demyelination binds to ApoE-containing lipid particles and is re-utilized or eliminated; indeed, cholesterol removal from damaged neurons restores axonal properties, reducing inflammation (Goodrum, 1991, Zhornitsky et al., 2016).

Cholesterol clearance also plays a role in the maintenance of myelin function. Neuronal-specific cytochrome P450, CYP46A1, is primarily responsible for brain cholesterol elimination; however, in several pathologic conditions, it has been found to be expressed in all glial cells (van de Kraats et al., 2014, Marangon et al., 2020, Lu et al., 2018).In EAE models, there was a reduction in CYP46A1 mRNA levels at the onset of disease, which persisted during the disease's peak (Lavrnja et al., 2017). 24-OH cholesterol, a product of CYP46A1, also plays a role in multiple sclerosis (MS). Not only are its levels altered in the CSF and serum of MS patients (Zhornitsky et al., 2016), but it also plays a pro-inflammatory role by stimulating the trafficking of T lymphocytes, after being synthesised by macrophages following the removal of myelin debris (Chalmin et al., 2015).

Cholesterol was discovered to be essential in microglia to resolve neuroinflammation in MS (Berghoff et al., 2021). Cholesterol is essential for the survival of microglia; however, microglia produce little cholesterol on their own and must rely on cholesterol supplied by astrocytes. Indeed, an excessive amount of cholesterol, as a result of myelin debris clearance in MS, is cytotoxic to microglia and inhibits further phagocytic activity (Qian et al., 2022). Unexpectedly, new sterol synthesis was found to be necessary only in microglia and not in other cell populations involved in myelin repair, *e.g.,* oligodendrocytes. Indeed, excessive cholesterol uptake from myelin debris in microglia triggers a negative feedback mechanism that inhibits the final synthesis of cholesterol by inhibiting the last enzyme, 24-dehydrocholesterol

reductase (DHCR24), which pushes towards the synthesis of desmosterol (DE), a direct precursor of cholesterol; DE stimulates Liver X receptor (LXR) to begin the secretory pathway of cholesterol from the cell, resulting in a less inflammatory and more permissive environment for repair (Berghoff et al., 2021).

1.3 Sphingolipids

Sphingolipids (SL) are a minor cell component that resides predominantly in the outer layer of the plasma membrane, with their hydrophilic head group facing the extracellular milieu. They were first described by J. L.W. Thudichum in the nineteenth century, when he identified for the first time a compound that was very abundant in the brain, naming it monoglycosylceramide (Wennekes et al., 2009, Feizi, 1985, Sonnino et al., 2006).

Sphingolipids represent a class of lipids consisting of a sphingoid base (which is simultaneously the skeleton and the hydrophobic tail), a *N*-acyl chain, and a head group. This compounds are synthesised in the RE from non-sphingolipid precursors and undergoes numerous modifications, leading to a vast family of molecules that play important roles in biological membranes, affecting many cellular functions (Gault et al., 2010, Harayama and Riezman, 2018).

Ceramide is the most elementary sphingolipid, consisting structurally of a fatty acid bound via an amide bond to the amino group of a sphingoid base. Sphingoid bases range from 12 to 22 carbon atom chain lengths in humans (Farwanah et al., 2007); these bases can be saturated, like sphinganine or dihydrosphingosine, or unsaturated, like sphingosine (Merrill, 2011). In the plasma membrane, ceramide increases rigidity and permeability; additionally, the membrane's curvature is affected by the length of the acyl chain: long chains generate a negative curvature, whereas short chains generate a positive one (Quinville et al., 2021).

The most represented sphingosine in mammals is D-*erythro*-(2S,3R)-sphingosine (*trans*-D-*erythro*-2-amino-4-octadecen-1,3-diol) which is an 18-carbon atoms long sphingosine with a double bond in positions 4 and 5 and two hydroxyl groups in positions 1 and 3.

Ceramide, containing an acyl chain and the sphingoid base, is the precursor of all other complex sphingolipids due to an additional substituent group in position C1.

Sphingolipids can be categorised in phosphosphingolipids, formed by ceramide and phosphocholine, namely SM or glycosphingolipids (GSLs) when the polar head contains one or more sugars.

GSLs can be further subdivided into neutrals when there is no charged sugar in the molecule, gangliosides when there are one or more sialic acid (Neu5Ac) residues, and sulfatides when they comprise a sulphate group (Schnaar and Kinoshita, 2015).

Ceramide, an highly hydrophobic SL, can be synthesised via *de novo synthesis* in the ER, the *salvage pathway* in the lysosomes, or being recycled from other more complex SLs at the plasma membrane levels (Schnaar and Kinoshita, 2015, Wennekes et al., 2009, Hannun and Obeid, 2011).

1.3.1 Sphingolipids metabolism

De novo biosynthesis of ceramide begins in the ER, where serine-palmitoyl-transferase (SPT) joins palmitoyl-CoA to form 3-ketosphinganine (Merrill, 2011); 3-ketodihydrospingosine/3-ketosphinganine can be can be acylated to dihydroceramide (dHCer) by one of the six isoform of ceramide synthase ($CerS_{1-6}$) specific for acyl chain length (Mizutani et al., 2005); subsequently dHCer is converted to ceramide by dihydroceramide desaturase (DES), the enzyme specific for inserting the double bond in C4 of the spingoid backbone in mammals (Merrill, 2011, Mencarelli and Martinez-Martinez, 2013).

Once formed ceramide can move to cis-Golgi and eventually plasma membrane or being subjected to different enzymatic activity, forming numerous other SLs (Tettamanti, 2004).

Ceramide is a precursor of sphingomyelin; it is transported via the ceramide transfer protein (CERT) to the lumen of the Golgi apparatus, where it and phosphatidylcholine serve as substrates for sphingomyelin synthase 1. Additionally, at plasma membrane levels, sphingomyelin synthase-2 catalyses the same reaction (Lahiri and Futerman, 2007).

Ceramide is the direct precursor of all GSLs, if it remains on the luminal side of the ER, it can be glycosylated to galactosylceramide (GalCer) by ceramide galactosyltransferase (CGT/GalCerS) and then converted to sulfatide by cerebroside sulfotransferase (CST). In contrast, when transferred to the cytosolic side of the Golgi apparatus via vesicular trafficking, it serves as a substrate for glucosylceramide synthase in the formation of glucosylceramide (Hannun and Obeid, 2011). Ceramide can also be phosphorylated to ceramide-1-phosphate by ceramide 1 phosphate kinase (Lahiri and Futerman, 2007). Ceramide can also be deacylated to sphingosine via ceramidase, which can follow two pathways: being used in the recycling pathway to reform SL or being phosphorylated to produce the bioactive molecule sphingosine 1-phosphate (S1P) via sphingosine kinase (SK) (Bartke and Hannun, 2009). Concerning sphingosine kinases, only two are known: SK1, which is mostly found in the cytosol, and SK2,

which is found in both the cytosol and the nucleus (Lahiri and Futerman, 2007). S1P, which functions as an intra and extracellular signalling molecule, is irreversibly cleaved by S1P lyase into ethanolamine-phosphate and a long chain aldehyde (hexadecenal) as one of the main reaction of catabolism of SLs (Hannun and Obeid, 2008).

The breakdown of complex sphingolipids into ceramide and then sphingosine, that is subsequently recycled, is termed the "salvage pathway" (Kitatani et al., 2008).

Ceramide, in return, can be obtained via the degradation of other sphingolipids. In late endosomes and lysosomes, sialidases 1 and 2, *β*-galactosidase and *β-N*-acetyl-hexosaminidase and the glycohydrolases (β-glucosidases and β-galactosidases) catalyse the sequential removal of sugar units from the terminal hydrophilic portion of glycosphingolipids to form ceramide (Tettamanti, 2004).

Another way to obtain ceramide is through the activity of acid or neutral sphingomyelinases, which disrupt sphingomyelin, releasing phosphocholine and Cer (Lahiri and Futerman, 2007).

So, in addition to the enzyme mentioned, the *salvage pathway* also includes ceramidases and (dihydro)ceramide synthases. In fact, it appears that there are different dihydroceramide synthases that are not found in the ER, but are activated in other compartments, such as late endosomes and lysosomes, in response to different signals that may reflect the non-proliferative cell status to direct the salvage pathway (Kitatani et al., 2008). In this regard, it is important to note that while dihydrosphingosine is predominantly produced by *de novo* sphingolipid biosynthesis, free sphingosine appears to be derived mostly from the turnover of glycosphingolipids, sphingomyelin, or ceramide (Kitatani et al., 2008).

However, even if there is no dihydrosphingosine desaturase, there is Δ-4 desaturase, which is a dihydroceramide desaturase capable of oxidising sphinganine to sphingosine (Ternes et al., 2002). As a result, both dihydrosphingosine and sphingosine are precursors of ceramide and other SLs and are involved in both the *de novo* and the *salvage pathway* (Tettamanti, 2004).

1.4 Glycosphingolipids

Glycosphingolipids are a large family of membrane sphingolipids, highly abundant on cell surface that mediate interactions between cells and their extracellular environment.

Glycosphingolipids are the most structurally diverse class of sphingolipids and are typically categorised as either acidic, neutral, or basic. They are ubiquitous components of the membranes of mammalian cells and are especially abundant in the nervous system.

Gangliosides, the sialic acid-containing glycosphingolipids, discovered in 1936 by Ernest Klenk, are thought to play several roles role in the development, differentiation, and function of vertebrate nervous systems (Ohmi et al., 2012).

In cells, gangliosides are predominantly localised in the plasma membrane's extracellular leaflet, where they are not uniformly distributed (Sonnino et al., 2006). On the cell surface, gangliosides participate in cell-cell recognition, adhesion, and signal transduction within caveolae, lipid rafts or glycosphingolipid-enriched microdomains interacting with other membrane components such as sphingomyelin and cholesterol (Anderson, 1998, Simons and Toomre, 2000, Hakomori et al., 1998). Colocalization of gangliosides with signalling molecules and adhesion molecules in microdomain structures suggests their involvement in the regulation of processes such as cell proliferation, survival, adhesion, and neuronal differentiation. In addition to cell plasma membranes, gangliosides have been found on nuclear membranes, and it has recently been proposed that they play crucial roles in modulating intracellular and intranuclear calcium homeostasis and the subsequent cellular functions (Ledeen and Wu, 2008) cell growth (Bremer et al., 1986) and differentiation (Russo et al., 2018), immune responses, cell transformation and degradation (Ene and Nicolae, 2015).

1.4.1 Glycosphingolipids metabolism

Over the past couple of decades, the biochemical pathways of glycosphingolipids metabolism and the intracellular sites of synthesis and degradation, in the endoplasmic reticulum/Golgi apparatus and lysosomes, respectively, have been systematically investigated (Futerman and Riezman, 2005, Futerman, 2006).

Galactosylceramide synthase (GalCerS), which catalyses the transfer of galactose from UDP-galactose to ceramide, converts ceramide to galactosylceramide (GalCer) in the ER lumen (Sprong et al., 1998). GalCer is then transferred to the Golgi apparatus, where it is modified by cerebroside sulfotransferase (CST), which adds a sulphate group to the 3'-OH of galactose to produce sulfatide, the most abundant sulfoglycolipid in mammalian brains, firstly described

by Thudichum in 1884 (Eckhardt, 2008). Sulfatide degradation occurs in lysosomes by arylsulfatase A (ASA) (Farrell and McKhann, 1971, Eckhardt, 2008).

Alternatively, ceramide is transported to the cytosolic side of the cis-Golgi apparatus via a CERT-independent mechanism, where it is glycosylated by glucosylceramide synthase (GCS), an enzyme that transfers glucose from UDP-glucose to the primary hydroxyl group of ceramide to form glucosylceramide (GlcCer) (Hanada, 2006, Hanada et al., 2009, Marza et al., 2009).

GlcCer can be transported across the Golgi complex via vesicular trafficking, or it can be transported to the trans Golgi compartments by the lipid transport protein FAPP2 (Buton et al., 2002, Halter et al., 2007, Gault et al., 2010).

When GlcCer flips into the Golgi lumen, the addition of another sugar residue leads to the formation of lactosylceramide (LacCer) that, once produced, cannot be translocated back to the cytosolic leaflet (Buton et al., 2002).

In order to form all other gangliosides, non-specific enzymes such as *N-acetyl*-galactosaminyltransferase, galactosyl-transferase, and sialyl-transferase add acetylgalactosamine, galactose, and sialic acid to lacCer (Lahiri and Futerman, 2007, Kolter et al., 2002b). Once formed gangliosides leaves the golgi network, as budding vescicles, and reach the external leaflet of plasma membranes (Tettamanti, 2004).

1.4.2 Gangliosides

LacCer is converted into more complicated glycosphingolipids whose accessory groups, glucose, galactose, *N*-galactosamine and *N*-acetylglucosamine, sites of bond vary and this determines their nomenclature: isoglobo-, lacto-, neolacto-, and ganglio series (Merrill, 2011).

Gangliosides are a class of sphingolipid containing residues of sialic acid, an acidic sugar. They have been classified based on exoses and sialic residues using the Svennerholm nomenclature (Svennerholm, 1963).

In this nomenclature G stands for ganglioside and each are characterized by the presence of:

- no sialic acid residues: A for asialo-ganglioside
- one sialic acid residues: M for monosialo-ganglioside
- two sialic acid residues: D for disialo-ganglioside
- three sialic acid residues: T for trisialo-ganglioside

Together with this definition, gangliosides are also named after zero (0 series), one sialic acid residues (a series), two sialic acid residues (b series), or three sialic acid residues (c series) linked to the 3-position of the inner galactose moiety, which distinguishes this second and complementary nomenclature (Kolter et al., 2002a, Sandhoff and Kolter, 2003).

Sialyl-transferases are substrate-specific and substrate-selective enzymes that convert lactosylceramide subsequently into GM3, GD3, and GT3.

The simplest ganglioside, GM3, is formed by the addition of a sialic acid residue to LacCer in a reaction catalysed by sialyl-transferase type I, namely GM3 synthase. Subsequently, a N-acetylgalactosamine transferase transfers N-acetylgalactosamine to GM3 to form GM2. Due to the addition of a galactose, GM2 can be converted to GM1a (monosialo-ganglioside of the *a* serie); GM1a is then subjected to a sialyl-transferase type IV, which adds a second sialic acid residue, synthesising GD1a (disialo ganglioside of the *a* serie) (Schnaar, 2019).

The subsequent addition of a sialic acid residue to GM3 by a sialyl-transferase type II, namely GD3 synthase, generates GD3; GD3 is converted into GT3 by a sialyl-transferase type III, namely GT3 synthase. The precursors of the b and c series, GD3 and GT3, undergo the same transformation as GM3 via the same enzymes. GD3 is the progenitor of GD2, GD1b, and GT1b, while GT3 is the progenitor of GT2, GT1c, and GQ1c (Lahiri and Futerman, 2007, Schnaar, 2019).

The gangliosides described thus far, despite being predominant in various organs and tissues and especially abundant in the brain, are only a few of the more than 200 identified species, which vary not only for the glycan head group but also for the moiety of sphingosine with different length and different saturation of the acyl chains (Sipione et al., 2020).

The enzymes involved in gangliosides biosynthesis, are membrane-anchored glycosyl transferases that exhibit a gradient of distribution in the Golgi apparatus. The initial phases of glycosylation take place in the cis-Golgi, while subsequent phases occur in the trans-Golgi (Tettamanti, 2004).

Different types of gangliosides are enriched based on developmental stage and cell type. In adult human tissues, 0 and c series gangliosides are only found in trace amounts. GM3 and GD3 are highly expressed during embryogenesis and postnatal development, while in adult tissue, these gangliosides are present at much lower levels and the expression pattern shifts from simple to complex gangliosides, including GM1, GD1a, GD1b, and GT1b. This transformation is governed primarily by the differential expression and intracellular

distribution of enzymes required for the biosynthesis of these glycosphingolipids (Yu et al., 2012, Yu et al., 2009).

For example, GD3 is highly expressed on the surface of neural stem cells (NSC) and regulates endocytosis and self-renewal by interacting with growth factor receptors such as epidermal growth factor receptor (EGFR). Nonetheless, as the neuronal line differentiates, a switch to more complex gangliosides such as GM1 occurs, and at the end of differentiation, there is an increased expression of the more complex gangliosides GD1a, GD1b, and GT1b (Sipione et al., 2020).

1.4.3 Sphingolipids and glycosphingolipids functions

Some SLs act as second messengers in many cellular pathways. Among sphingolipids, the most studied second messengers are sphingosine 1-phosphate (S1P) and ceramide, nowadays referred to as bioactive molecules. Their balance, a concept defined as "sphingolipid rheostat", and their regulatory effect on different pathways determine the fate of cells (Grassi et al., 2019b). These two lipids are balanced in a physiological context, with S1P acting as a pro-survival lipid in numerous cellular responses such as the regulation of proliferation, cell growth, cell migration, and also inflammation, whereas Cer mediates signal transduction leading to cell death at an high concentration as happens, for example, in oligodendrocytes during MS (Dasgupta and Ray, 2019, Grassi et al., 2019b, Coelho et al., 2010).

Among sphingolipids, glycosphingolipids have a variety of structural and functional roles, including calcium homeostasis in neurons and, more broadly, survival, proliferation, development, differentiation, autophagy, apoptosis, and ageing (Sipione et al., 2020). For example, KO mice for GlcCer synthases are embryo-lethal, whereas other mutants for GlcCer synthase only in neurons result in abnormal cerebellar development and death within three weeks (Yu et al., 2009). It is well known that glycosphingolipids, mostly gangliosides, interact with growth factor receptors, modulate cell growth, and inhibit receptor-associated tyrosine kinases in many cells' events. GM3 inhibits phosphorylation and dimerization of EGFR and the insulin receptor (IR), but GM1 and GD1a have no effect on these processes (Schnaar, 2019).

Gangliosides in particular have been identified as pro survival, and regulators of differentiation in the developing brain by modulating the effects of ceramide and the induction of apoptosis

(Yu et al., 2009). For example, GD3 synthase null mice, lacking both b- and c-series gangliosides, exhibit normal myelination with no demyelinating process in the brain (Kawai et al., 2001). Instead, when *N*-acetylgalactosamine transferase, which transfers N-acetylgalactosamine to GM3 and GD3 to form GM2 and GD2 respectively, is absent, mice do not produce complex GLs, but even if the CNS is still functional they exhibit axonal degeneration, increased presence of unmyelinated zones, and dysfunction of ion channels due to their incorrect localization; moreover, aspermatogenesis occurs in males (Lahiri and Futerman, 2007, Takamiya et al., 1996, Jackman et al., 2009). Taken together, these studies suggest a role for gangliosides in axon-glial interaction.

Functionally, the GalCer-sulfatide axis is also particularly important.

Oligodendrocytes, the myelinating cells of the CNS, perform a sequential biosynthesis of GalCer and sulfatide in the CNS. In mature oligodendrocytes, the synthesis of GalCer and sulfatide begins at the onset of terminal differentiation and remains constant (Poduslo and Miller, 1985). GalCer and its derivative sulfatides are the most prevalent and abundant long-chain fatty acid lipids in myelin. These lipids are found in lipid rafts, GalCer- and sulfatide-rich domains in oligodendrocyte membranes. They regulate the distribution of multiple myelin proteins, which has a profound effect on the survival, proliferation, and differentiation of oligodendrocytes (Aureli et al., 2015).

Even though they are not myelin-specific lipids, they play a significant role in nerve conduction. This has been proven in mice lacking the UDP-galactose/ceramide galactosyltransferase (CGT) enzyme, which converts Ceramide to GalCer. As a result, they do not produce GalCer and neither sulfatide, resulting in a decrease in myelin stability, abnormal axon-glial interaction, and slow nerve conduction (Ozgen et al., 2016, Saher et al., 2011).

This correlates with the role of interaction between the oligosaccharide chain of these glycosphingolipids and two gangliosides, GD1a and GT1b, on the surface of the axon, which, along with the myelin-associated glycoprotein (MAG), mediates the long-term stability of axon-myelin. Indeed, the trans-interactions between GalCer and sulfatide and the gangliosides present in the outer leaflets of two myelin sheaths stabilize the myelin wrapping forming a specialised “glycosynapse” (Aureli et al., 2015).

GalCer is not only the precursor for sulfatide, but it also appears to be involved in myelin formation and maturation, whereas sulfatide participates in the maintenance of the long-term stability of myelin structure, specifically affecting the sheaths’ integrity and stability.

Mice lacking cerebroside sulfotransferase (CST), which adds the sulphate group to the 3'-OH of galactose to produce sulfatide, do not synthesise sulfatide at all; however, they have thinner, but apparently normal, myelin, despite the fact that degeneration of the nodal areas is observed during ageing, leading to degeneration as a result of the unusual location of the Na^+ and K^+ channels. All this suggests that GalCer and sulfatide might represent not only structural components of the myelin sheath but also active players in myelin formation and maintenance (Grassi et al., 2016).

1.5 Lipid Rafts and Caveolae

K. Simons and G. Van Meer proposed the hypothesis of lipid rafts to answer the question: "How are the different molecular compositions of cell compartments developed and maintained?" observing the composition of cell's membranes of polarised epithelial cells. The apical and basolateral portions are indeed different in composition: the former has a GLS:phospholipids:cholesterol ratio of 1:1:1, whereas the latter, while cholesterol is equally distributed, has an higher amount of phospholipid with respect to GLS (Simons and van Meer, 1988b). Intrinsic properties on certain membrane lipids are responsible for the lateral order found in biological membranes and their organisation leads to the segregation of specific lipids into membrane domains, which are *"ordered structures that differ in lipid and/or protein composition from the surrounding membrane"* (Simons and Van Meer, 1988a).

These microdomains are rich in SLs and cholesterol, as well as a large amount of phospholipids and few proteins, especially Src kinase family proteins and small G-proteins (Hakomori, 2000); in fact, the organisation of these rafts supports various signal transduction phenomena; in this regard, it is necessary to affirm and emphasize that are the interactions between lipids, not lipid-protein interactions, that drive segregation (Sonnino et al., 2006).

The greater stimulation of segregation in lipid and protein clusters is primarily due to the presence of gangliosides, whose hydrophilic and bulkier head groups, rather than the head groups of the more abundant glycerophospholipids, induce membrane segregation and a positive curvature, resulting in the formation of microdomains (Sonnino et al., 2018).

Indeed, gangliosides are naturally predisposed to laterally segregate and form hydrogen bonds and hydrophobic interactions with other SLs and cholesterol (Sipione et al., 2020).

Erythrocytes provided one of the earliest observations of GLs aggregates on membrane surfaces nearly forty years ago (Tillack et al., 1983). Although the existence of lipid rafts was previously hypothesised, they have been known for a long time; however, there were limitations in their study until the identification of a biochemical method capable of isolating them. One of the first indications of the existence of these domains was the observation that cell membranes are not completely soluble in non-ionic detergents such as Triton X-100 and consequently, many authors refer to these structures as "detergent-resistant membranes" (DRM) (Brown and Rose, 1992).

The lipid rafts are, after all, small and dynamic membrane domains formed by the lateral segregation of sphingolipids; They are ordered structures with a very short half-life, from micro to milliseconds, in which we also find many proteins and receptors along with lipids, and their aggregation within these domains allows for crucial signalling (Sonnino and Prinetti, 2013). In principle, each cell has specialised membrane domains in which a subset of proteins appears to direct the formation of specific multi-molecular complexes, thereby enabling intracellular and extracellular signalling activity (Sonnino and Prinetti, 2013). Through interaction with membrane proteins, such as the Src family protein kinases and receptors anchored to glycosylphosphatidylinositol (GPI), these lipid platforms have key cellular function and can regulate signal transduction pathways via membrane metabolism (Sonnino et al., 2014).

The heterogeneity and dynamic nature of lipid rafts contribute to the large number of membrane-transduced signals. There are many glycosyl-hydrolases and glycosyl-transferases in the plasma membrane that enable the addition or removal of sugar residues from membrane glycolipids. As an example, ceramide, can derive from the hydrolysis of SM but also from the removal of oligosaccharide chains from gangliosides. This dynamism involves a reorganisation of the membrane's structure that modulates the interaction of glycolipids with raft-associated proteins (Sonnino et al., 2014). Membrane domains are not only distinguished by their unique lipid composition, but also by the presence of distinct subsets of membrane proteins. In this regard another form of signalling platform is caveolae. Caveolae, characterized by the presence of caveolins, are flask-shaped invaginations of the plasma membrane, enriched in cholesterol and GSLs, that have been implicated in cell signalling (Hooper, 1999). Caveolins are palmitoylated protein that form an hairpin structure throughout the membrane, with their *N*- and *C*-terminal domain located on the cytosolic side of the membrane (Hooper, 1999); in caveolae are present 3 tissue specific isoforms of caveolins, caveolin-1, caveolin-2 and caveolin-3 (Sonnino and Prinetti, 2009). Cav1 and Cav2 are prevalently found in adipocyte, endothelial cells and fibroblast whereas Cav-3 is prevalently found in smooth muscle cells (Boscher and Nabi, 2012). In part, caveolae can be compared to lipid rafts due to their resistance to detergents and similar lipid composition to that of these microdomains (Hakomori, 2000). However, contrary to lipid rafts, caveolae are not ubiquitously expressed in all cells, indeed they were found in endothelial cells, adipocytes, smooth muscle cells and fibroblasts (Sonnino and Prinetti, 2009). Similar to lipid rafts,

caveolae are clusters of lipids and proteins that regulate signalling mechanisms; in fact, inside caveolae are found many proteins involved in signal transduction: non receptor tyrosine kinases (Fyn, Src, Ras, Yes), nitric oxide synthase (NOS), epidermal growth factor receptor (EGFR), insulin receptor (IR), platelet-derived growth factor receptor (PDGFR), phospholipase C and others (Hooper, 1999).

2. Multiple sclerosis

Multiple sclerosis (MS) is a chronic inflammatory demyelinating disease of the central nervous system (CNS) with a variety of clinical presentations (Lemus et al., 2018).

This disease has been known for a very long time: indeed, It was initially described in 1400, but it wasn't until the 19th century that a correlation between the heterogeneous clinical phenotype of patients at various stages of the disease and the change observed in post-mortem examinations was observed (Kumar et al., 2011), leading the neurologist Charcot to coin the name *Sclérose en plaques* (Pearce, 2005), a term that would in time became Multiple Sclerosis (Zalc, 2018). In the past decade, the ratio of females to males affected by MS as the total amount of patients, has increased. MS is estimated to affect 2.8 million people worldwide, so it has a significant functional and financial impact on the global life expectancy (Thompson et al., 2018, Walton et al., 2020).

The clinical pathological spectrum of this disease is very heterogeneous and different types can be distinguished. The most common phenotype is relapsing-remitting (RRMS) form, diagnosed in 85% of patients, characterized by alternating periods of neurological dysfunction (relapsing) and periods of relative clinical stability devoid of new symptoms (remitting) (Kalincik, 2015). The majority of patients with RRMS progress to secondary progressive multiple sclerosis (SPMS), which is characterised by periods of progressive impairment due to continuous myelin-damaging attacks that result in severe disability (Rovaris et al., 2006). Ten % of patients are instead diagnosed with primary progressive multiple sclerosis (PPMS), in which the disease progresses without the initial relapsing-remitting form (Ransohoff et al., 2015). Individual episodes of demyelination of the CNS may also occur, and could transform into MS only if additional risk factors are present; otherwise, this condition is known as isolated clinical syndrome (ICS) (Miller et al., 2012). Each of these subtypes is distinguished by varying degrees of inflammation, demyelination, remyelination, and axonal loss (Kantarci et al., 2014).

Diagnosis is usually done via magnetic resonance imaging (MRI), CSF analysis, and visual evoked potentials (Kaminska et al., 2017). Loss of motor and sensory function due to immune-mediated inflammation, demyelination, and axonal damage characterises patients with MS (Karussis, 2014).

Neurodegeneration is associated with chronic inflammation regardless of the stage of the disease, although the level of inflammation is higher during the early relapsing phase (Lassmann, 2014).

Demyelination refers to all processes involving myelin damage with or without preservation of axonal integrity, which can be of traumatic, genetic, or autoimmune nature, resulting in impaired nerve conduction and neurodegeneration due to loss of physical and metabolic support of the axons (Hanafy and Sloane, 2011, Ferrer, 2018).

MS is mainly a disease of the white matter, characterized by focal confluent plaques of demyelination, with variable axonal degeneration and astrocytic gliosis combined with microglial activation (Zalc, 2018, Lassmann, 2014); is associated with inflammation (neuro-inflammation) and BBB leakage (Pearce, 2005).

Remyelination is a spontaneous process through which demyelinated axons are re-covered with new myelin sheaths, resulting in the formation of shadow plaques. These plaques are lesions that resemble demyelinated regions; their myelin sheaths are thin, with enlarged internodes, and their myelin density is lower than that of healthy white matter; despite this, functional recovery occurs (Munzel and Williams, 2013). Remyelination occurs during clinical remissions, but this process is inhibited as the disease progresses, and significant axonal loss is observed (Thompson et al., 2018, Podbielska et al., 2013).

Unfortunately, there is no cure for this disease, only disease-modifying therapies that primarily target the inflammatory component to slow the disease's progression (Thompson et al., 2018).

MS is now considered an autoimmune-based pathology in which demyelinated parts of its specific targeted organ, the brain, are characterised by immunological reactivity dominated by autoreactive lymphocyte T cells, $CD4^+$ (T helper 1 (Th1) and T helper 17 (Th17)) and cytotoxic/suppressor $CD8^+$T-cells, that enter the CNS through damaged BBB and induce an inflammatory cascade resulting in demyelination and axonal loss (Lubetzki and Stankoff, 2014).

It was believed that Th1 and Th17 lymphocytes play the major role in demyelination, since they recognise myelin antigen bound to major histocompatibility complex class II (MHCII) on antigen presenting cells (APCs), likewise dendritic cells at the BBB or microglial cells. After entering the CNS, Th1 proliferate and secrete toxic cytokines such as interferon-gamma (IFN-

γ) and tumour necrosis factor-alpha (TNF-α), thereby causing inflammatory damage and recruitment of other immune cells (^{macrophages} and B cells), thereby creating a loop of pro-inflammatory enhancement that results in demyelination and axonal degeneration (Lubetzki and Stankoff, 2014, Munzel and Williams, 2013).

Cytotoxic/suppressor CD8+T-cells are CNS antigen-specific, restricted to MHC class and secretors of IFN-γ and perforin; are the most abundant lymphocyte in MS lesions and seems to be able to regulate MS, inhibiting the disease (Sinha et al., 2015). Cytotoxic $CD8^{+}$T cells may play a crucial role in the demyelination, because oligodendrocyte and/or myelin antigens can be recognized by $CD8^{+}$T cells due to MHCI expression under inflammatory or stress conditions (Lubetzki and Stankoff, 2014). However, EAE into $CD8^{+}$ null mice, have a more severe progression, whereas experimental transfer of MOG-induced $CD8^{+}$T cell in wildtype B6 mice doesn't induces EAE pathology, besides this transfer reduce disease severity in other classical induced EAE models (York et al., 2010).

Moreover, it has been demonstrated that a drug commonly used to limit the progression of pathology has a proliferative effect on cd8+ cells, thereby implementing the cytotoxic effect against the more aggressive CD4+ cells (Tyler et al., 2013).

Since no autoantigen has been found, viral infection, environmental factors, way of life, and genetic predisposition are the only known con causes of Multiple Sclerosis.

Several studies have identified smoking and vitamin D deficiency as risk factor; retinoid receptor for vitamin D (VDR) induces OPC differentiation, and vitamin D increases OPC differentiation. Others have suggested that Epstein Barr virus, Herpes simplex types 1 and 2, measles, and rubella may influence MS development. (Thompson et al., 2018, Lemus et al., 2018, Lutton et al., 2004, Dulamea, 2017).

3. Glial Cells in myelin development and remyelination

In the adult mammalian CNS, glial cells or neuroglia consist of astrocytes, oligodendrocytes, and microglia. Sixty – ninety percent of a human brain's cells are glial cells (Sherman and Brophy, 2005, Aggarwal et al., 2011a).

The term glia, derived from the Greek word for glue, reflects Rudolf Virchow's nineteenth-century belief that these cells had the function of holding the nervous system together. It is now common knowledge that glia play a variety of roles, including modulation of homeostatic functions, myelination, synaptic function, and response to neural injury (Domingues et al., 2016).

Even though all three are related to the CNS, their embryonic origins are distinct.

Oligodendrocytes (OLs) and astrocytes originate from the neuroectoderm. Microglia instead are myeloid cells of hematopoietic origin that migrate to the CNS via the bloodstream during the early stages of embryonic development (Barres, 2008). OLs and astrocytes have the same origin: radial glial cells (RGCs) which are neural stem cells positive to neuroepithelial stem cell protein (nestin+) that maintain self-renewal and have differentiation properties (Miron et al., 2011, Magistri et al., 2016). Sonic hedgehog (SHH) and fibroblast growth factor (FGF) direct the differentiation of the oligodendrocyte progenitor cells (OPC) (A2B5+, PDGFR+, and NG2+). IGF-1, and T3 promote the differentiation of pre-oligodendrocytes/immature oligodendrocytes (O4+/ GalC+) (Miron et al., 2011). Ciliary neurotrophic factor (CNTF) and bone morphogenic proteins (BMPs) start astrocytic commitment (Magistri et al., 2016).

Myelin damage observed during MS is not confined to the cells responsible for its production: the oligodendrocyte. All glial cells participate both during myelin development, synapse formation, BBB formation and during disease such MS where loss of myelin sheaths and oligodendrocytes death together with astrogliosis and activated microglia are observed (Barres, 2008, Lassmann, 2014, Domingues et al., 2016).

Remyelination is the spontaneous process by which demyelinated axons receive new myelin sheaths, thereby leading to functional recovery (Munzel and Williams, 2013). Animal models of MS and some MS patients exhibit spontaneous remyelination; however, in humans it is ineffective due to the small number of OPCs near the lesion that are unable to differentiate

into myelin-producing cells. Those that differentiate, initially form thin, short myelin sheets that temporarily but not permanently restore motor/sensory function(Abu-Rub and Miller, 2018). OPCs must differentiate into myelin-producing oligodendrocytes in order to remyelinate (Alizadeh et al., 2015). However, within lesions there are many dead oligodendrocytes and, even if they are continuously replaced by new ones, these are not able to differentiate. From study of post-mortem MS brain, it has been estimated that around 70 % of MS lesions that remain demyelinated, contain plentiful OPCs, suggesting a failure of differentiation and the other 30 % contain few or no OPCs, indicating failure of recruitment (Kotter et al., 2006).

3.1 Oligodendrocytes

At various stages of their development, OLs , which originate from neuroectodermal cells in the subventricular zone, express membrane-bound surface antigens, several of which are GSLs (Barres, 2008).

Oligodendrocyte precursor cells (OPCs) are called NG2-glia because they express the oligodendroglial differentiation of nerve/glial antigen 2 (NG2). These cells, with self-renewal properties, are present in both the developing and adult brain and make up 5-10% of the adult CNS's cell population (Ferrer, 2018). During brain development and adulthood, mature oligodendrocytes produce myelin (Barres, 2008, Domingues et al., 2016).

Myelin biogenesis requires the extension of OLs processes, recognition and adhesion to the axon, stabilisation, and the formation of compact and non-compact myelin with specialized axon-glial contact domains (Jackman et al., 2009). Each axon is covered in numerous myelin segments (internodes), which are separated by nodes of Ranvier in which are found numerous sodium channels that facilitate rapid saltatory nerve conduction; consequently, myelin provides electrical insulation and metabolic support to axons (Domingues et al., 2016, Podbielska et al., 2013).

At the beginning of the myelination process, oligodendrocytes produce between 5,000 and 50,000 μm^2 of myelin per cell each day, which is directly proportional to the production of myelin lipids. By the end of the myelination process, oligodendrocytes have produced approximately 40% of the total lipids in the human brain (Pfeiffer et al., 1993, Norton, 1981).

Myelin, wrapping the axons in a spiral fashion is composed of lipids and proteins that are distributed according to charge, lipo- or hydrophilicity, and relative molecular weight. The lipid content of myelin is about 80% of its total dry weight, indeed, myelin has a distinct lipid composition containing all the major lipid classes; in comparison to other plasma membrane in which the molar ratio of cholesterol, phospholipids, and glycosphingolipids is 25:65:10, in myelin is 40:40:20 allowing for the close packing and organisation of molecules within the membrane (Chrast et al., 2011, O'Brien, 1965).

High Cholesterol content is required for proper myelin assembly, and the supply/synthesis of this molecule governs this process, suggesting that signalling systems that drive myelin biogenesis may be coupled to cholesterol metabolism (Saher et al., 2005).

The myelin membrane also contains ethanolamine plasmalogens, whose levels correlate with myelination with a peak between 30 and 40 when myelination is complete (Schmitt et al., 2015, Braverman and Moser, 2012). Ethanolamine plasmalogens reduce membrane fluidity and strengthen intermolecular hydrogen bonds. High plasmalogen levels in myelin may increase membrane packing density and stability (Han and Gross, 1990, Paltauf, 1994). Plasmalogens may protect unsaturated membrane lipids from oxidation and provide lipid mediators for inflammatory reactions (Farooqui et al., 2000).

3.1.1 Oligodendrocytes in MS

For a long time, it was believed that adult OLs were not involved in remyelination; however, these cells, when survive to myelin damage, extend their plasma membrane around nude axon (Duncan et al., 2018). Moreover, in animal models of toxin-induced demyelination, it was shown that OPCs, which are highly proliferative and motile cells expressing PDGF receptor alpha (PDGFαR), and are NG2+, reach the lesion site differentiating into immature OLs that have the capacity to transform into myelinating OLs, thus contributing to myelin repair in the adult CNS (Ffrench-Constant and Raff, 1986, Sherman and Brophy, 2005).

Following myelin damage and before producing new myelin sheaths, however, OPCs must undergo activation, migration, proliferation, and differentiation. The result is a compact myelin layer that is thinner and shorter than those formed during myelination during development (Cunniffe and Coles, 2021).

Remyelination may fail due to a defect at any stage of the process: OPCs proliferation and recruitment, OLs survival, proliferation, migration, maturation; moreover, a deficiency of pro-regenerative factors or an excess of inhibitory factors, combined with the oligodendrocyte's intrinsic composition, may limit the ability to recover axons (Franklin and Ffrench-Constant, 2017). Remyelination is often inconclusive because the cells with remyelination potential are randomly distributed within the CNS and are distant from germinal zone, thus difficult to reach (Domingues et al., 2016).

Other several factors are likely to impair remyelination: the presence of myelin debris still present in the glial scar, which can prevent axonal regeneration and inhibit OPCs differentiation (Podbielska et al., 2013).

Furthermore, several studies have found that the potential for remyelination decreases with age, because aged OPCs are less reactive to factors that induce differentiation. Furthermore, it has been s that the myelin sheath of elderly mice can be repaired through heterochronic parabiosis with a young animal. Lastly, there may be variations in the potential for remyelination based on the location of damage, such as paraventricular lesions being less amenable to safeguard than subcortical regions (Cunniffe and Coles, 2021).

3.2 Astrocytes

Astrocytes are the most abundant and heterogeneous glial population in the CNS (Hamby and Sofroniew, 2010). Astrocytes have almost countless functions as regulators of CNS homeostasis, through control of ion, pH, neurotransmitter metabolism, and roles in the development and maintenance of the BBB, and in synaptogenesis and myelination (Sofroniew and Vinters, 2010, Ullian et al., 2001).

Astrocytes originate from the neural embryonic progenitor cells that reside in the lumen of neural tube, although they can also be formed indirectly via radial glia (Kessaris et al., 2008). Even though the heterogeneity of these cells is quite complex, Ramón y Cajal's classification based on morphological differences is still used to classify them as type 1 and type 2 astrocytes. In the grey matter, type 1 or protoplasmic astrocytes embed blood vessels and synapses to promote BBB and synapses functions. (Barres, 2008).

Type 2 astrocytes, also known as fibrous astrocytes, are found in the white matter, and have elongated morphology due to their alignment with myelinated fibres (Barres, 2008, Sofroniew and Vinters, 2010, Butt et al., 1994). It is generally accepted that astrocytes support OLs function (Domingues et al., 2016).

Moreover, astrocytes can be diverse in their ability to react to CNS insults, ranging from inactive (quiescent), as in normal resting CNS, to active-reactive when, upon injury or insult in CNS, astrocytes activated resulting in astrogliosis (glial scar) (Domingues et al., 2016, Nash et al., 2011, Matyash and Kettenmann, 2010, Kohler et al., 2021, Barres, 2008).

We do not exactly know whether astrogliosis is beneficial or harmful, but in the first phase of CNS injury, it is an essential and protective response. In the subsequent phase, reactive astrocytes release toxic chemicals and construct physical barriers to impede axonal regeneration (Zhan et al., 2017).

The first evidence of interplay between astrocytes and OLs on myelination was suggested not long time ago, in the 80's, when type 1 astrocytes were identified to expand OPCs from neonatal rat optic nerve and which was lately found to be mediated by a soluble growth factors identified as platelet-derived growth factor (PDGF) and fibroblast growth factor (FGF2); this two growth factors are potent mitogens for OPCs inhibiting their premature differentiation (Domingues et al., 2016). In particular there is new evidence that astrocyte play a positive role in the remyelination process by forming glial scar that prevents self-reactive leucocyte from migrating from lesion area to a non-damaged healthy area (Kiray et al., 2016). Moreover, it was suggested, that astrocytes are required during cuprizone induced demyelination in by secreting a variety of factors, such as the chemokines CCL2, CCL3, but mostly CXCL10 to attract inflammatory cells, such as microglia to the lesion, indeed in astrocyte ablated in GFAP kinase transgenic mice showed impaired microglial clearance of debris (Skripuletz et al., 2013).

It has also been highlighted that Ciliary neurotrophic factor (CNTF) in culture medium, probably secreted by reactive astrocyte within lesion *in vivo*, has property enhancing generation, maturation, and survival of oligodendrocytes playing a positive role in remyelination process increasing myelin oligodendrocyte glycoprotein (MOG) expression (Salehi et al., 2013).

3.3 Microglia

The brain is an immune privileged organ (Glezer et al., 2007) where typical cells fulfilling the immune response fail to get there due to the BBB, indeed the CNS is equipped with specialized resident immune cells: microglia. Such cells originate from a myeloid precursor and creep into the brain just after birth to remain there throughout life; are equipped with self-renewal capacity via colony stimulating factor 1 receptor (CSF-1) stimulation in response to cytokines (*e.g.,* IL-34) secreted by neuron and other glial cells that initiate a cascade of signal via AKT and ERK pathway that allows proliferation and survival of these immune cells (Elmore et al., 2014, Colonna and Butovsky, 2017).

Microglia mediate the selective elimination of non-functional synapses during brain development by phagocytosing complement proteins (e.g. C3 and C1q) deposited on synapses and bound to complement receptors on microglia surface (Barres, 2008).

Microglia act as sentinel cells for intruders and is on the frontline during neuro-inflammation. In the CNS there are also "*Perivascular, subdural meningeal and choroid plexus macrophages which are non-parenchymal macrophages that mediate immune responses at brain boundaries*" [cit. (Goldmann et al., 2016, Aguzzi et al., 2013)].

Microglia participate in immune surveillance and pathogen scavenging, they play a crucial role in myelin repair after injuries caused by many CNS diseases (e.g., MS). Microglia, in particular, play an important role in removing damaged myelin debris, facilitating repair, and in promoting the proliferation and differentiation of OPCs into OLs by secreting multiple protein factors. (Neumann et al., 2009, Domingues et al., 2016).

Microglia activate in response to injury by undergoing morphological changes, emitting branched protrusions, and migrating to the lesion site, releasing cytokines, neurotrophic factors, and acting as a phagocyte when required. This function is conducted during both development and adulthood (Neumann et al., 2009, Aguzzi et al., 2013).

Microglia have always been phenotypically categorised like macrophages, the phenotypes of which vary according to the activity conducted: M1 with pro-inflammatory phenotype for the response against the pathogen and M2 with anti-inflammatory phenotype that promotes the removal of debris and creates an environment conducive to regenerations. However, this strict definition is no longer entirely accepted as evidence have shown the existence of

additional phenotypes of microglia, including brain zone and disease-dependent microglia (Napoli and Neumann, 2009, Neumann et al., 2009, Colonna and Butovsky, 2017). For example exist: axon tract-associated microglia (ATM), damage associated microglia (DAM), injury responsive microglia (IRM), Human AD microglia (HAM); microglia inflamed in multiple sclerosis (MIMS), lipid-droplet-accumulating microglia in aging (LDAM) and DARK microglia mostly related to aging (Paolicelli, 2022, Garcia-Revilla et al., 2019).

In response to IFN-γ or lipopolysaccharide (LPS), M1 activated microglia promotes the transcriptional activation of nuclear factor-kB (NF-kB), increase expression of CD86 and MHC-II, and secrete pro-inflammatory cytokines including TNF, IL-1, IL-12, reactive oxygen species (ROS) and reactive nitrogen species (NOS); whereas, M2 state acts as an anti-inflammatory secreting cell via activation of STAT6 pathway, blocking pro-inflammatory cytokines, clearing debris, promoting tissue repair, releasing neurotrophic factors and anti-inflammatory factors (IL-4, IL-6, IL-10, IL-13, IL-1RA, FIZZ1, and PPARγR) (Stansley et al., 2012, Neumann et al., 2009, Orihuela et al., 2016, Choi et al., 2017).

When there is no pathogen that activates the innate immune response microglia require “find me signals” to migrate within a lesion site. Some molecules released by cells at lesion sites elicit a specific response from microglia via their receptors: migration and activation, secretion of a plethora of cytokines, chemokines, and growth factors that stimulate a more damaging event before restoring the environment and stimulating brain repair.

One of these signals is ATP released from a damaged neuron, which is recognised by the purinergic receptor P2X4R and induces reactive microgliosis (Glezer et al., 2007, Napoli and Neumann, 2009, Zabala et al., 2018).

3.3.1 Lipids and membrane domain in microglia

Microglia morphology and functions are extremely affected by lipids compositions, in particular a changes in lipid rafts composition often lead to altered cells communications (Antonucci et al., 2012). In addition, evidence suggests that high cholesterol levels increase the expression of pro-inflammatory genes in microglia, whereas polyunsaturated fatty acids appear to have an anti-inflammatory effect on these cells (Indaram et al., 2015, Ebert et al., 2009).

In these cells, lipid rafts take part in multiple processes. In microglial cells, for instance, lipid rafts have been implicated in the induction of reactive oxygen species (ROS) by lysophosphatidylcholine (LysoPC), which leads to caspase-1 activation and subsequent IL-1β processing (Grassi et al., 2020). Other evidence of the involvement of lipid rafts in microglia is the interaction between a currently unknown receptor, ganglioside GM1, and the -syn protein, which results in the internalisation of α-synuclein (α-syn), a key player in the pathogenesis of Parkinson's disease (PD) Other evidence of the involvement of lipid rafts in microglia is the interaction between a receptor, for now, unknown receptor, ganglioside GM1 and the α-syn protein itself, that leads to the internalisation of α-synuclein (α-syn), a key player in the pathogenesis of Parkinson's disease (PD) (Park et al., 2009).

Microglia are structurally and metabolically regulated by caveolins, membrane adaptor proteins associated with lipid rafts. The transition between a resting phenotype and an immunoinflammatory phenotype has been linked to a change in caveolin isoform expression. Caveolin-1 (Cav-1) levels are low during the inactive state of cells, while caveolin-3 (Cav-3) levels are elevated. Cav-3 expression decreases concurrently with changes in cell morphology upon microglia activation, whereas Cav-1 expression increases. Cav-1 in these cells improves mitochondrial function and acts as a negative regulator of microtubule stability, and since lipid raft marker flotillin-1 levels increase concurrently with Cav-1 levels, it has been hypothesised that lipid rafts are involved in the regulation of the morphological changes associated with the inactive-active state transition (Niesman et al., 2013a).

3.3.2 Microglia in MS

In multiple sclerosis, the repair mechanism is ineffective, and the causes must be looked for primarily in the immune system and the individual's age. Macrophages and microglia play a crucial role in the removal of myelin debris, which contains factors that inhibit the differentiation of OPCs, and in the release of neurotrophic factors against OPCs (Neumann et al., 2009, Domingues et al., 2016).

In animal models of MS, such as experimental autoimmune encephalomyelitis (EAE), it is evident that microglia play a negative role by enhancing neuroinflammation, but it is also

known that microglia play a positive role (Miron et al., 2013, Colonna and Butovsky, 2017, Voss et al., 2012).

M1 and M2 phenotypes characterise MS and subsequent neurodegeneration. In MS, there is neuroinflammation, demyelination, removal of myelin debris, and remyelination; during these events, M1 pro-inflammatory phenotype changes to M2 anti-inflammatory phenotype (Neumann et al., 2009, Bogie et al., 2014). In this regard, we can identify four additional phenotypes: M1 is cytotoxic, M2a is activated and involved in repair and regeneration, M2b is immunoregulatory, and M2c is deactivating (Hirbec et al., 2019). These categorizations however are more related to in vitro experiment than in vivo, because as already described there exist multiple area-, disease- and phase-dependent phenotype (Ransohoff, 2016). In addition, these phenotypes coexist throughout the various stages of the disease, and it has been established that microglia has a dual function to induce inflammation as M1-like, which is neurotoxic and oligodendrocyte-damaging, and to reduce inflammation as M2-like, which is known to promote repair (Peferoen et al., 2015).

Since both microglia and macrophages are present in the CNS during diseases such as MS, one of the primary goals has been to characterise microglia in comparison to macrophages, with whom they share certain surface markers (F4/80+/CD11+). In humans and mice, transmembrane protein 119 (TREMM 119) was discovered to be expressed exclusively by microglia and not by macrophages (Chu, Shi et al. 2018). In addition, other microglial specific markers were identified: the transmembrane 9 lectin sialic acid-binding immunoglobulin-like lectin H (Siglec-H), and the purinergic receptor P2RY12 (Konishi et al., 2017, Timmerman et al., 2018).

The innate immunity triggering receptor expressed on myeloid cells 2 (TREM2), which functions as a lipid sensor and transmits intracellular signals to promote microglia fitness during ageing, and stimulate the ability to respond to prolonged demyelination, is essential to this process. In cuprizone-induced demyelination models in mice, it has been observed that microglia with low levels of this protein do not promote remyelination because they do not increase the expression of genes involved in phagocytosis and lipid metabolism (Poliani et al., 2015).

4. Human remyelination-promoting antibody rHIgM22

Regardless of the cause, MS research aims to find a therapy that could improve remyelination. The only FDA-approved drugs are symptomatic therapies that reduce inflammation by limiting pathology's progress. The first drug was fingolimod, and now there are many drugs with various targets. Fingolimod, an analogue of S1P, reduces inflammatory response by binding S1PR3 on the surface of T lymphocytes and inhibiting their migration; Moreover, it has been demonstrated that fingolimod can modulate resident glial cells, thereby enhancing remyelination (Halmer et al., 2014, Miron et al., 2010).

In any given scenario, the immune response is either the cause or effect of OL's death. This plays a significant role in the pathophysiology of MS; for example, clinically CFS of MS patients was enriched in various antibodies against myelin proteins: MBP, PLP, MAG, and MOG, which have been described as autoantibody targets in MS, and different sphingolipids, like anti glycolipid antibodies have been reported (Zamvil and Steinman, 1990, Steinman, 1993, Steinman et al., 1993, Steinman, 1995, Kerlero de Rosbo et al., 1993, Jaskiewicz, 2004, Meinl and Hohlfeld, 2002, Sela et al., 1982, Lubetzki et al., 1989, Bansal et al., 1994, Endo et al., 1984, Ilyas et al., 2003).

Increased anti-GD1a antibodies in MS sera may impair OPC maturation (Marconi et al., 2005). MS patients have a higher antibody response to sulfatides, and sulfatide levels are proportional to pathology progression, indicating that sulfatide is a prognostic factor for the onset and progression of MS (Kanter et al., 2006, Quintana et al., 2008, Moyano et al., 2013, Haghighi et al., 2013). Other studies have demonstrated how these antibodies interact with OLs to modify the membrane's sphingolipid composition, resulting in demyelination based on the extracellular matrix (ECM) protein content of the culture (Ozgen et al., 2014). These antibodies may play a role in the development of demyelinating diseases, but they may also be effective immunological treatment (Rodriguez et al., 2009).

Some new therapies include remyelination-promoting IgM antibodies. Remyelination-promoting IgMs target OLs and myelin antigens. They react to self-antigens and have a lower affinity than classic antibodies. These antibodies induce a calcium influx into astrocytes and OPCs (Paz Soldan et al., 2003).

The human monoclonal IgM antibody 22 (rHIgM22) is a recombinant antibody, isolated by screening the serum of a patient with Waldenström macroglobulinemia, a rare, low-grade cancer characterised by IgM-secreting clonal cells in the bone marrow (Dimopoulos et al., 2016b, Dimopoulos et al., 2016a). A phase I multicenter, double-blind, placebo-controlled study (NCT01803867) evaluating the safety, tolerability, pharmacokinetics, and immunogenicity of a single dose of rHIgM22 in clinically stable MS patients for at least three months has been completed. All participants continued disease-modifying MS treatments. In all study groups, fifty-five participants received rHIgM22 and seventeen received placebo. None of the dose levels studied showed dose-limiting toxicities or serious adverse events (Dulamea, 2017).

rHIgM22 binds specifically to myelin and induces calcium influx in OLs, thus promoting remyelination in mouse models of MS: Theiler's murine encephalitis virus (TMEV) model, experimental allergic encephalomyelitis (EAE) model, and lysolecithin-induced demyelination model (Mitsunaga et al., 2002); Binding of rHIgM22 is abolished in CNS tissue slices from CST-KO mice (this enzyme adds a sulphate group to the 3'-OH of galactose to produce sulfatide (Wright et al., 2009)), indicating that this antibody binds to myelin and OLs.

Literature suggests that rHIgM22's binding target may be DRM/lipid rafts and that its biological activity depends on lipid raft organisation (Wright et al., 2009, Howe et al., 2004).

Moreover, data obtained in our lab showed the involvement of different glycosphingolipids in rHIgM22 binding at the oligodendrocytes cell's surface, suggesting that reorganization of lipid membrane microenvironment might be relevant in its biological activity (Grassi et al., 2015, Grassi et al., 2023).

Although it is extremely promising as a remyelinating promoting therapeutics, its mechanism of action is not completely understood; it is not yet known how it acts , if directly on OLs or their precursors OPCs. Although it binds to the OLs selectively, only from a certain moment of differentiation in *in vitro* experiments (unpublished), in purified cultures of OLs there are no effects; However, if mixed glial cells cultures is treated with the antibody, the proliferation of all glial populations increase, among which the highest increase is found in astrocytes (Grassi et al., 2019a); rHIgM22 also induces a time-dependent increase of the PDGFα receptor (PDGFαR) in mixed glial cultures and this may stimulates OPCs proliferation in mixed glial cultures.

Enhanced extracellular release and intracellular synthesis of the bioactive sphingolipid S1P have also been observed; However, in the presence of an inhibitor selective for the PGFαR, only the release of S1P is unaffected. Regarding this event, no biosynthetic enzyme of S1P production, SK1 and SK2 are affected by rHIgM22 treatment (Grassi et al., 2019a).

Microglia are also directly influenced by rHIgM22 activity: *in vitro* experiments demonstrated an increase in phagocytosis following the binding of rHIgM22 to CNS myelin. Y. Zorina and her collaborators proposed a model to explain this increased phagocytosis: rHIgM22 binds myelin debris via the Fc domain and targets it for phagocytosis by microglia, which binds it via receptor 3 of the complement system (CR3), determining the opsonisation of the debris (Zorina et al., 2018). Therefore, based on the current state of knowledge, the pro-reparative effect of the rHIgM22 antibody is not only due to a selective action on OPCs and OLs, but rather involves all glial cell populations (Grassi et al., 2019a).

In pre-myelinating OLs, rHIgM22 promotes myelination independent of immunomodulation and anti-apoptotic signalling. rHIgM22 binds to CNS tissues like O4, an anti-sulfatide antibody (Howe et al., 2004).

rHIgM22 exerts its biological activity by inhibiting apoptotic signalling and differentiation in OPCs; Ca2+ influx, via CNQX-sensitive AMPA channels, is needed for the inhibition of apoptotic signalling pathways in TMEV mice and primary rat OLs. This is achieved by reducing caspase-3 and caspase-9 cleavage and altering caspase gene expressions (Howe et al., 2004, Watzlawik et al., 2010).

In addition, literature strongly suggests that the biological activity of rHIgM22, may require a multimolecular complex consisting of Lyn and the cell surface molecules integrin αvβ3 and PDGFαR (Watzlawik et al., 2010, Watzlawik et al., 2013a). These observations have led to the hypothesis that the pentameric structure of rHIgM22 could facilitate the clustering of a lipid antigen and stabilise lipid raft domains. In addition, it may be responsible for the reorganisation of Lyn, integrin αvβ3, and PDGFαR into a signalling complex that promotes OPCs survival and proliferation (Watzlawik et al., 2010, Wright et al., 2009). Signalling through this complex determines Lyn activation, followed by activation of the ERK ½ MAPK cascade, which inhibits caspase 3 and caspase 9 and OPCs differentiation, promoting OPCs proliferation (Watzlawik et al., 2013a, Watzlawik et al., 2013b). For rHIgM22-mediated inhibition of apoptotic signalling and differentiation in isolated OPCs, PDGF is required. Neurons and astrocytes produce PDGF, which promotes OPCs survival *in vivo* and *in vitro* by stimulating

OPCs proliferation. In fact, IgM-mediated OPCs proliferation is only detectable in cultures with significant numbers of astrocytes, microglia, and OPCs, thus mixed glial cultures, but not in purified OPCs cultures (Watzlawik et al., 2013a).

AIM OF THE STUDY

Multiple sclerosis (MS) is the most common demyelinating disease of the central nervous system (CNS), that primarily affects young adults. MS is a chronic inflammatory disease caused by an autoimmune attack. Currently, there is no cure for this disease; only disease-modifying therapies are available, mainly aimed at targeting the inflammatory component to slow disease progression (Lemus et al., 2018, Thompson et al., 2018).

MS is characterised by myelin loss due to oligodendrocyte death, followed by axon degeneration. Thus, myelin-forming oligodendrocytes are regarded as the main cell population involved in the disease. However, all glial cell populations are involved in diverse roles for proper myelin formation and, on the other hand, in the demyelinating process that characterises MS. Indeed, astrocytic gliosis and microglial activation are sustained in lesion sites, being associated with inflammation and alterations in blood-brain barrier (BBB) permeability (Lassmann, 2014, Karussis, 2014, Pearce, 2005, Domingues et al., 2016, Barres, 2008). However, activation of astrocytes and microglia can follow different patterns, and some of them are not detrimental to the disease's progression but rather exert protective effects.

At the early stages of MS, endogenous myelin-repair mechanisms are activated in acute inflammatory lesions, leading to some functional recovery and clinical remission. However, myelin repair mechanisms are not highly efficient, at least in humans, thus in general, the disease develops into a progressive form. Effective remyelination implies proliferation, recruitment, migration, and differentiation of OPCs, orchestrated by a variety of signals. On the other hand, several factors are hampering the myelin repair process, including astrocytic scarring as well as the presence of myelin debris at the lesion sites (Thompson et al., 2018, Podbielska et al., 2013).

Among all glial cells, microglia's role stands out. In physiological circumstances, microglia play multiple roles, including synapsis pruning (the removal of unnecessary synapses) and acting as a brain surveillant, sensing homeostasis, or polarising to become a pathogen scavenger in response to various insults. Microglia are activated in response to injury by undergoing morphological changes, becoming ameboid, with fewer and shorter processes, and migrating to the lesion site, releasing cytokines, neurotrophic factors, and acting as a phagocyte when required. The role of different microglia phenotypes can be detrimental, contributing to the progression of the disease; however, it can also be protective, facilitating the repair mechanisms. Following myelin damage, microglia in particular exert a fundamental and limiting effect by removing myelin debris, thereby facilitating the remyelination process

(Barres, 2008, Aguzzi et al., 2013, Napoli and Neumann, 2009, Neumann et al., 2009, Lloyd and Miron, 2019, Domingues et al., 2016).

Improving the efficiency of the endogenous myelin-repair mechanisms seems to be a valuable therapeutic approach to cure MS. Very promising in this sense is the treatment with the recombinant human antibody IgM22 (rHIgM22). This antibody has proven to effectively promote remyelination in different mouse models of chronic demyelination (Eisen et al., 2017, Warrington et al., 2000, Howe et al., 2004, Pirko et al., 2004). While it has been shown that rHIgM22 is able to bind selectively to myelin forming OLs and to induce anti-apoptotic signals in pre-myelinating OLs, some pieces of evidence suggest that its action seems to target other glial cells than OLs. Indeed, rHIgM22 stimulates microglia to proliferate and phagocytise myelin debris through the antibody F_C domain bound to myelin being recognised by complement receptor three (Zorina et al., 2018).

Data obtained in our laboratory demonstrated the involvement of diverse glycosphingolipids in rHIgM22 binding at the cell surface (Grassi et al., 2015, Grassi et al., 2023). Moreover, rHIgM22 treatment was able to induce changes in the sphingolipid pattern of oligodendroglial cells(S. Grassi et al. , 2021), suggesting that the reorganisation of the lipid membrane microenvironment may be involved in the biological activity of rHIgM22. Indeed, existing literature suggests also that the binding target of rHIgM22 could be associated with detergent-resistant membranes (DRM) or lipid rafts (Wright et al., 2009, Howe et al., 2004).

Because microglia play a significant role in the remyelination process, as they are the protagonists of an event that protects and promotes myelin repair, microglia have been the focus of this thesis.

Biochemical analyses of primary microglia (PM) are complex and expensive. Approximately 10% of the total glial cells in the nervous tissue are comprised of these cells (Soulet and Rivest, 2008), so isolation of microglia from mixed glial cells leads to a low yield.

On the other hand, the BV-2 cell line is widely used because it retains the morphological, phenotypic, and functional characteristics described for freshly isolated primary microglia and has functional markers of macrophages (Blasi et al., 1990). Moreover, Zorina Y. and colleagues (Zorina et al., 2018) analysed the effects of rHIgM22 in both PM and the BV-2 cell line and concluded that the effects were comparable. Consequently, all experiments were conducted on the BV-2 cell line.

The main purpose of this thesis was to determine whether the effect mediated by rHIgM22 in microglia was mediated by a mechanism of action similar to that observed in the oligodendroglial lineage, *i.e.*, by exerting changes in the sphingolipid patterns. However, the lipid composition of this cell population, under basal conditions, has never been reported, so the first focus of this PhD work has been to characterise the lipid composition of these cells.

BV-2 cells are an immortalised murine microglial cell line that grows semi adherent, where adherent and floating cells may represent two different sub-populations. Furthermore, it has been reported in the literature that culture conditions affect not only protein expression but also the composition of certain lipid classes (Frechin et al., 2015). Thus, the first analyses have been focused on characterising adherent and floating cells' culture features, and the expression of proteins supposedly involved in rHIgM22's mechanism of action in other glial cells. Then, the lipid patterns have been analysed with a combination of traditional chromatographic techniques and mass spectrometry analysis for selected lipid classes.

Since my preliminary data showed that sphingolipids are expressed at a low level in these cells, we optimised the application of a technique commonly employed in my laboratory to these cells: metabolic labelling experiments employing a tritiated sphingolipid precursor, allowing the detection of possible effects of the rHIgM22 antibody on the lipid profile of microglia with high sensitivity.

MATERIALS AND METHODS

MATERIALS

All reagents were of analytical grade. Ca^{2+} and Mg^{2+}-free HBSS, D-Glucose, BSA fraction V, HEPES, trypsin, sodium pyruvate, poly-D-lysine, PBS, Na_3VO_4, $MgSO_4$, DNase I, EDTA, trypan blue solution, methanol, chloroform, calcium chloride, were purchased from Sigma Aldrich (Darmstadt, Germany); penicillin/streptomycin, bovine foetal serum, RPMI1640, DMEM high glucose, and glutamine from *Euroclone* Spa (Pero, Milan, Italy). Membrane for dialysis Spectra/Por MWCO 12-14 kD were purchased from spectrumlabs.com.

Anti-integrin αV #60896; Anti-integrin β3 #4702; Anti-c-SrC #2109; Anti-AKT #9272; Anti-Lyn #2732; Anti Cav-1 Cell #3267 (D46G3); Anti β- actin #3700; goat anti-mouse or goat anti-rabbit horseradish peroxidase-linked secondary antibodies; all the antibodies described so far have been purchased from Cell Signalling Technology, Inc. (Danvers, MA, USA). Anti GAPDH immunological sciences MAB10578; Anti-Fyn Santacruz #4023 Anti PrP (SAF 32) Cayman No. 189720.

LiteABlot Plus and LiteABlot Turbo Chemiluminescent Substrate were purchased from *Euroclone* Spa (Pero, Milan, Italy). [1-^{3}H]sphingosine (radiochemical purity over 98%; specific radioactivity of 1.36 Ci/mmol) was prepared by specific chemical oxidation of the primary hydroxyl group of sphingosine followed by reduction with sodium boro[^{3}H] hydride as previously described (Prinetti et al., 2001). High performance thin layer chromatography (HPTLC) silica gel plates and solvents were purchased from Merck (Darmstadt, Germany). [^{3}H]-sphingomyelin, isotopically labelled at the sphingosine moiety, was synthesized and purified in our laboratories (Riboni et al., 1994).

Human IgM from human serum has been purchased from Sigma Aldrich.

rHIgM22 antibody was kindly provided by Acorda Therapeutics, Inc. (Ardsley, NY, USA) under a Research Agreement between University of Milano and Acorda Therapeutics (Prof. Alessandro Prinetti as the Principal Investigator).

METHODS

1. Cell cultures

1.1 BV-2 cell line

BV-2 cells, is a microglial cells line derived from C57BL/6 mouse brain, transformed by recombinant retrovirus (v-raf/v-myc). It was purchased from Cell Bank IRCCS AOU San Martino IST, Genova, Italy.

These cells are a continuous culture that grows semi-adherent and has a microglial morphology. This model expresses the nuclear v-myc and the cytoplasmic v-raf oncogene products as well as the env gp70 antigen at surface level. BV-2 cells have morphological, phenotypical and functional markers of macrophages (Blasi et al., 1990).

All the demonstrated experiments were conducted using a complete medium: RPMI 1640 medium (*Euroclone*) supplemented with 10% of heat-inactivated foetal bovine serum (*Euroclone*), 2 mM glutamine, 100 U/mL penicillin and 100 µg/mL streptomycin, at 37°C with 5% of CO2.

1.2 Astrocytes

Purified astrocytes were obtained from mixed glial cells (MGCs) using a modified version of the protocol from McCarthy and de Vellis (McCarthy and de Vellis, 1980). Briefly, MGCs were cultured for 8-10 days to allow the stratification of astrocytes and oligodendrocytes before being subjected to a shaking procedure (20 hours, 200 rpm). This procedure, which removes oligodendrocytes and microglia, was repeated three times, allowing a week to pass between each shaking. Astrocytic cell layers were then detached using trypsin-EDTA, plated on poly-D-lysine coated dishes and cultured for two weeks in DMEM high glucose containing 10% heat inactivated FBS, 100 U/mL penicillin, 100 µg/mL streptomycin, 1 mM sodium pyruvate, and 2 mM glutamine.

2. Growth curve

In each experiment, BV-2 cells were seeded at $1.5x10^4$ cells/cm^2 and $3x10^4$ cells/cm^2 in a 100Ø petri dish containing 10 mL of complete medium. Every 24 hours, n°1 p100 for each density was analysed by counting the number of cells in the Neubauer chamber and after adherent and floating cells were centrifuged at 3000 rpm for 10 minutes at 4°C. Following cell lysis with lysis buffer, protein concentration was determined using the DC assay protein kit (Biorad) described below.

3. Cells viability test with trypan blue dye

Upon reaching the confluence of 80-90%: the floating cells were collected and subjected to centrifugation 110 rpm, 10 min RT; The adhesive cells were detached from the support with EDTA 0.02% in PBS (3ml/ Flask T75, 3 minutes in incubator at 37°C with 5% CO2) and centrifuged 110 rpm, 10 minutes, RT. In both cases cells where resuspended in complete culture medium and an aliquot (20 µL) was mixed with an equal amount of Trypan blue dye. 10 µL of suspension was analysed in the Neubauer chamber. Cells were counted, blue coloured cells have been identified as dying or dead cells.

4. Lyophilisation

In order to continue with the lipid analysis, cells were lysed with H_2O following cells collection. To prevent deterioration, the samples were subsequently frozen in liquid nitrogen and subjected to the freeze-drying process overnight.

5. Total lipid extraction

Freeze-dried samples were subjected to lipid extraction.

Samples were resuspended with 50 µL of iced-cold H_2O and extracted with 1.5 mL of the solvent system $CHCl_3/CH_3OH$ (2/1) (v/v) and subjected to mixer at 1200 rpm for 20 minutes at 24°C and then centrifugation at 13200 rpm for 20 minutes at 24 °C. At the end the supernatant, composed by the total lipid extract was transferred to a new *Eppendorf* tube.

The obtained pellet was subjected to total lipid extraction twice time more using the same solvent system described, and then it was used to quantify protein as described below.

6. Two phase partitioning with modified Folch method

This process aims at separating the most hydrophobic lipids from the most hydrophilic lipids. The total lipid extracts were dried under nitrogen flow (N_2) and resuspended in a volume of 500 µL $CHCl_3$:CH_3OH 2:1 (v/v) and subjected to two-phase partitioning. Initially 20% of sample's volume, in water was added. Then the samples were placed in a thermomixer at 900 rpm for 20 minutes at 24°C and then centrifuged at 13200 rpm for 20 minutes at 24°C. After the procedure, two phase were obtained: the superior *aka* aqueous phase containing gangliosides and an organic phase containing all the other lipids. A second partitioning was performed on the organic phase, adding twice the volume added of water, of CH_3OH: H_2O 1/1 (v/v) and the protocol was repeated. At the end, both phases were dried under N_2 flow and resuspended in $CHCl_3$:CH_3OH 2/1 (v/v).

7. Alkaline methanolysis

This process aims at removing glycerophospholipids from the organic phase.

Organic phases were dried under nitrogen flow (N_2) and resuspended in 100 µL of $CHCl_3$, sonicated and vortexed, then it was added 100 µL of NaOH 0.6N in CH_3OH and samples were placed in a thermomixer at 600 rpm for 3 hours at 37°C. The samples were left 12h at least or overnight at room temperature. The reaction was blocked adding 120 µL of HCl 0.5 M in CH_3OH. 180 µL CH_3OH, 700 µL $CHCl_3$ and 170 µL H_2O were added to the samples, which were then placed in a thermomixer at 1100 rpm for 20 minutes at 24°C and then centrifuged at 13200 rpm for 20 minutes at 24°C. Two phase where obtained, the aqueous phase was not analysed.

8. Dialysis

This process is designed to remove salts and other impurities from aqueous phases that would otherwise interfere with HPTLC analysis. The aqueous phases were N_2 dried and then resuspended in ultra-distilled water. A glass beaker was filled with decarbonated water and membrane filters Spectra/Por (cut-off: 12-14 Kda) were placed at the upper end of the Eppendorf. The samples were placed on a floating support into the water in the beaker and left floating in agitation at 4 ºC for 48 hours. Every 24 hours ultra-distilled water was replaced. At the end of the process samples were lyophilised and resuspended in $CHCl_3$:CH_3OH 2/1 (v/v) for HPTLC analysis of ESI mass spectrometry Analysis.

9. Thin layer chromatography (TLC)

TLC was used to separate the lipids present in the aqueous and organic phases on a one-dimensional silica gel-packed glass plate.

The samples were seeded along an imaginary line 1.5 cm from the bottom edge of the plate, together with appropriate standards to enable the identification of individual bands based on their co-migration. The plate was then immersed in a pre-saturated chromatographic chamber containing a solvent system in volume such that the plate was not immediately immersed up to the imaginary line of 1.5 cm, allowing the separation of all the lipids contained in the sample rising for capillarity in a controlled manner.

Various solvent systems were used depending on the type of sample to be analysed:

- $CHCl_3$:CH_3OH:H_2O (chloroform-methanol-water) 110:40:6 (v/v/v) for general analysis of organic phase
- $CHCl_3$:CH_3OH:CH_3COOH:H_2O (chloroform-methanol-acetic acid-water) 30/20/2/1 (v/v/v/v) for phospholipids analysis
- $CH_3(CH_2)_4CH_3$:$C_4H_8O_2$ (*n*-hexane- ethyl acetate) 3/2 (v/v) for cholesterol analysis
- $CHCl_3$:CH_3OH:NH_3 (2N) (chloroform-methanol-ammonia) 70/30/3 (v/v/v) to separate neutral glycosphingolipids
- $CHCl_3$:CH_3OH:H_2O (chloroform-methanol-water) 70/25/4 (v/v/v) for sulfatide analysis
- $CHCl_3$:CH_3OH:$CaCl_2$ 0.2% (chloroform-methanol-calcium chloride) 55/45/10 (v/v/v) for ganglioside analysis in aqueous phase.

Then specific colorimetric sprays were applied:

- Anisaldehyde for general lipid detection

Anisaldehyde was prepared in the laboratory by mixing 0.5 ml 4-methoxybenzaldehyde with 50 mL glacial acetic acid and 1 mL of 97% sulphuric acid. The TLC was completely sprayed with the reagent, allowed to evaporate, slightly under the hood, and then put in the stove 20 minutes at 120°C. All the lipids present in the sample, and the standards, were shown in different colours according to their characteristics.

- Aniline for selective glycolipid detection

Aniline was prepared in the laboratory by mixing 4g of diphenylamine and 4 mL aniline in a mixture of 20 mL 85% phosphoric acid and 200 mL acetone. The TLC was slightly sprayed with the reagent and put in the stove 15 minutes at 20°C. Lipids of interest are highlighted by grey-green and blue colours.

- Cresyl violet for selective sulfatide detection

Cresyl Violet was prepared in the laboratory by mixing 0,01g of cresyl violet acetate with 50 mL of aqueous solution 1% acetic acid. TLC was immersed in the solution for 3-5 minutes to allow the red-violet staining of sulfatide and then rinsed with bleaching solution (30 mL aqueous solution 1% acetic acid with 10 mL methanol) to remove excess staining.

- Ehrlich reagent for selective detection of gangliosides

Ehrlich reagent was prepared in the laboratory by mixing 1.5 g of p-dimethylaminobenzaldehyde with 200 mL ethanol and 50 mL 37% hydrochloric acid. The TLC was sprayed with the reagent and then, rapidly covered, above and below, with glasses previously heated to 120°C, and in the end placed in the stove for 20-30 minutes at 120°C.

- Phosphorus reactive for selective phospholipid detection

Phosphorus reactive spray was prepared in the laboratory by mixing a 1st solution (16 g ammonium molybdate in 120 mL water) with a 2nd, filtered, solution (80 mL 1st solution, 40 mL of 37% hydrochloric acid and 10 mL mercury) and 200 mL sulphuric acid; at the

end the final solution was make up to the final volume of 1 L with water (Vaskovsky and Kostetsky, 1968).

10. Protein quantification

10.1Protein quantification for lipids analysis

The sample analysed is the pellet obtained after total lipid extraction, digested over-night with NaOH 1N.

The protein quantification was performed through DC assay (*Bio-Rad*). The assay was performed in 96 well plates following the protocol supplied with the *Bio-Rad* DC assay kit. The samples, diluted to NaOH 0.05N, were analysed in triplets, like the protein standard, bovine serum albumin (BSA in NaOH 0.05N), at different concentrations. 25 µL reagent A and 200 µL reagent B, both supplied with the kit, were added to each well. After 15 minutes of incubation, the absorbance at 750 nm was measured with the spectrophotometer. The samples readings were compared with the ones of the standard.

10.2Protein quantification for protein expression

The sample analysed is a cells lysate in Lysis Buffer (LB) composed by 10 mM Tris-HCl pH 7.5, 150 mM NaCl, 5 mM EDTA, 1 mM Na_3VO_4, 1 mM PMSF, 75 mU/mL aprotinin.

The protein quantification was performed through DC assay (*Bio-Rad*). The assay was performed in 96 well plates following the protocol supplied with the *Bio-Rad* DC assay kit. The samples were analysed in triple, like the protein standard, bovine serum albumin (BSA in LB), at different concentrations. 25 µL of reagent A+S and 200 µL of reagent B, both supplied with the kit, were added to each well. Reagent A+ S is made at the moment of use: every 1 mL of reagent A, 25 µL of reagent S are added. After 15 minutes of incubation, the absorbance at 750 nm was measured with the spectrophotometer. The samples readings were compared with the ones of the standard.

11. Mass spectrometry analysis

The cells collected at optimal confluence (80-90 % of confluence) or in over-confluence were lysed in water, lyophilized, subjected to total lipid extraction and two-phase partitioning as described previously. Organic and aqueous phase where subjected to alkaline methanolysis and dialysis, respectively. Equal amount of dialysed aqueous phase of both adherent and floating cells collected at optimal confluence (equivalent to 1 mg of protein) and different amount of adherent cells (equivalent to 6.3 mg of protein) and floating cells (equivalent to 7.2 mg of protein) from cells collected in over-confluence were analysed through ESI negative mass spectrometry to characterize ganglioside. Equal amount of methanolized organic phase from adherent and floating cells (equivalent to 1 mg of protein) collected at 80-90 % of confluence were analysed through ESI positive mass spectrometry to characterize Cer, SM and neutral GLs molecular species.

This analysis was conducted through UNITECH OMICs (University of Milan, Italy) using ExionLC AD system (SCIEX) connected to TripleTOF, 6600 System (SCIEX) equipped with Turbo V, Ion Source with ESI Probe.

The samples were separated on Kinetex EVO C18 – 2.1 x 100 mm, 1.7µm (Phenomenex) as mobile phase A, water: acetonitrile (60:40) and as mobile phase B, 2-propanol: acetonitrile (90:10), both containing 10 mM ammonium acetate and 0.1% formic acid. The flow rate was 0.4 mL/min, and the column temperature was set at 45°C. The elution gradient was set as below: 0–2 min (45% B), 2–12 min (45–97% B), 12–17 min (97% B), 17–17.10 min (97–45% B), and 17.10–20 min (45% B).

- Aqueous phase over confluent: MS spectra were collected over the m/z range of 300-2000 Da in negative polarity, operating in PIS (Product Ion Scan). The collision energy has been set to -90 (CES 20).
- Aqueous phase 80-90 % of confluence: MS spectra were collected over an m/z range of 350-2500 Da in negative polarity, operating in IDA® mode (Information Dependent Acquisition). Collision energy was set at -70 (CES 20).
- Organic phase 80-90% of confluence: MS spectra were collected over an m/z range of 140-2000 Da in positive polarity, operating in IDA® mode (Information Dependent Acquisition). Collision energy was set at 35 (CES 15).

Data processing was conducted using MS-DIAL software.

12. Electrophoresis and western blot analysis

Adherent and floating cells separately were lysed with lysis buffer (10 mM Tris-HCl pH 7.5, 150 mM NaCl, 5 mM EDTA, 1 mM Na_3VO_4, 1 mM PMSF, 75 mU/mL aprotinin).

To evaluate Integrin αV-β_3, Lyn, Fyn, c-Src, PDGFαR, Cav-1, AKT and PrP (SAF32) expression, the samples were analysed using electrophoresis on a polyacrylamide gel in denaturing conditions. The samples were suspended in *Laemmli buffer* (1x: 62.5 mM Tris-HCl pH 6.8, 2% SDS, 5% 2-mercaptoethanol, 0.01% Bromophenol blue, 10% glycerol) and boiled for 5 minutes at 100°C before being analysed.

The electrophoresis run was performed using a Mini protean II unit, produced by *Bio-Rad*. To obtain optimal resolution, a stacking gel was polymerized on top of the resolving gel. A solution of 25 mM Tris, 192 mM glycine, 0.1% SDS, pH 8.3 was used as *running buffer*. The proteins were separated using 10% polyacrylamide gels.

After electrophoresis separation, proteins were transferred to polyvinylidene difluoride (PVDF) membranes, at 200 mA, 3 hours at 4°C with a wet blotting (*Bio-Rad*). The transfer buffer used was *Blotting buffer* 1x (25 mM Tris-HCl, 192 mM glycine, 15 % methanol, pH 8.0-8.5).

In order to evaluate Integrin αV-β_3, Lyn, Fyn, c-Src, PDGFαR, Cav-1, AKT expression, the membranes after transfer, then blocked with 5% milk in TBS with 0.05%-Tween20, incubated overnight with Integrin αV (1:1000), anti-Integrin β_3 (1:1000), Lyn (1:1000), Fyn (1:1000), c-Src (1:1000), PDGFαR (1:500), Cav-1 (1:1000), AKT (1:1000) and anti-PDGFαR (1:500) primary antibodies diluted in BSA 5% in TBS with 0.05%-Tween20 and finally with a goat anti-rabbit horseradish peroxidase-linked secondary antibody (1:5000) for all except PDGFαR, for which the goat anti-rabbit horseradish peroxidase-linked secondary antibody was 1:2500.

In order to evaluate PrP (SAF32), GAPDH and β-actin expression, the membranes after transfer were blocked with 3% milk in TBS with 0.05%-Tween20, incubated overnight with anti-PrP (SAF32) (1:2000), anti GAPDH (1:1000) and anti-β-actin (1:1000) in BSA 1% in TBS with 0.05%-Tween20, and finally with a goat anti-mouse horseradish peroxidase-linked secondary antibody (1:3000).

Bound antibodies were visualized by ECL (LiteABlot Plus and LiteABlot Turbo Chemiluminescent Substrate). For quantitative measurements, membranes were acquired by

UVITEC Cambridge technology (*Eppendorf*). Image analysis was performed using NINE Alliance software.

13. Metabolic labelling experiment to assess sphingolipids turnover

To observe quantitatively and qualitatively the variation of the sphingolipid pattern at different time, cells were seeded to the density 1.5 $x10^4/cm^2$ in petri dishes of 100 Ø, each with 10 mL of complete medium.

- 24 hours after seeding, cells that were to be analysed at 48 h of chase were fed with [1-^{3}H] sphingosine at a concentration of 3.68 x 10^{-8} mol/L, which does not involve biological activity. Therefore, this administration of [1-^{3}H] sphingosine does not change the viability and morphology of the treated cells. After two hours of feeding (pulse), the medium was removed and its radioactivity quantified, and the medium was replaced with new complete medium without [1-^{3}H] sphingosine for 48 hrs of chase. During pulse period cells incorporate radioactive sphingosine efficiently and during chase period they acylate the tritiated precursor to form ceramide and other complex sphingolipids.
- 48 hours after seeding, cells that were to be analysed at 24 hours of chase, were fed with [1-^{3}H] sphingosine at a concentration of 3.68 x 10^{-8} mol/L for two hours, then the medium was removed, and its radioactivity quantified, and was replaced with new complete medium without [1-^{3}H] sphingosine for 24 hrs of chase.
- 60 hours after seeding, cells that were to be analysed at 12 hours of chase, were fed with [1-^{3}H] sphingosine at a concentration of 3.68 x 10^{-8} mol/L for two hours, then the medium was removed, its radioactivity quantified, and then was replaced with new complete medium without [1-^{3}H] sphingosine for 12 hrs of chase.

At all-time points, cells were collected at 80-90 % of confluence on ice. Floating cells were obtained by centrifuging at 3000 rpm for 10 minutes, 4°C. Adherent cells were detached with PBS and Na_3VO_4 1mM, centrifuged at 3000 rpm for 10 minutes at 4°C. At the end adherent and floating cells, separately, were lysed with water.

Due to this protocol all sphingolipids were radioactively labelled and analysed through HPTLC and submitted to digital autoradiography (*TRacer Beta-Imager*, *Biospace,* Paris, FR). All radioactive sphingolipids were quantified by M3 Vison software (*Biospace*, Paris, FR).

14. Metabolic labelling experiment and treatment with antibodies

14.1 Effects of rHIgM22 of sphingolipids pattern of cells collected in over-confluence

To observe quantitatively and qualitatively the effect of rHIgM22 on the sphingolipid pattern, cells were seeded to the density $3x10^4/cm^2$ in petri dishes of 100 Ø, each with 10 mL of complete medium. 24 hours post seeding, cells were fed with [1-^{3}H] sphingosine at a concentration of 3.68 x 10^{-8} mol/L. After two hours of feeding (pulse), the medium was removed and its radioactivity quantified, and the medium was replaced with new complete medium without [1-^{3}H] sphingosine for 48h of chase. After the first 24h of chase, 24 hours treatment with 10 µg/mL of rHIgM22 or control IgM was conducted. Cells were collected in over-confluence on ice. Floating cells were obtained by centrifuging medium after chase at 3000 rpm for 10 minutes, 4°C. Adherent cells were detached with PBS and Na_3VO_4 1 mM and centrifuged at 3000 rpm for 10 minutes at 4°C. Adherent and floating cells separately, were lysed with water.

Due to this protocol all sphingolipids were radioactively labelled and analysed through HPTLC and submitted to digital autoradiography (^{T}Racer Beta-Imager, Biospace, Paris, FR). All radioactive sphingolipids were quantified by M3Vison software (Biospace, Paris, FR).

14.2 Effects of rHIgM22 of sphingolipids pattern of cells collected at 80-90% of confluence at steady state metabolic labelling settings

To observe quantitatively and qualitatively the effect of rHIgM22 on the sphingolipid pattern, cells were seeded to the density 1.5 x10^4/cm^2 in petri dishes of 100 Ø, each with 10 mL of complete medium.

60 hours post seeding, cells that were to be analysed at 48 hrs of chase were fed with [1-^{3}H] sphingosine at a concentration of 3.68 x 10^{-8} mol/L. Therefore, this administration of [1-^{3}H] sphingosine does not change the viability and morphology of the treated cells. After two hours of feeding (pulse), the medium was removed and its radioactivity quantified, and the medium was replaced with new complete medium without [1-^{3}H] sphingosine for 12h of chase. During chase time 12 hours treatment with 10 µg/mL of rHIgM22 or control IgM was conducted. Cells were collected at 80-90% of confluence, on ice. Floating cells were obtained by centrifuging medium after chase at 3000 rpm for 10 minutes, 4°C. Adherent cells were detached with PBS and Na_3VO_4 1 mM, and then centrifuged at 3000 rpm for 10 minutes at 4°C. Adherent and floating cells, separately, were lysed with water. Due to this protocol all sphingolipids were radioactively labelled and analysed through HPTLC and submitted to digital autoradiography (^{T}Racer Beta-Imager, *Biospace*, Paris, FR). All radioactive sphingolipids were quantified by M3Vison software (*Biospace*, Paris, FR).

15. Statistical analysis

Experiments were run in triplicate, unless otherwise stated. Data are expressed as mean value ±SD and were analysed by Student-T test.

RESULTS

1. Characterization of BV-2 cell line

The BV-2 cell line is a widely used microglial model instead of primary microglia because it retains the morphological, phenotypical, and functional properties described for freshly isolated primary microglia (Blasi et al., 1990). In the literature, there are more than four thousand articles about BV-2 cells, a murine immortalised microglia cell line. However, under basal conditions, *i.e.,* when no activating stimulus is applied, little information is found for this cell line.

BV-2 cells are round, and small (10-15 µm Ø) (Gibson et al., 2012), when cultured in a complete medium, 10% FBS, under basal conditions.

The BV-2 cell line is a semi adherent cell culture, in which both adherent and floating cells are always present when kept in culture. To assess whether floating cells were partially dead cells, we evaluated the viability of the floating cells using the trypan blue exclusion method. The test showed that floating cells are, on average, 94% alive (**Table 1**). Since adherent cells are used to maintain and expand the culture, we assumed that they were alive, at least to a greater extent than 98 percent; thus, their vitality has not been evaluated.

Viability of floating cells			
	Vital	Dead	% Of viability
Cells number (x 10^4)	407.5	32.5	92.6
	287.5	10.0	96.6
□	347.5	213.0	94.2

Table 1 ***Viability of BV-2 floating cells.*** *Floating cells were collected, centrifuged at 1100 rpm, 10 minutes and then cells were counted in Neubauer chamber using trypan blue as a discriminating dye between living and dead or dying cells. Cell's membrane of dead or dying cells is no longer preserved, allowing the dye to enter cells, and turning them blue.* No *statistical analysis were available, further experiments are needed .*

Two different situations of confluence were analysed, characterising the specific features of both adherent and floating cells, sub-populations of this microglial cell line.

BV-2 cells replicate rapidly. They achieve the optimal confluence for analysis in 72 hrs when seeded at a density of $1.5x10^4$ cells/cm^2 after this time they grow over-confluent; if, on the other hand, BV-2 cells are seeded at twice the density described, they reach over confluence

in 72h. To better characterise BV-2 growing conditions, two growth curves of BV-2 cells, differing in seeding density, were performed. Every 24 hours after seeding, until reaching over-confluence for each seeding density, cells were collected, counted in the Neubauer chamber, and after lysis, their protein content was quantified. The growth curves of cells seeded at $1.5x10^4/cm^2$ (panel a) and $3x10^4/cm^2$ (panel b) are shown in **Figure 1**. Both curves derive from the number of cells collected every 24 hours from each subpopulation.

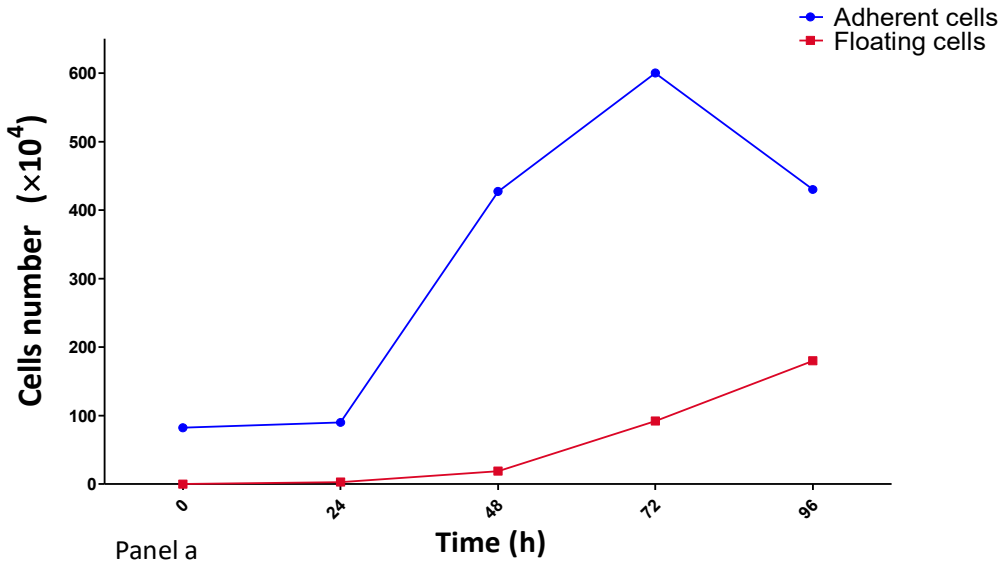

Panel a

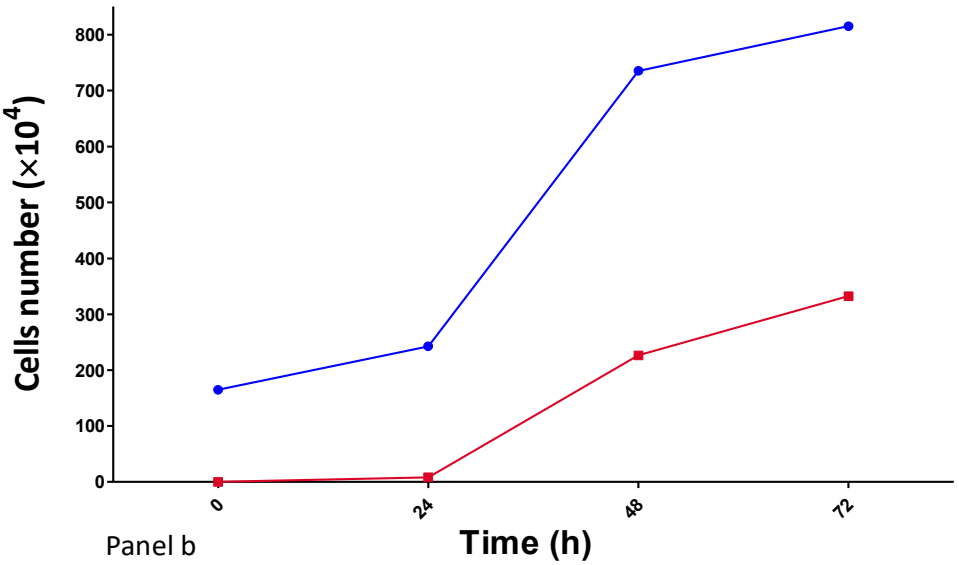

Panel b

Figure 1 *(**Panel a)** **Growth curve of BV-2 cells seeded at 1.5x10^4/cm^2**. BV-2 cells were seeded at 1.5x10^4/cm^2 into five petri dish 100Ø. Every 24h after seeding, adherent and floating cells were detached or collected, respectively, and counted in Neubauer chamber. Afterwards the protein content was quantified. The experiment was conducted three times. **(Panel b) Growth curve of BV-2 cells seeded at 3x10^4/cm^2.** BV-2 cells were seeded at 3x10^4/cm^2 into four petri dish 100Ø. Every 24h after seeding, adherent and floating cells were detached or collected, respectively, and counted in Neubauer chamber. Afterwards the protein content was quantified. The experiment was conducted once.*

Regarding the two confluence states, after 72 hours of culturing, adherent and floating cells are differently distributed for each seeding density. Similarly, also the protein content varies between adherent and floating depending on the confluence considered. In case of cells seeded at 1.5x10^4 cells/cm^2 after 72 hrs, proteins are divided into 80% and 20% for adherent and floating cells, respectively, whereas for cells seeded at 3x10^4 cells/cm^2 proteins are divided into 56% and 44% for adherent and floating cells, respectively (**Table 2**).

Protein content of BV-2 cells 72h after seeding					
	seeding density	**Sample**	**Cells number (%)**	**protein (mg)**	**protein (%)**
optimal confluence	1.5x10^4	Adherent cell	86.2 ± 2.0	1.2 ± 0.6	79.7 ± 9.1
		Floating cells	11.8 ± 2.0	0.3 ± 0.2	20.3 ± 9.1
over-confluence	3x10^4	Adherent cell	71.0	1.1	55.9
		Floating cells	29.0	0.9	44.1

***Table 2** **BV-2 Protein content 72h after seeding.** BV-2 cells were seeded at 1.5x10^4/cm^2 and 3x10^4/cm^2 reaching optimal confluence or over-confluence in 72h, respectively. Adherent and floating cells were detached or collected, respectively, and counted in Neubauer chamber. Afterwards the protein content was quantified. The Statistical analysis, expressed as mean value with ± SD, were performed only for samples of cells collected at optimal confluence; for cells collected in over confluence are necessary further experiments to gain statistical data.*

72 hours are required for cells seeded at a density of $3x10^4/cm^2$ to attain over-confluence, and even though the protein content varies depending on the confluence reached, in over-confluence it must be considered that floating cells may potentially consist of adherent cells that have detached from their support due to a shortage of area.

BV-2 cells were found to be responsive to rHIgM22 (Zorina et al., 2018), even if the exact mechanism in these cells is still unknown. However, literature suggests that rHIgM22 antibody effects on oligodendrocyte precursor cells (OPCs) are mediated by the recruitment and activation of a multimolecular complex formed by Lyn, integrin αvβ3 and PDGFαR, promoting OPCs' survival and proliferation (Watzlawik et al., 2013a).

Thus, we assessed the expression levels of these proteins and of other proteins possibly involved in the formation of similar signalling complexes in BV-2 cells. Expression levels were compared between adherent and floating cells.

Together with the kinase Lyn, directly involved in the multi-molecular complex recruited by rHIgM22 in OPCs, the levels of other kinases of the Src family, Fyn and c-Src, were also analysed (Watzlawik et al., 2010).

In addition, the expression of caveolin-1 (Cav-1), a membrane adaptor protein enriched in lipid rafts, that has been identified as a structural and metabolic regulator of microglia, was evaluated (Niesman et al., 2013b). It has been shown that the expression of the caveolins, both isoforms 1 and 3, changes in microglia, when passing from a patrolling state to an active state. In the patrolling state microglia express at high levels Cav-1 and at low levels Cav-3 while in the activated state the expression levels of the two isoforms are inverted (Niesman et al., 2013b).

Moreover, the expression of PrP, a GPI anchored protein usually regarded as a lipid raft marker, involved in many cellular functions such as cell proliferation, cell signalling, and protection against stress (Legname, 2017, Linden, 2017), and AKT, or protein kinase B, a non-raft marker and a fine regulator of cells' survival, proliferation, and metabolism (Song et al., 2005), were evaluated.

For all of the antigens examined, which are present in both sub-populations, adherent cells appear to have a slightly higher expression than floating cells; however, these differences are very small, and the analysis was conducted on a small number of samples, insufficient to gain statistical significance for the data, so the results of this analysis must be considered qualitative (**Figure 2**).

As shown in Figure 2, western blot analysis revealed that all the antigen examined are expressed at similar levels in both sub-populations, except for Integrin β_3 and the kinase c-Src that are more expressed in adherent cells.

Very interestingly, our results indicated the absence of PDGFα receptor expression in both sub-populations under basal conditions (**Figure 2**). PDGFαR is indeed one of the main components of the multimolecular complex recruited by rHIgM22 in OPCs. Thus, the lack of expression of this receptor suggests that the effect of rHIgM22 on microglia might be mediated by a completely different molecular mechanism. Also interesting is the absence of Cav-1 in BV-2 cultured in a complete medium under basal conditions (**Figure 2**).

***Figure 2* Antigen expression of BV-2 cells seeded at 1.5x10^4/cm^2.** *Cells were seeded at 1.5x10^4/cm^2, after 72h they were collected and lysed in lysis buffer (as described in Materials and Methods). Adherent and floating cells were analysed separately. The same amount of protein (20 µg) for all samples (except for those used to assess the expression of PDGFαR (80 µg) and AKT (50 µg)) were separated by SDS-PAGE (10%) and transferred onto PVDF membranes. Membranes were probed by western blotting using specific antibodies for the antigen shown and then normalized with housekeeping genes anti-GAPDH/anti-b-actin antibodies.*

Integrin α_V (135-140 KDa)

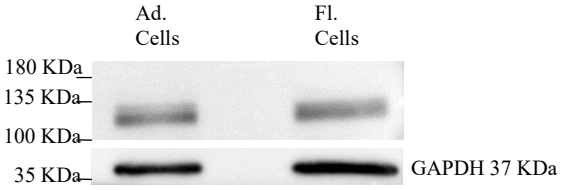

Integrin β_3 (97-110 KDa)

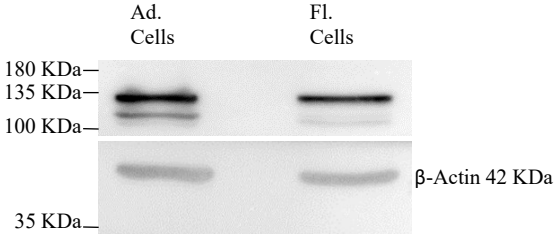

PDGFαR (190 KDa)

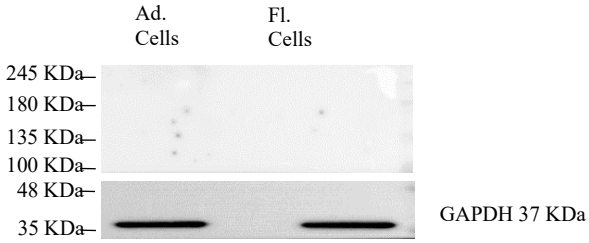

Lyn (60 KDa)

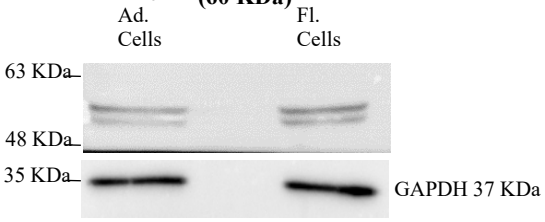

c-Src (60 KDa)

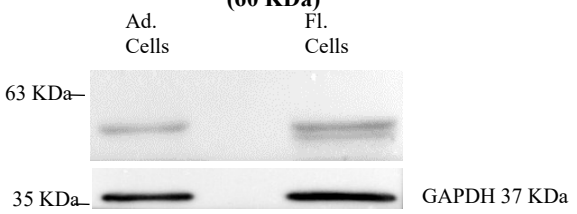

Fyn (59 KDa)

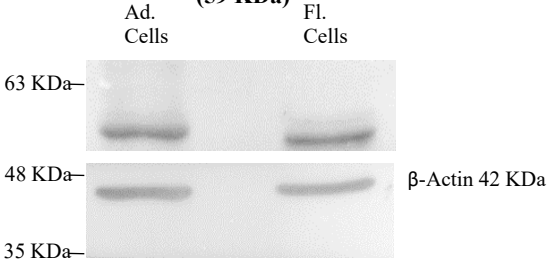

Cav-1 (21 KDa)

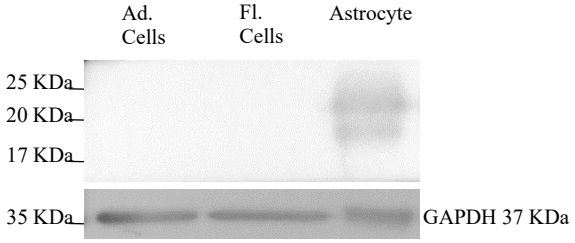

AKT (60KDa)

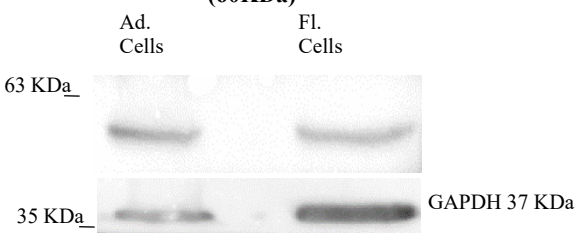

PrP (Saf32) (30-15 KDa)

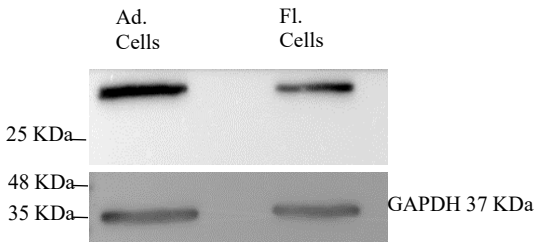

2. Analysis of endogenous lipids in BV-2 cells

It is well known that the lipid composition of cultured cells differs depending on whether cells are growing in a high- or low-crowding area (Frechin et al., 2015). In vitro, the available growth area affects the viability, proliferation, and adhesion of cells, as well as the reorganisation of the cell membrane, cytoskeleton, and adhesion mechanism. These events, referred to as “contact inhibition” and “local cell crowding” (Puliafito et al., 2012, Frechin et al., 2015) are characterised by changes in the expression of autophagic marker genes, focal adhesion kinases (FAK), and pathways associated with MAPK and mTOR signalling (Trajkovic et al., 2019).

Notably, FAK expression varies between high-density and low-density cell crowding, influencing cell homeostasis via ABC transporters, one of which, ABCA1, is directly associated with the reorganisation of membrane lipids (Frechin et al., 2015). Considering these findings, the pattern of membrane lipids in the two previously described states of confluence was investigated.

BV-2 cell lipids were analysed by thin layer chromatography (TLC) and ESI-mass spectrometry (ESI-MS) to characterise any lipid differences between cells collected at optimal (80-90% of confluence) or over confluence.

2.1 Analysis of endogenous lipids from cells collected at optimal confluence

BV-2 cells were seeded at a density of 1.5 x 10^4 cells/cm^2; once optimal confluence was reached, floating cells were harvested, and adherent cells were detached. Samples were processed as described in Materials and Methods. To identify each class of lipids in BV-2 cells, the organic and aqueous phases obtained were analysed by TLC using specific solvent systems and colorimetric assays.

The more hydrophobic lipids, such as phospholipids, cholesterol, sphingolipids, and glycosphingolipids, are found in organic phases, whereas the more hydrophilic lipids, *e.g.,* gangliosides, are found in aqueous phases.

1.1.1 Analysis of phospholipids

The specific analysis of phospholipids via TLC using the solvent system $CHCl_3$: CH_3OH: CH_3COOH: H_2O (30/20/2/1) (v/v/v/v) and the colorimetric assay for phosphorus, shown in (**Figure 3**) enabled us to identify a very distinctive characteristic of this cell line. BV-2 cells are enriched in phosphatidylcholine (PC). Indeed, densitometric analysis confirms that PC is the predominant phospholipid in both adherent and floating cells, without identifying differences between the two sub-populations for this or the other phospholipids (**Table 3**).

Although PC is the predominant phospholipid in the brain (Choi et al., 2018), as in many other tissues, this result is highly relevant when compared to other glial populations, such as oligodendrocytes, where phosphatidylethanolamine (PE) is the predominant phospholipid (Fressinaud et al., 1990) .

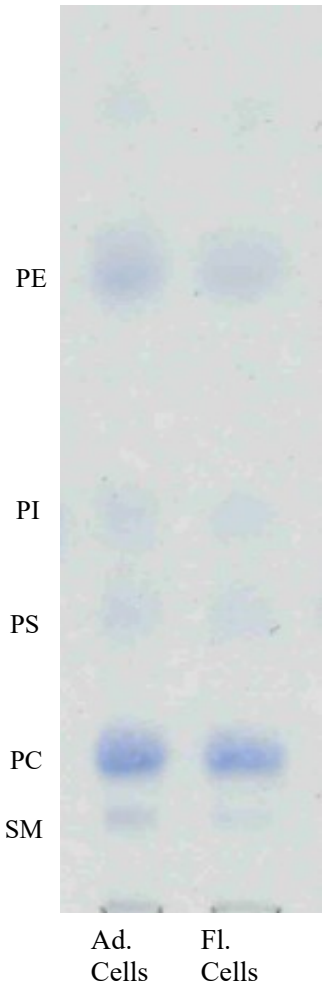

<u>Figure 3</u> ***Analysis of phospholipids in organic phase of cells collected at optimal confluence.*** *BV-2 cells were seeded at 1.5x10^4/cm^2 and, after 72 h, samples were processed as described in Materials and Methods. Equal amounts of organic phase (equivalent to 400 µg of protein) from adherent and floating cells were analysed via HPTLC with the $CHCl_3$: CH_3OH: CH_3COOH: H_2O (30/20/2/1) (v/v/v/v) and the colorimetric assay phosphorus reactive spray for phospholipids (Vaskovsky V.E., Kostetsky (1968).*

Phospholipids			
Optimal confluence			
% Of total			
Lipid	**Adherent cells**	**Floating cells**	***p***
PE	27.9 ± 0.6	22.4 ± 5.2	0.611
PC	39.0 ± 12.0	35.0 ± 7.7	0.300
SM	17.9 ± 10.9	22.2 ± 5.1	0.637

Table 3 ***Densitometric analysis of phospholipids present in the organic phase of BV-2 cells collected optimal confluence.*** *Thin-layer chromatography-based densitometric analysis of phospholipids in the organic phase (**Figure 3**). The data derive from three distinct experiments involving optimally confluent cells. ImageJ software was used to conduct the densitometric analysis. The values displayed are in arbitrary units ±SD calculated using an unpaired t-test.*

Normally, in the brain, phospholipids are lower in percentage compared to those present in other organs (heart, kidney, and liver), indeed, phospholipids are estimated to be 60% of total lipids, whereas in other organs represent 90% (Choi et al., 2018).

Although PC is the most abundant phospholipid in the brain, the discovery is noteworthy when considering other glial cells, such as oligodendrocytes, in which PE is the predominant phospholipid (Fressinaud et al., 1990).

1.1.2 Analysis of cholesterol

Cholesterol is a hydrophobic lipid that is highly abundant within membranes; it serves the crucial function of stabilising all the other lipids within the two leaflets, thereby regulating their fluidity (Sonnino and Prinetti, 2010).

Unlike other lipids, quantitative TLC analysis can be performed to easily determine the concentration of cholesterol in a sample using cholesterol standards at known concentrations. Indeed, it has been determined that both sub-populations of BV-2 contain the same amount of cholesterol, which can be expressed as nmol/mg of protein (**Figure 4**).

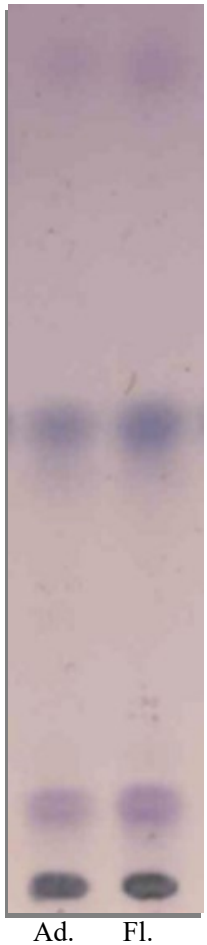

Cholesterol nmol/mg		
Cells collecting conditions	**Adherent cells**	**Floating cells**
optimal confluence	18.3 ± 5.6	18.6 ± 5.8

***Figure 4* Cholesterol analysis in organic phase of BV-2 cells collected at optimal confluence**. *BV-2 cells were seeded at 1.5x10^4/cm^2. After 72 hours, samples were processed as described in Materials and Methods. Using the solvent $CH_3(CH_2)_4CH_3$:$C_4H_8O_2$ (n-hexane-ethyl acetate)(3:2) (v/v) and the colorimetric assay anisaldehyde reactive spray, an equal amount of organic phase (equivalent to 90 µg of protein) from adherent and floating cells was analysed by TLC. Three distinct analyses were conducted with optimally confluent cells. NINE Alliance software was used to conduct the densitometric analysis.*

1.1.3 Analysis of sphingolipids

Sphingolipids (SL) are a class of lipids formed by a backbone of sphingosine or sphinganine, namely a sphingoid backbone that also functions as a hydrophobic tail; when combined with an acyl chain, they form the simplest SL, ceramide (Cer). The addition of an head group to Cer leads to the formation of more complex sphingolipids, such as sphingomyelin (SM) and glycosphingolipids (GSLs), that are divided into neutral, acidic, or sulphated (Merrill, 2011).

Based on their physico-chemical properties, SLs can be either hydrophilic or hydrophobic. Cer, SM, neutral GLS, and sulfatide are the most hydrophobic SLs, whereas gangliosides are the most hydrophilic.

Using a two-phase partitioning (as described in Materials and Methods), it was possible to separate the more hydrophobic SLs in the organic phase and the highly hydrophilic gangliosides in the aqueous phase. All described lipid classes were analysed using thin-layer chromatography and mass spectrometry. Each analysis was conducted on three distinct experiments, unless otherwise specified.

In all the organic phase analysed by TLC, there are bands co-migrating with the standards of Cer, glucosylceramide (GlcCer), PE, lactosylceramide (LacCer), lysophosphatidylcholine (LysoPC), PC, and SM (**Figure 5**). For all lipids identified in the organic phase that were analysed with the solvent system $CHCl_3$: CH_3OH: H_2O (chloroform: methanol: water) (110/40/6) and the colorimetric assay anisaldehyde, which detects all lipids non-specifically, a densitometric analysis was performed (**Table 4**), demonstrating changes in the distribution of two SLs, Cer and SM.

In order to obtain more quantitative information and to analyse the different molecular species for each lipid, mass spectrometry analysis was also conducted for some lipid classes, as detailed below.

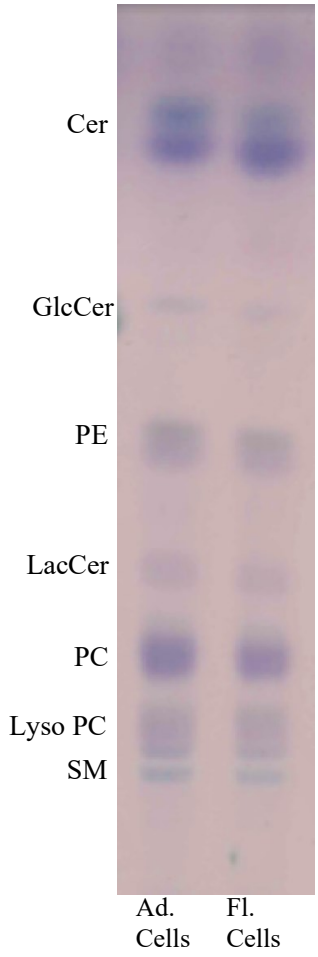

Figure 5 ***Organic phase of BV-2 cells collected at optimal confluence****. BV-2 cells were seeded at 1.5x10^4/cm^2 . After 72 hours, samples were processed as described in Materials and Methods. Equal amounts of organic phase (equivalent to 150 µg of protein) from adherent and floating cells were analysed via TLC using the solvent system $CHCl_3$: CH_3OH: H_2O 110/40/6 (v/v/v) and the anisaldehyde reactive spray colorimetric assay.*

1.1.3.1 Ceramide and sphingomyelin

Densitometric analysis of each lipid present in the organic phase subjected to TLC analysis revealed some quantitative differences between the two sub-populations (**Table 4**); Significantly higher Cer levels were found in floating cells than adherent cells, suggesting the hypothesis that floating cells are in a different activation status and perhaps in a pre-apoptotic condition. SM is significantly more prevalent in adherent cells than in floating cells.

Mass spectrometry analysis was performed on the organic phase subjected to alkaline methanolysis (as described in Materials and Methods). In fact, even though thin-layer chromatography is a well-established method, it has limitations in the detection of extremely rare lipid species as well as in the detection of different molecular species. Mass spectrometry is an analytical method capable of ionising atoms and/or molecules, separating them, and detecting them as gaseous ions based on their mass/charge ratio (m/z), hence revealing the structure of unknown molecules present in a sample. The advantage of mass spectrometry is that it is able to analyse unknown substances from tiny sample quantities. Indeed, mass spectrometry allowed for the identification of the molecular species of Cer and SM.

In terms of the chain length of the sphinganine or sphingosine backbone, adherent and floating cells are composed of the same ceramide molecular species. In addition to confirming the densitometric data (**Table 4**) that floating cells have more ceramide than adherent cells, **Figure 6** shows that the two sub-populations have different distributions of different molecular species.

It was also possible to obtain information on the fatty acids (acyl chains) present within the identified molecular species of ceramides using this semi-quantitative technique. For the majority of those detected, it was possible to define a wide variety of fatty acids based on chain length, including some that were acetylated (**Figure 7**;**Figure 8**).

Lipid in organic phase			
Optimal confluence			
% Of total			
Lipid	**Adherent cells**	**Floating cells**	***p***
Cer	**10.9 ± 3.5**	**18.8 ± 2.4**	**0.035***
GlcCer	15.1 ± 1.8	12.5 ± 2.8	0.242
PE	14.9 ± 1.6	15.9 ± 2.5	0.608
LacCer	13.7 ± 1.6	11.7 ± 2.7	0.315
PC	16.0 ± 1.2	14.1 ± 1.1	0.116
SM	**14.6 ± 1.0**	**12.7 ± 0.5**	**0.041***
Lyso PC	14.6 ± 0.4	14.4 ± 0.9	0.727

***Table 4* Densitometric analysis of lipids present in organic phase of BV-2 cells collected at optimal confluence.** *Densitometric analysis of lipids in the organic phase analysed by thin layer chromatography (**Figure 5**). Three separate experiments were conducted with cells collected at optimal confluence. The densitometric analysis was performed using ImageJ software, and the values displayed are in arbitrary units with ±SD determined using an unpaired t-test. * p<0.05*

molecular species of ceramide	mass spectrum area	
	Adherent cells	**Floating cells**
Cer (sphingosine 18:2)	295.9	435.0
Cer (sphingosine 18:1)	26527.4	27850.4
Cer (sphinganine 18:0)	464.0	317.1
Cer (sphinganine 14:0)	2635.2	9105.6
Cer (sphingosine 17:1)	145.2	202.6
Cer (sphinganine 16:0)	363.6	1675.8
Total	30431.3	39586.6
Ratio	1.30	**Floating > adherent**

Table 5 ***Mass spectrometry analysis of methanolized organic phase of cells collected at optimal confluence****. BV-2 cells were seeded at 1.5x10^4/cm^2*. After 72 hours, samples were processed as described in Material and Methods. *Through ESI mass spectrometry, an aliquot of methanolyzed organic phase (equivalent to 1 mg of protein) from adherent and floating cells was analysed. The displayed data are arbitrary units of mass spectrum area for various molecular species of ceramide, distinguished by the length of their sphinganine or sphingosine backbone chains.*

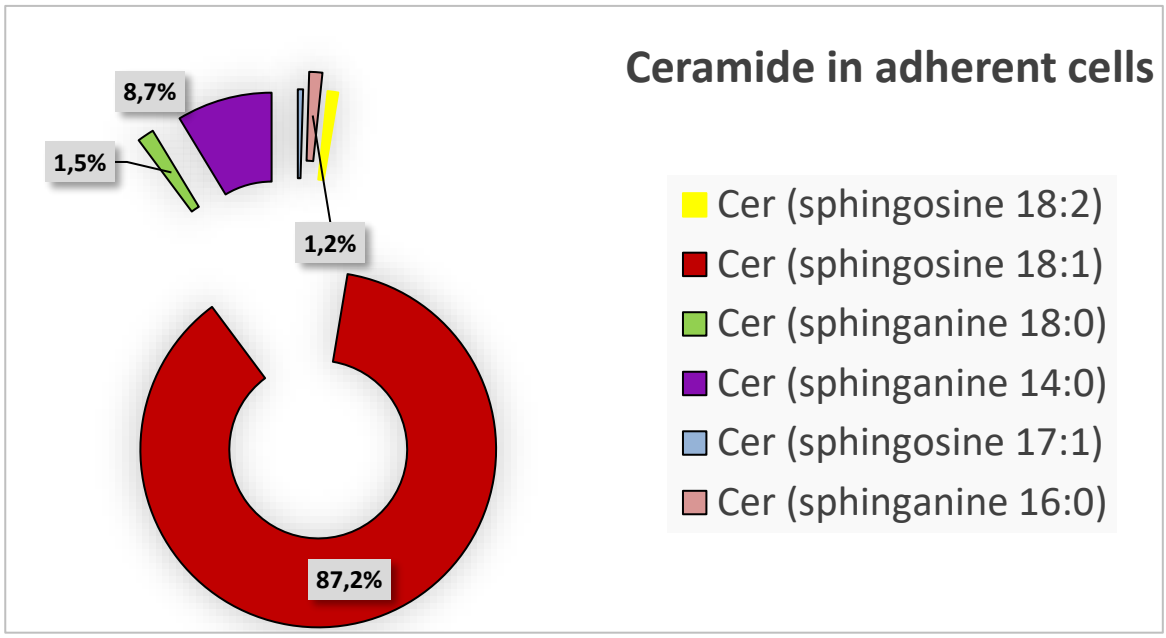

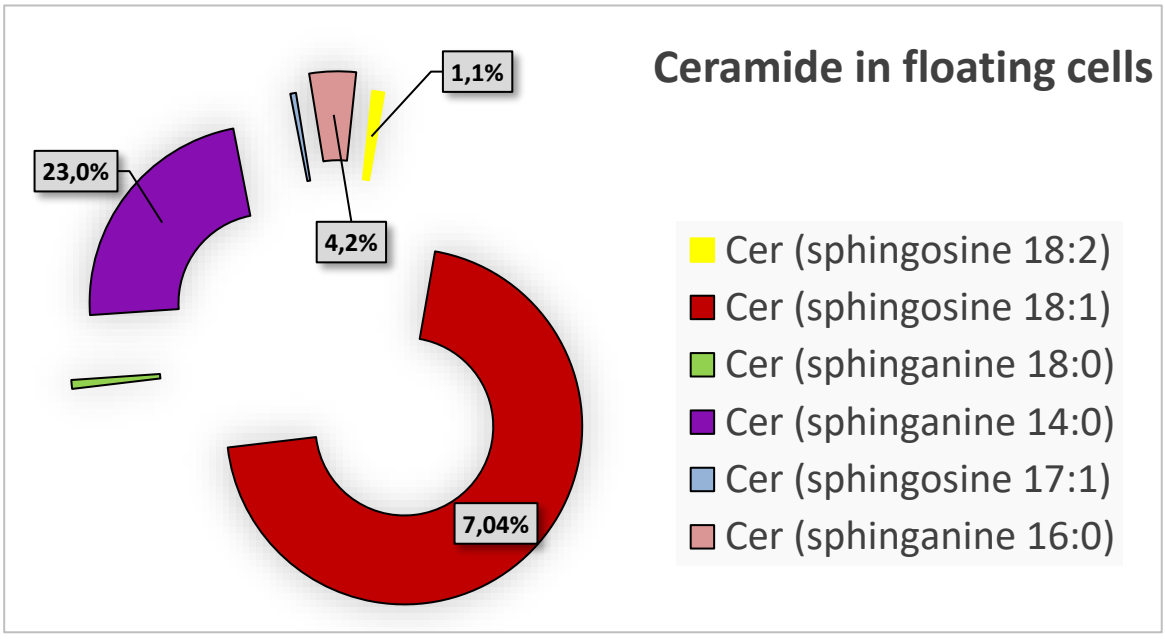

Figure 6 ***Ceramide molecular species analysed with ESI mass spectrometry analysis in methanolyzed organic phase of BV-2 cells collected at optimal confluence.*** *The percentage representations of distinct ceramide molecular species, distinguished by the length of their sphinganine or sphingosine backbone chains, are shown in (**Table 5**). Unrepresented data are less than or equal to 1%.*

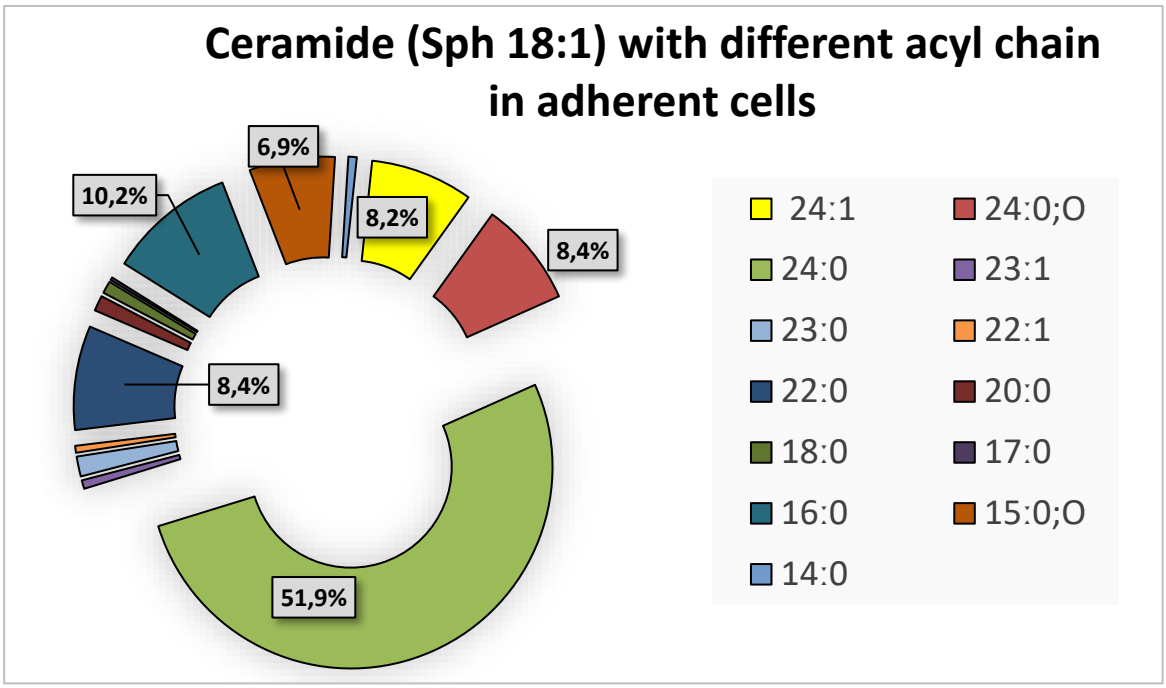

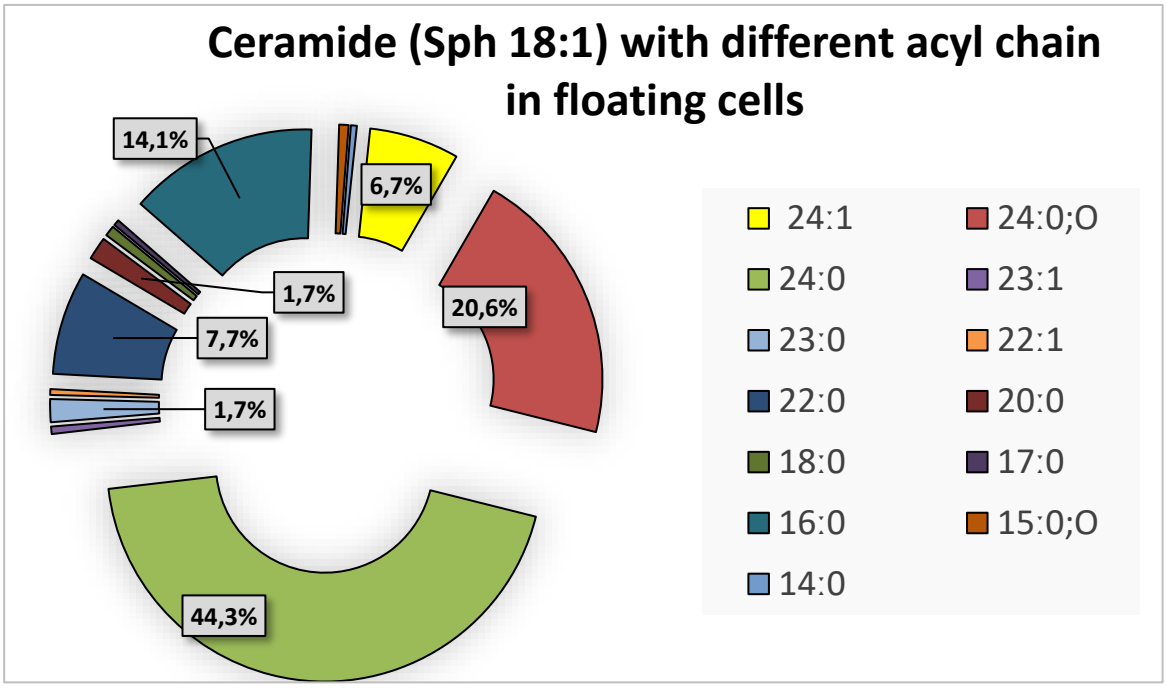

***Figure 7** Different acyl chain of ceramide molecular species with sphingosine (C18:1).* *Different acyl chain of ceramide molecular species with sphingosine (C18:1) detected by ESI mass spectrometry on methanolyzed organic phase of optimally confluent BV-2 cells. Data expressed as a percentage of various fatty acid chain lengths. The percentage of unrepresented data is less than or equal to 1.5%.*

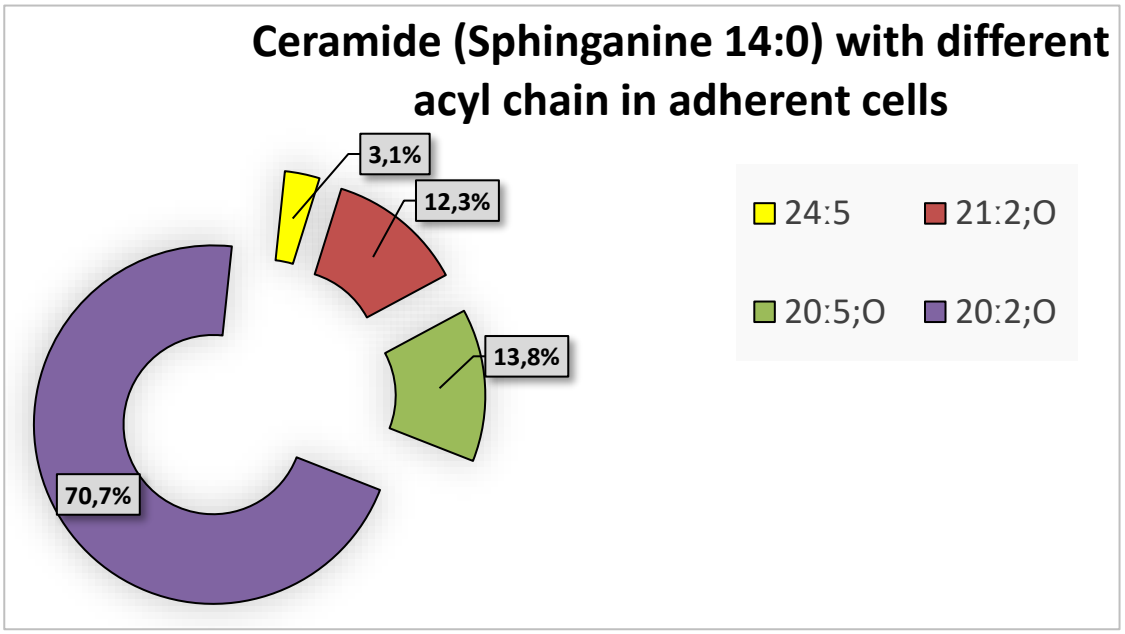

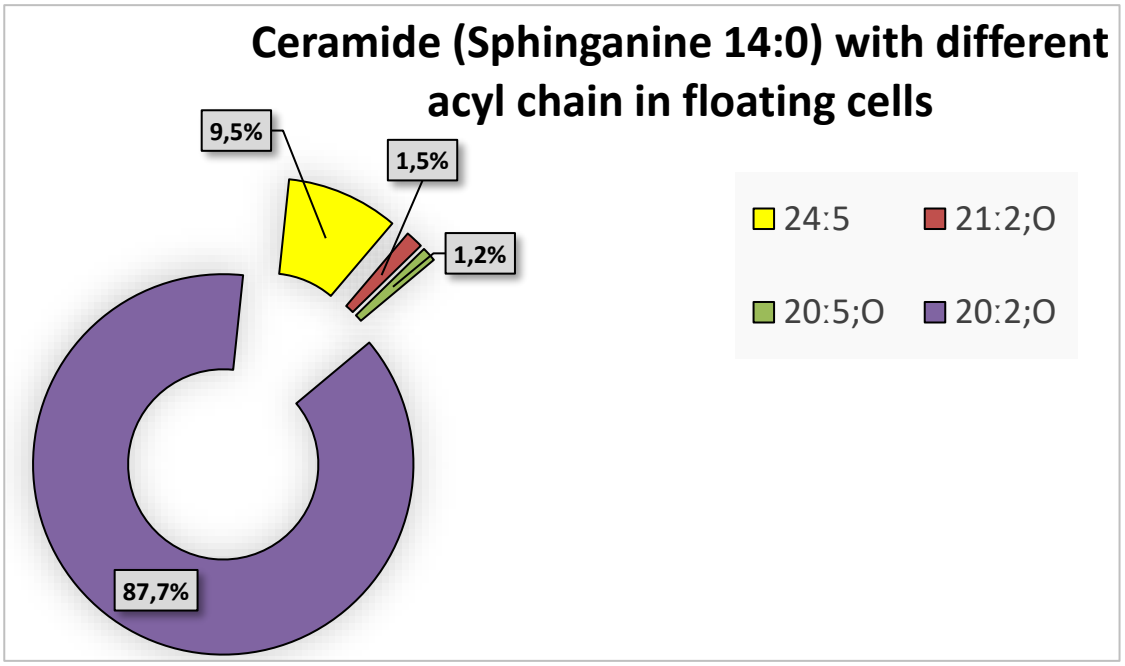

Figure 8 ***Different acyl chain of ceramide molecular species with sphinganine (C14:0).*** *Different acyl chain of ceramide molecular species with sphinganine (C14:0) detected by ESI mass spectrometry analysis of methanolyzed organic phase of optimally confluent BV-2 cells. Data expressed as a percentage of various fatty acid chain lengths. Unrepresented data are less than or equal to 1%.*

Regarding SM, ESI mass spectrometry analysis confirmed the difference between adherent and floating cells (**Table 6**) which had been detected by densitometric analysis (**Table 5**). Using mass spectrometry, several molecular species of SM with distinct backbone types were distinguished. Different distributions of sphinganine and sphingosine backbone chain length were observed between the two sub-populations of the same molecular species (**Figure 9**). Nonetheless, this distinct distribution between adherent and floating cells is less pronounced than that of Cer molecular species. Again, for the most abundant molecular species of SM, it has been possible to identify the wide range of acyl chains, which are differently distributed between adherent and floating chains (**Figure 10**; **Figure 11**).

Molecular species of sphingomyelin	**mass spectrum area**	
	Adherent cells	**Floating cells**
SM (sphingosine 19:2)	932.8	12.8
SM (sphingosine 18:2)	17777.2	4808.6
SM (sphingosine 18:1)	978622.5	36658.4
SM (sphinganine 18:0)	37259.9	11870.0
SM (sphingosine 17:1)	8112.3	2154.8
SM (sphinganine 16:0)	357.7	157.9
Total	1043062.4	385591.5
Ratio	2.7	**Adherent ≥ floating**

Table 6 ***Sphingomyelin mass spectrometry analysis of methanolized organic phase of cells collected at optimal confluence.*** *BV-2 cells were seeded at $1.5x10^4/cm^2$. After 72 hours, samples were processed as described in Material and Methods. Through ESI mass spectrometry, 1 mg of methanolyzed organic phase from adherent and floating cells was analysed. The displayed data are arbitrary units of mass spectrum area for various molecular species of sphingomyelin, distinguished by the length of their sphinganine or sphingosine backbone chains.*

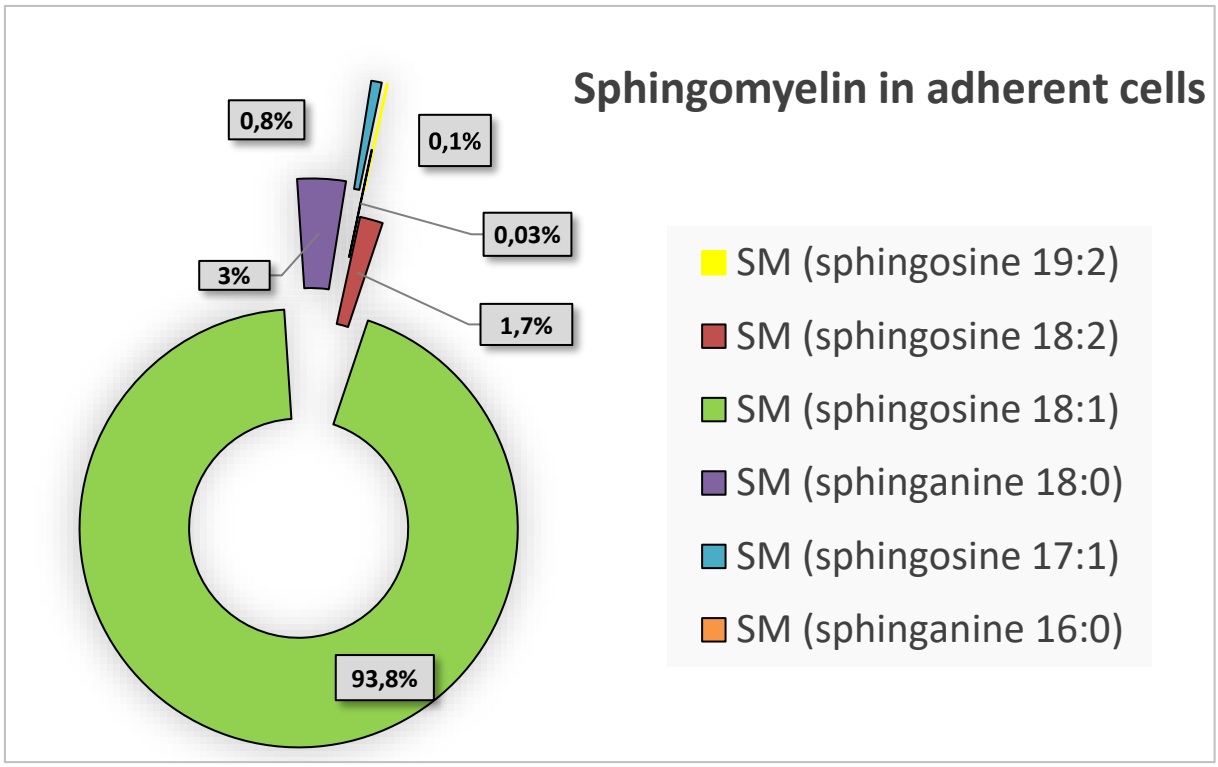

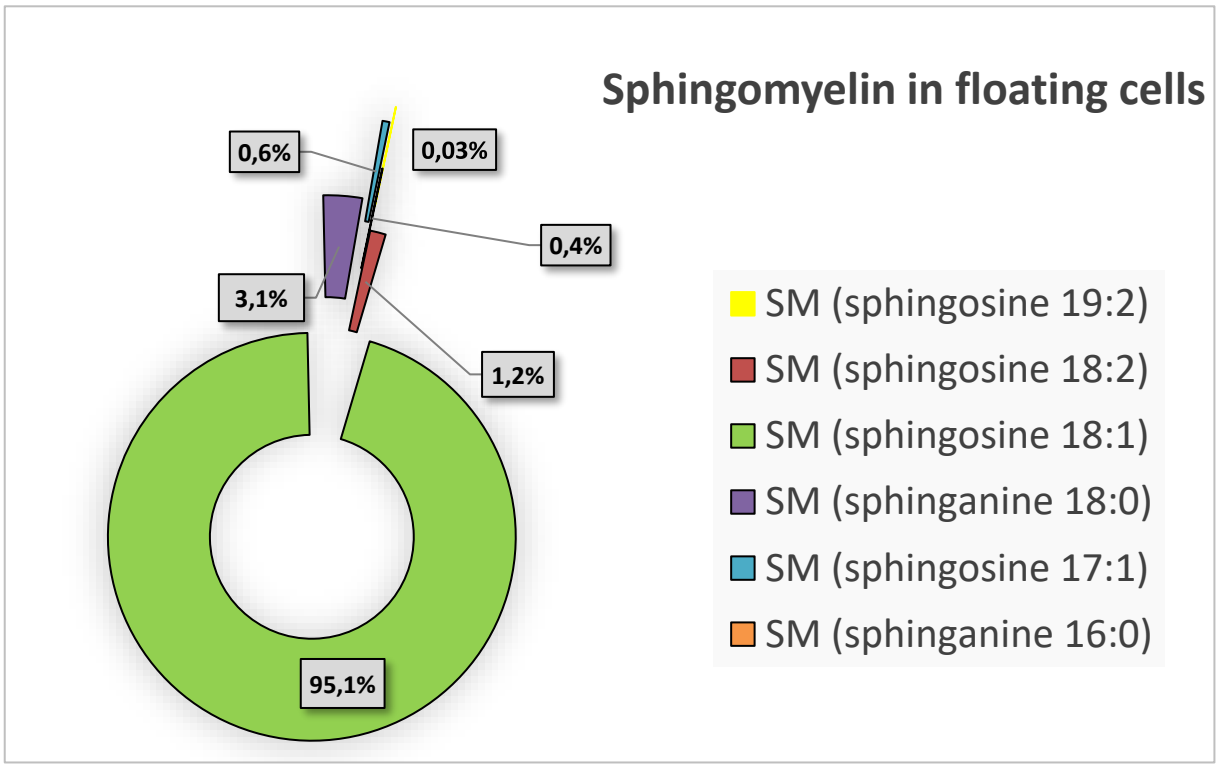

***Figure 9** Sphingomyelin molecular species analysed with ESI mass spectrometry analysis in methanolyzed organic phase of BV-2 cells collected at optimal confluence.* *Percentage representations of the various molecular species of sphingomyelin distinguished by the length of their sphinganine or sphingosine backbone chains shown in **Table 6**.*

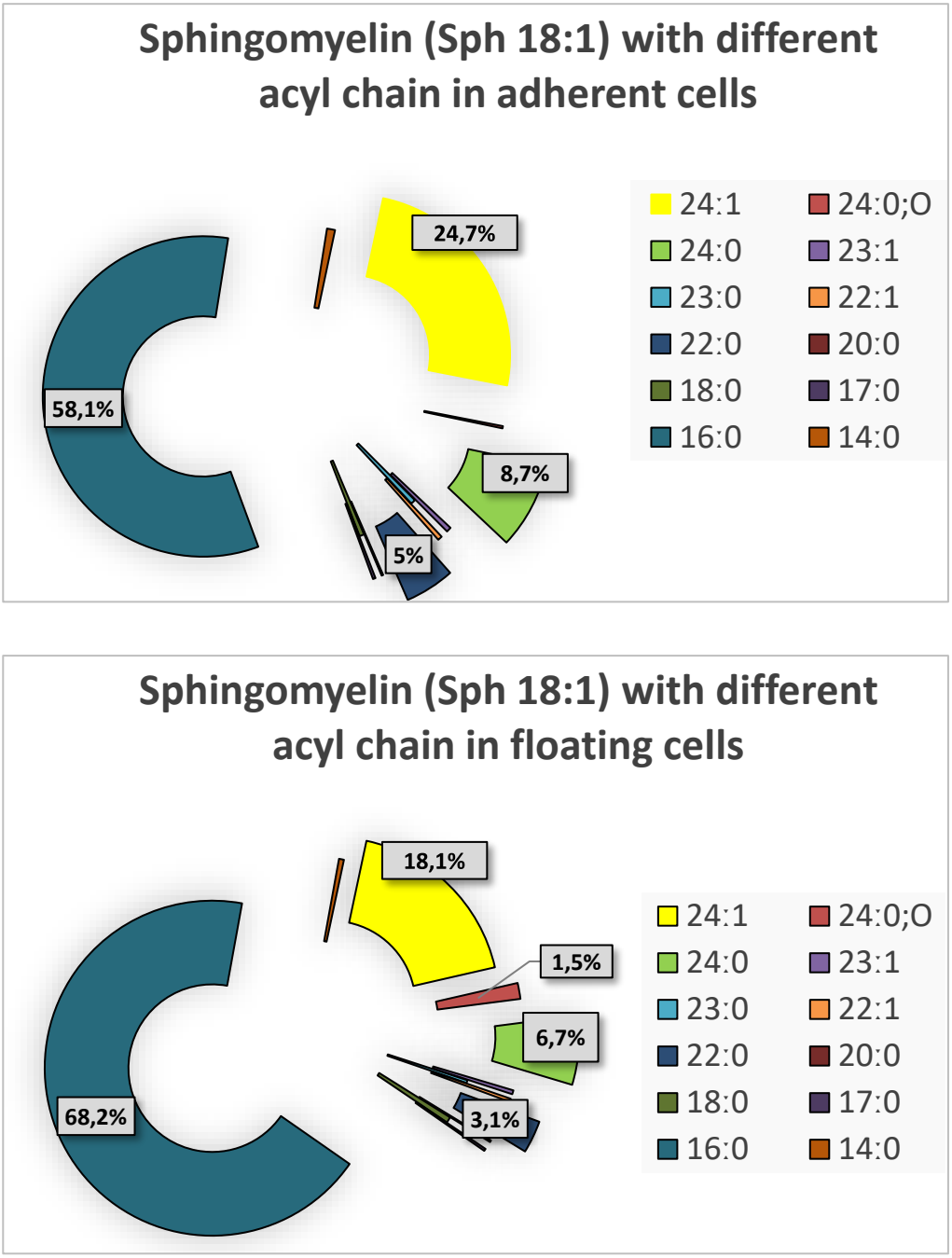

Figure 10 ***Different acyl chain of sphingomyelin molecular species with sphingosine (C18:1).*** *Different acyl chain of sphingomyelin molecular species with sphingosine (C18:1) evaluated with ESI mass spectrometry analysis on methanolyzed organic phase of optimally confluent BV-2 cells. Data expressed as a percentage of various fatty acid chain lengths. The percentage of unrepresented data is less than 1.5%.*

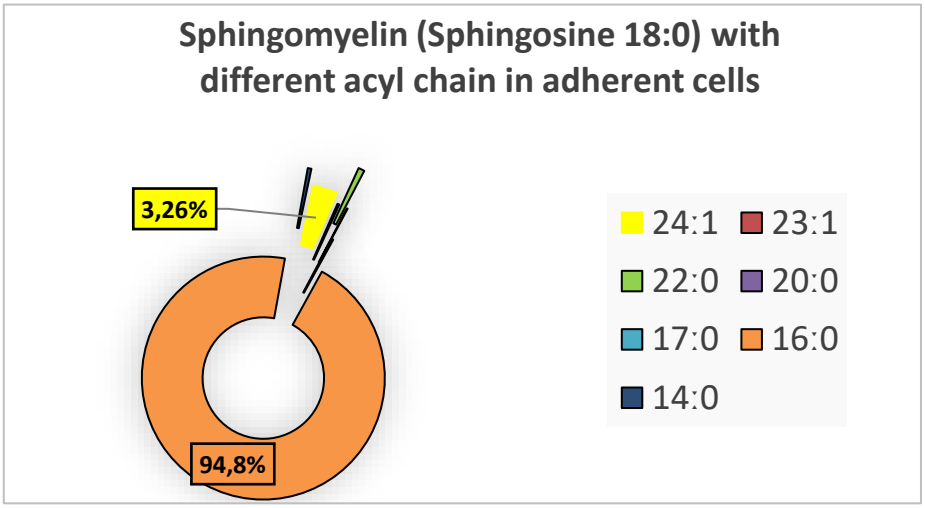

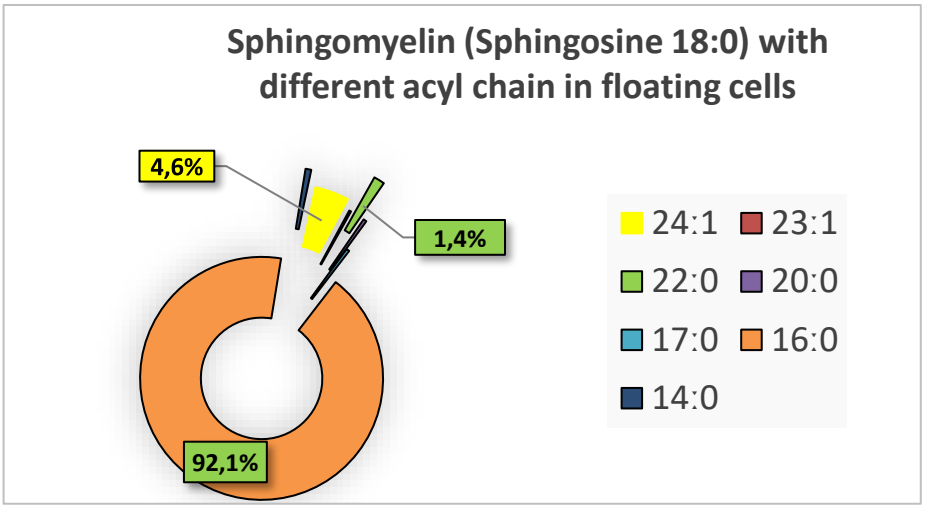

***Figure 11* Different acyl chain of sphingomyelin molecular species with sphinganine (C18:0).** *Different acyl chain of sphingomyelin molecular species with sphinganine (C18:0) detected by ESI mass spectrometry analysis on methanolyzed organic phase of optimally confluent BV-2 cells. Data expressed as a percentage of various fatty acid chain lengths. The percentage of unrepresented data is less than or equal to 1%.*

1.1.3.2 Analysis of neutral glycosphingolipids

Cer with a one or more neutral or uncharged sugars as the carbohydrate head group form neutral GLs (Merrill, 2011).

To accurately determine the presence of neutral GLs, the organic phase was subjected to alkaline methanolysis (as described in Materials and Methods) to remove all phospholipids, which can alter the migration of neutral GLs and interfere with their identification. Using the solvent system $CHCl_3$: CH_3OH: H_2O 110/40/6 (v/v/v) and the colorimetric assay Aniline, specific for reducing sugars, it was possible to determine the difference between the organic phase and the methanolyzed organic phase (**Figure 12**).

Due to their similar structures, neutral GLs such as GlcCer and GalCer co-migrate with the solvent used, preventing their correct discrimination; therefore, the methanolyzed organic phases were analysed with a different solvent system, allowing the separation these two lipids using known concentration standards for the two GLs analysed. This analysis enabled the identification of the complete absence of GalCer in both sub-populations. Moreover, using known concentration standards, it was possible to densitometrically assess the enrichment of GlcCer in adherent cells versus floating cells (**Figure 13**).

However, neutral GLs were difficult to characterise by TLC due to their low concentration relative to the sample examined. Therefore, mass spectrometry analysis has proven to be fundamental. Also, the semiquantitative differences between the two sub-populations have been confirmed for GlcCer and identified for LacCer and TrihexosylCer (**Table 7**;**Table 8**;**Table 9**).

Furthermore, it was possible to identify the molecular species of the GLs identified, although they are not as numerous as those detected for Cer and SM. Nonetheless, the acyl chains which vary most for the most abundant GLS, GlcCer, are distributed equally between the two sub-populations (**Figure 14**).

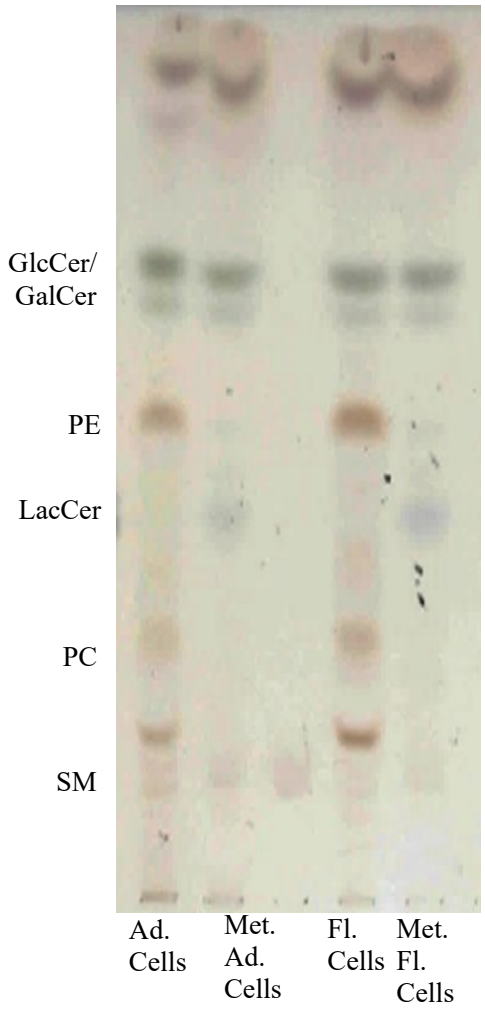

***Figure 12* analysis of organic and methanolyzed organic phase of cells collected at optimal confluence.** *BV-2 cells were seeded at 1.5x10^4/cm^2. After 72 hours, samples were processed as described in Material and Methods. Equal amount of organic and methanolyzed organic phase (equivalent to 1,5 mg of protein) from adherent and floating cells were analysed by $CHCl_3$: CH_3OH: H_2O 110/40/6 (v/v/v) and the colorimetric assay Aniline reactive spray.*

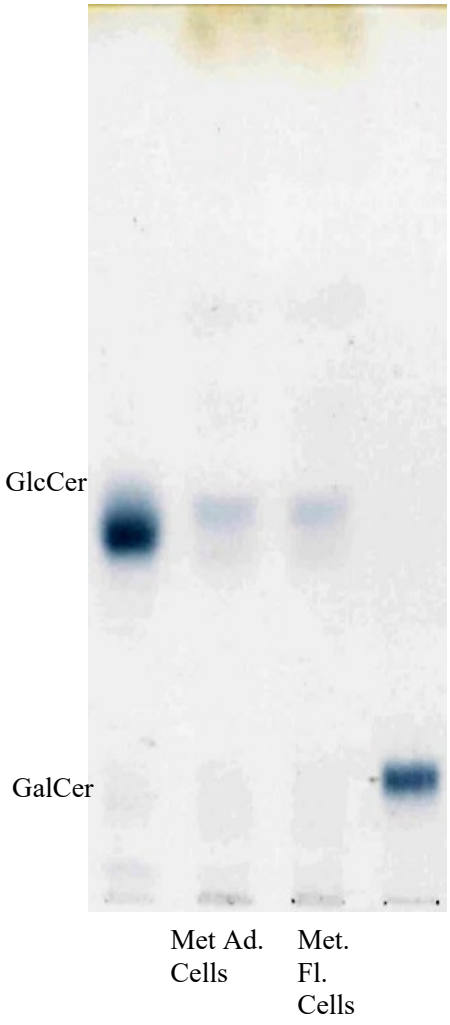

GlcCer	µg/mg
Adherent	0.57 ± 0.2
floating	0.41 ± 0.1

Figure 13 ***Analysis of methanolized organic phase of cells collected at optimal confluence.*** *BV-2 cells were seeded at 1.5x10^4/cm^2. After 72 hours, samples were processed as described in Material and Methods. Using the solvent system $CHCl_3$: CH_3OH: NH_3 (2N) 70/30/3 (v/v/v) and the colorimetric assay Aniline reactive Spray, TLC analysis was performed on an aliquot of methanolyzed organic phase (equivalent to 1.5 mg of protein) from adherent and floating cells. The data derive from three distinct experiments involving optimally confluent cells. ImageJ software was used to analyse densitometric data from three separate experiments, with ±SD analysed using an unpaired t-test. These values were quantified and are expressed as µg of glucosylceramide per mg of protein of each sample.*

molecular species of glucosylceramide	mass spectrum area	
	Adherent cells	**Floating cells**
GlcCer (sphingosine C 18:1)	192722.6	46736.9
Ratio	4.12	**Adherent > Floating**

Table 7 ***Glucosylceramide mass spectrometry analysis on methanolized organic phase of cells collected at optimal confluence.*** *BV-2 cells were seeded at* $1.5x10^4/cm^2$. After 72 hours, samples were processed as described in Material and Methods. *Through ESI mass spectrometry, an aliquot of methanolyzed organic phases (equivalent to 1 mg of protein) from adherent and floating cells was analysed. The displayed information represents arbitrary units of mass spectrum area for the unique molecular species of glucosylceramide formed by sphingosine C:18 chain length.*

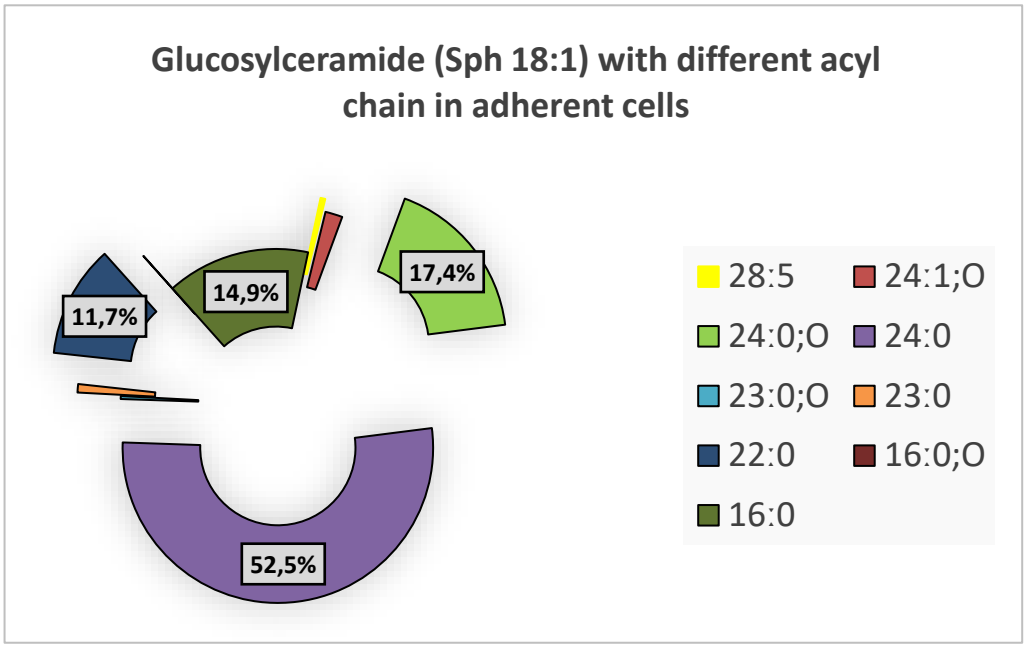

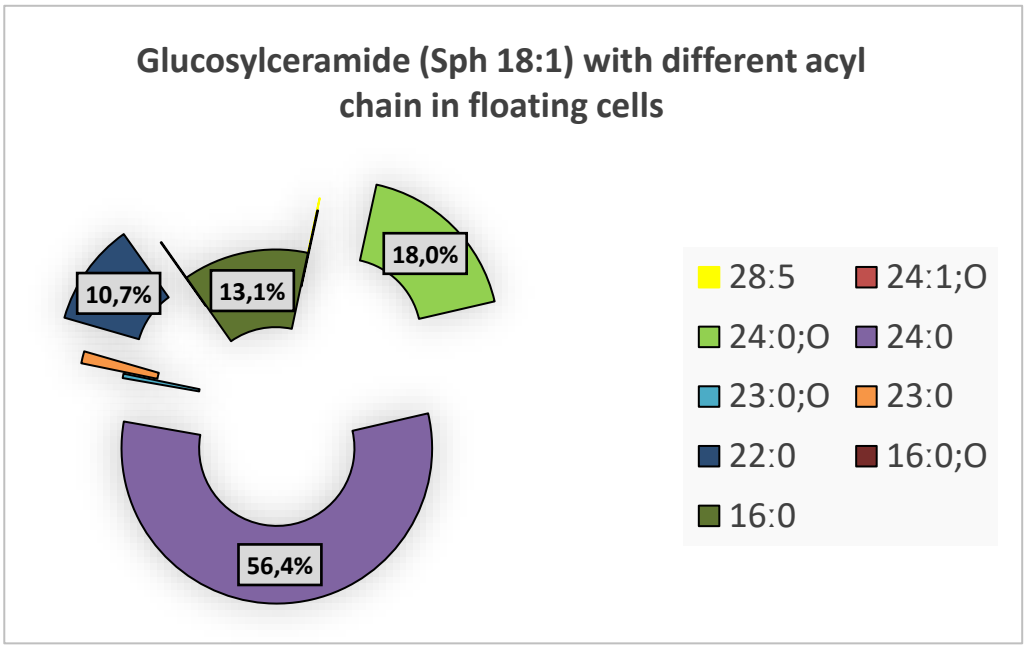

Figure 14 ***Different acyl chain of glucosylceramide molecular species with sphingosine (C18:1).*** *Different acyl chain of glucosylceramide molecular species with sphingosine (C18:1) evaluated by ESI mass spectrometry on methanolyzed organic phase of optimally confluent BV-2 cells. The data is expressed as a percentage of various fatty acid chain lengths. The percentage of unrepresented data is less than 2%.*

Molecular species of lactosylceramide	mass spectrum area	
	Adherent cells	**Floating cells**
LacCer (sphingosine C 18:1)	106.3	93.2
Ratio	1.14	**Adherent > floating**

Table 8 ***Lactosylceramide mass spectrometry analysis on methanolized organic phase of cells collected at optimal confluence.*** *BV-2 cells were seeded at 1.5x10^4/cm^2. After 72 hours, samples were processed as described in Material and Methods. Through ESI mass spectrometry, an equal amount of methanolyzed organic phase (equivalent to 1 mg of protein) from adherent and floating cells was analysed. The displayed information consists of arbitrary units of mass spectrum area for the unique molecular species of lactosylceramide formed by sphingosine C:18 chain length.*

molecular species of trihexosylceramide	mass spectrum area	
	Adherent cells	**Floating cells**
TrihexosylCer (sphingosine C 18:1)	17.9	37.9
TrihexosylCer (sphinganine C 18:0)	4.3	27.1
Total	22.2	65.0
Ratio	2.9	**Floating > adherent**

Table 9 ***Trihexosylceramide mass spectrometry analysis of methanolyzed organic phase of cells collected at optimal confluence.*** *BV-2 cells were seeded at 1.5x10^4/cm^2. After 72 hours, samples were processed as described in Material and Methods. Through ESI mass spectrometry, an equal amount of methanolyzed organic phase (equivalent to 1 mg of protein) from adherent and floating cells was analysed. According to the length of the sphinganine or sphingosine backbone chain, the displayed data represent arbitrary units of the mass spectrum area of various molecular species of trihexosylceramide.*

1.1.3.3 Analysis of sulfatide

Sulfatide is a GLs derived from GalCer by the addition of a sulphate group to the 3'-OH group of galactose via cerebroside sulfotransferase (CST) (Merrill, 2011). Sulfatide is highly abundant in myelin and is among the main lipid targets for the rHIgM22 antibody (Grassi et al., 2023). Sulfatide has been found to be absent in primary microglia (Fitzner et al., 2020) as well as its direct precursor, which we identified to be absent in BV-2 cells (**Figure 13**). Due to an accelerated biosynthetic pathway from GalCer to sulfatide, sulfatide may have been present even in the absence of the precursor, and because of this, the TLC analysis was conducted with a specific solvent system, $CHCl_3$:CH_3OH: H_2O C:M: 70/25/4 (v/v/v) and the colorimetric assay cresyl violet on the methanolyzed organic phases. Surprisingly, despite the fact that the antibody has already been shown to induce a biological effect on BV-2 cells (Zorina et al., 2018) and that sulfatide is one of the major lipid targets for this antibody (Grassi et al., 2023), sulfatide was found to be absent in both sub-populations of the BV-2 cell line (**Figure 15**).

Figure 15 ***Sulfatide analysis in methanolized organic phase of BV-2 cells collected at optimal confluence.*** *BV-2 cells were seeded at 1.5x10^4/cm^2. After 72 hours, samples were processed as described in Material and Methods. Using the solvent system $CHCl_3$:CH_3OH: H_2O 70/25/4 (v/v/v) and the colorimetric assay cresyl violet, an equal amount of methanolyzed organic phase (equivalent to 1 mg of protein) from adherent and floating cells was analysed via TLC.*

1.1.3.4 Analysis of gangliosides

Extremely hydrophilic lipids, such as gangliosides, can be effectively enriched in aqueous phases obtained via the two-phase Folch modified method. Gangliosides are sialic acid-containing glycosphingolipids thought to play a role in the development, differentiation, and function of vertebrate nervous systems (Ohmi et al., 2012).

GM1 and GD1a are the only gangliosides present in BV-2 cell sub-populations (**Figure 16**). The distribution of these two gangliosides differs slightly between the two sub-populations, and densitometric analysis revealed an enrichment of ganglioside in adherent cells (**Table 10**).

After determining the limits of TLC analysis for other classes of SLs and considering the small number of gangliosides present in relation to the sample analysed, an equal amount of the dialyzed aqueous phase was analysed by mass spectrometry.

This analysis enabled us to identify distinct molecular species of gangliosides yet identified via TLC analysis, distinguished by the length of their ceramide chains. In addition to these two, two other gangliosides, GM2 and GD1b, were identified, albeit in tiny amounts.

The densitometric analysis was confirmed by this more sensitive analysis, which showed a greater quantitative difference between the two sub-populations in terms of the total amount of gangliosides and better defined the enrichment of the different gangliosides between the two populations, identifying each as enriched in GD1a compared to all others, with the sole higher concentration of this particular lipid in floating cells (**Table 11**).

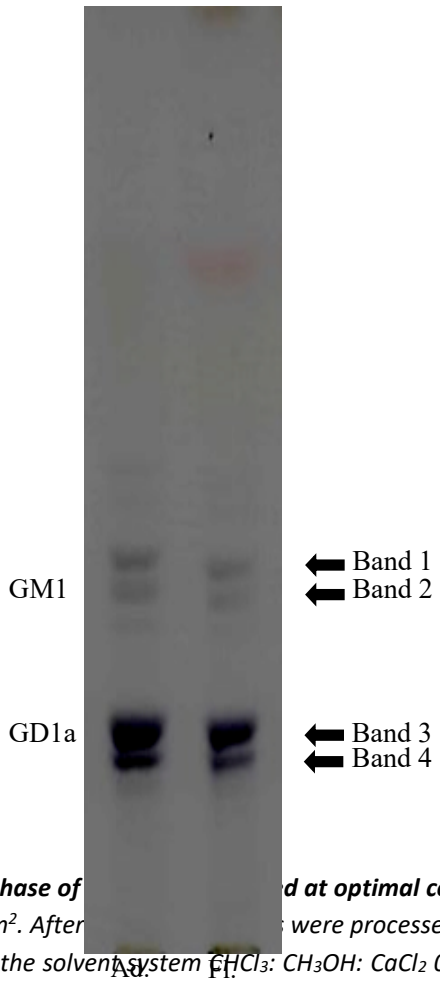

Figure 16 ***Aqueous phase of d at optimal confluence****. BV-2 cells were seeded at 1.5x10^4/cm^2. After were processed as described in Material and Methods. Using the solvent system $CHCl_3$: CH_3OH: $CaCl_2$ 0.2% 55/45/10 (v/v/v) and the colorimetric assay Ehrlich reactive spots, an equal amount of dialyzed aqueous phase (equivalent to 1.5 mg of protein) from adherent and floating cells was analysed by TLC.*

Ganglioside								
Optimal confluence								
Densitometric units				***P***	**% Single band**		**% Combined bands**	
		Ad. cells	**Fl. cells**		**Ad. cells**	**Fl. Cells**	**Ad. cells**	**Fl. Cells**
GM1	band n°1	17.4 ± 1.6	11.8 ± 1.2	0.07	25.9	22.5	48.7	45.9
	band n°2	15.3 ± 2.4	12.2 ± 4.2	0.16	22.8	23.4		
GD1a	band n°3	18.2 ± 3.0	15.3 ± 4.8	0.66	27.1	29.1	51.3	54.1
	band n°4	16.3 ± 3.3	13.1 ± 7.0	0.66	24.2	25.0		
Total		67.0	52.4		**Adherent > floating**			
Ratio		1.3						

***Table 10** Densitometric analysis of lipids present aqueous phase of BV-2 cells collected at optimal confluence.* *Densitometric analysis of lipids in the aqueous phase analysed by thin layer chromatography (**Figure 16**). The data derive from three distinct experiments involving cell collected at optimal confluence. The densitometric analysis was performed using ImageJ software, and the values displayed are arbitrary units with ±SD calculated using an unpaired t-test.*

Ganglioside	mass spectrum area		% Total (combined mass spectrum area)	
	Ad. cells	Fl. cells	Ad. cells	Fl. cells
GM2 (34:1)	3.23	1.10	1.97	1.75
GM1 (34:1)	2.49	1.06		
GM1 (42:2)	1.32	0.33		
GM1 (42:1)	5.35	1.67	5.59	4.85
GD1a (44:2)	1.18	0.01		
GD1a (42:2)	50.95	15.27		
GD1a (42:1)	42.79	22.75		
GD1a (41:2)	3.67	1.04		
GD1a (34:1)	53.04	19.81	92.43	93.37
GD1b (40:1)	0.03	0.02	0.02	0.03
Total	164.05	63.06	**Adherent > floating**	
Ratio	2.60			

Table 11 ***Mass spectrometry analysis of dialysed aqueous phase of cells collected at optimal confluence.*** *BV-2 cells were seeded at 1.5x10^4/cm^2. A*fter 72 h, samples were processed as described in Materials and Methods. *Similar amount of dialysed aqueous phase (equivalent to 1 mg of protein) from adherent and floating cells were analysed trough ESI mass spectrometry. The analysis was conducted by UNITECH OMICs (University of Milan) and Peakview software was used for data processing. The results are presented in the form of a mass spectrum (arbitrary units). or the relative abundance of ions as a function of their mass/charge ratio. All gangliosides identified are distinguished as different molecular species differing in ceramide chain length.*

2.2 Analysis of endogenous lipids from cells collected in over-confluence

Since it has been reported in the scientific literature that changes in cell confluence are associated with alterations in the lipid pattern, several of the previously presented analyses have been repeated on cells collecte ence (Frechin et al., 2015).

BV-2 cells were seeded at a density amples were processed as described in Materials and Methods To identify d in BV-2 cells, the organic and aqueous phases were analysed by TLC using s ystems and colorimetric assays.

2.2.1 Analysis of phos

The analysis of the organic phase v lvent system and phosphorous reagent confirmed the peculiar characteris ine, which was also observed for cells collected at optimal confluence (**Tab** nts the majority of phospholipids (**Figure 17**). Even if the analysis has been per e, densitometric analysis reveals that the difference between PC and PE is ced than in cells collected at optimal confluence

Figure 17 ***analysis of phospholipids in organic phase of cells collected in over-confluence***. *BV-2 cells were seeded at* $3_x10^4/cm^2$. After 72 h, samples were processed as described in Materials and Methods. *Equal amount of organic phase (equivalent to 400 µg of protein) from adherent and floating cells were analysed trough HPTLC using the solvent system* $CHCl_3$*:* CH_3OH*:* CH_3COOH*:* H_2O *(30/20/2/1) (v/v/v/v) and the colorimetric assay phosphorus reactive spray for phospholipids (Vaskovsky V.E., Kostetsky (1968)).*

Phospholipids		
over-confluent		
% Of total		
Lipid	**Adherent cells**	**Floating cells**
PE	8	21
PC	63	53
SM	29	27

Table 12 ***Densitometric analysis of phospholipids present in the organic phase of BV-2 cells collected in over-confluence****. Thin-layer chromatography-based densitometric evaluation of phospholipids in the organic phase (****Errore. L'origine riferimento non è stata trovata.****). The data is derived from a single analysis of over-confluent cells, no statistical analyses were available. ImageJ software was used to conduct the densitometric analysis. The data displayed are arbitrary units.*

2.2.2 Analysis of cholesterol

Even the organic phases from over-confluent cells were subjected to quantitative TLC analysis of cholesterol. This analysis revealed that the amount of cholesterol in the two sub-populations is equivalent (**Figure 18**). In addition, this information is remarkably similar to that obtained from cells collected under optimal confluence conditions (**Figure 4**).

Cholesterol nmol/mg		
Cell collecting conditions	**Adherent cells**	**Floating cells**
over-confluence	20.0 ± 8.7	17.9 ± 1.9

***Figure 18* Cholesterol analysis on organic phase of BV-2 cells collected in over-confluence.** *BV-2 cells were seeded at a density of $3x10^4/cm^2$. After 72 h, samples were processed as described in Materials and Methods. Using the solvent $CH_3(CH_2)_4CH_3$: $C_4H_8O_2$ (3:2) (v/v) and the colorimetric assay anisaldehyde reactive spray, equal amounts of organic phase (equivalent to 90 µg of protein) from adherent and floating cells were analysed via TLC. NINE Alliance software was used to conduct the densitometric analysis. Three distinct experiments were conducted on over-confluent cell samples.*

2.2.3 Analysis of sphingolipids: ceramide and sphingomyelin

The analysis of organic phases in over-confluent cells revealed the presence of lipids co-migrating with standards of Cer, GlcCer, PE, LacCer, LysoPC, PC, and SM (**Figure 19**).

However, in over-confluence conditions, densitometric analysis revealed that the differences found in ceramide and sphingomyelin in organic phases of cells collected at optimal confluence are no longer present (**Table 4**). Only a difference in PE has been identified between the two sub-populations (**Table 13**).

Also, when two-confluence cells are compared to adherent cells, the percentage ratio between Cer and GlcCer changes. Cells collected at optimal confluence have more GlcCer than Cer, while overconfluent cells have the opposite.

This information also identifies a precise metabolic situation in which cells collected at the optimal confluence level, approximately 80-90%, may be more metabolically active than cells collected at over confluence, which contain a larger amount of Cer, which is also listed as a pro-apoptotic bioactive molecule.

A mass spectrometry analysis of the organic phases of cells collected from a situation of over-confluence has not been performed due to the insignificance of the minor differences observed.

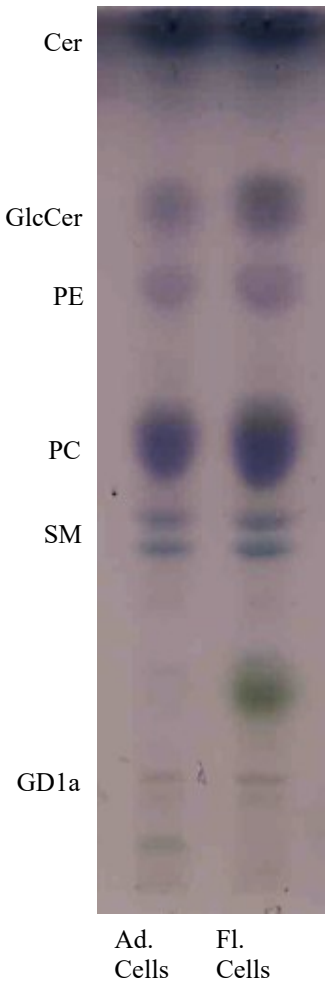

Figure 19 ***Organic phase of BV-2 cells collected in over-confluence****. BV-2 cells were seeded at a density of 3x10^4/cm^2. After 72 h, samples were processed as described in Materials and Methods. Equal amount of organic phase (equivalent to 150 µg of protein) from adherent and floating cells was analysed by HPTLC using the solvent system $CHCl_3$: CH_3OH: H_2O 110/40/6 (v/v/v) and the anisaldehyde reactive spray colorimetric assay.*

Lipids in organic phase			
over-confluent			
% Total			
Lipid	**Adherent cells**	**Floating cells**	***p***
Cer	19.0 ± 7.9	16.0 ± 4.5	0.690
GlcCer	12.0 ± 2.2	8.0 ± 4.7	0.429
PE	**7.0 ± 0.4**	**16.0 ± 0.9**	**0.01****
LacCer	14.0 ± 3.2	12.0 ± 4.1	0.731
PC	17.0 ± 1.2	19.0 ± 1.1	0.317
SM	15.0 ± 1.6	13.0 ± 1.8	0.446
Lyso PC	16.0 ± 0.1	15.0 ± 4.6	0.847

Table 13 ***Densitometric analysis of lipids present organic phase of BV-2 cells collected in over-confluence.*** *Thin-layer chromatography-based densitometric evaluation of lipids present in the organic phase (**Figure 19**). Data derive from three different experiments of cells collected in over-confluence. The densitometric analysis was performed using ImageJ software, and the values displayed are arbitrary units with ±SD determined using an unpaired t-test. ** p<0.01.*

2.2.4 Analysis of gangliosides

In comparison to cells collected at optimal confluence, cells collected at over-confluence appear to be enriched in gangliosides.

However, the main problem that emerged when analysing the aqueous phase of cells collected at optimal confluence was obtaining enough material to conduct the analysis. Indeed, BV-2 cells are, in general, poor in ganglioside content (**Figure 21**) and the enrichment shown is attributable, in part, to the higher amount of sample analysed, which was easily obtained by collecting cells over-confluent. Due to the large amount of sample resulting from the aqueous phases of cells collected in over-confluence and analysed by TLC, an increased number of gangliosides was detected. However, TLC analysis was only performed once, and the densitometric analysis (**Table 14**) revealed clearly that adherent cells contain a greater amount of ganglioside than floating cells; however, only minor differences between the two sub-populations were evaluated, even if the bands corresponding to different ganglioside species are distributed slightly differently.

To confirm these results, gangliosides analysis via ESI mass spectrometry was conducted on the same sample.

Mass spectrometry confirmed the enrichment of gangliosides in adherent cells (**Table 15**) and identified a small number of molecular species for each ganglioside yet identified by TLC (**Figure 21**). However, this analysis was not as in-depth as those previously presented; there is no information about molecular species distinguished by sphingoid backbone or acyl chain length.

Nonetheless, it was possible to obtain semiquantitative information based on differences in the proportion of Cer at different carbon atom lengths for each identified ganglioside. Specifically, a different distribution between the two cell sub-populations was confirmed for each ganglioside, which the TLC was not able to clarify.

In respect of the cells' collecting condition, in cells collected at 80-90% confluence, certain lipids, such as GalNacGD1a, were not observed. Furthermore, the distribution of lipids differs, although ganglioside GD1a remains the most abundant lipid in both populations and especially in floating cells.

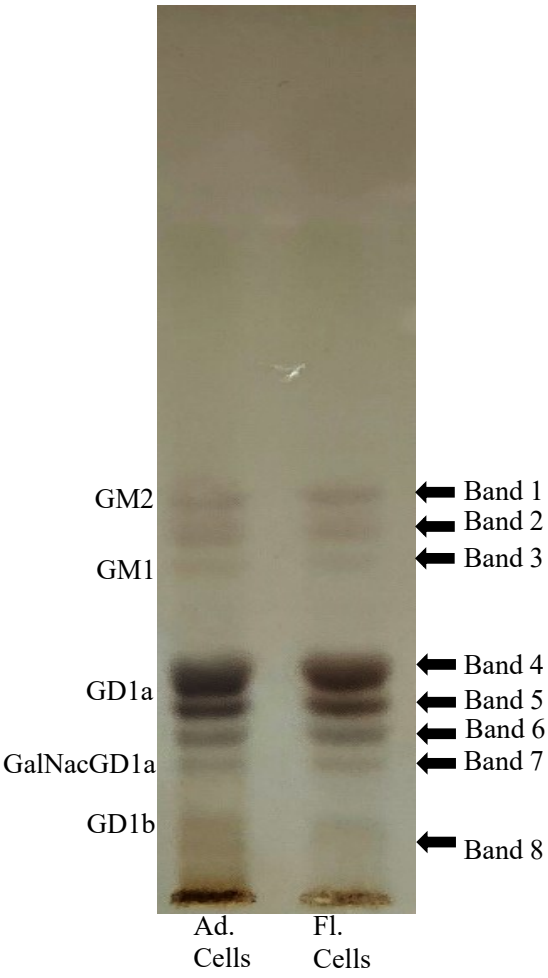

<u>Figure 20</u> Aqueous phase of BV-2 cells collected in over-confluence*. BV-2 cells were seeded at a density of 3x10^4/cm^2; After 72 h, samples were processed as described in Materials and Methods. Dialysis was conducted on aqueous phases. Equal amount of dialyzed aqueous phase (equivalent to 15 mg of protein) from adherent and floating cells was analysed by HPTLC employing the solvent system $CHCl_3$: CH_3OH: $CaCl_2$ 0.2% 55/45/10 (v/v/v) and the colorimetric assay Ehrlich reactive spray.*

Ganglioside							
Over confluence							
Densitometric units				% Single band		% Combined bands	
		Ad. cells	Fl. cells	Ad. cells	Fl. cells	Ad. cells	Fl. cells
GM2	band n°1	40.4	32.8	11.0	11.2	11.0	11.2
GM1	band n°2	43.6	29.0	11.8	9.9	24.4	18.3
	band n°3	46.3	24.7	12.6	8.4		
GD1a	band n°4	51.2	56.0	13.9	19.1	27.6	36.8
	band n°5	50.5	51.7	13.7	17.6		
GalNacGD1a	band n°6	47.6	48.4	12.9	16.5	24.9	27.6
	band n°7	44.1	32.6	12.0	11.1		
GD1b	band n°8	44.8	17.9	12.2	6.1	12.2	6.1
Total		368.7	293.2	**Adherent > floating**			
Ratio			1.3				

Table 14 ***Densitometric analysis of lipids present aqueous phase of BV-2 cells collected in over-confluence.*** *Densitometric analysis of lipids in the aqueous phase analysed by thin layer chromatography (figure 17). This is a single experiment with data expressed as the volume of each band and then as a percentage of the total. A portion of the sample was also analysed using ESI mass spectrometry. ImageJ software was used to conduct the densitometric analysis.*

Ganglioside	mass spectrum area		% Total (combined mass spectrum area)	
	Ad. cells	Fl. cells	Ad. cells	Fl. cells
GM2(34:1)	1.6	0.7	1.0	0.7
GM1(42:1)	4.8	2.6	11.6	9.9
GM1(40:1)	0.5	0.3		
GM1(34:1)	12.8	7.9		
GD1a (43:2)$^{-2H}$	N.D.	0.8	69.7	72.3
GD1a (42:3)	1.1	0.8		
GD1a (42:2)	17.4	14.1		
GD1a (34:1)	89.1	62.5		
GD1a (41:2)	0.6	0.5		
GD1a (34:3) (OH)	0.9	0.7		
GalNacGd1a (34:1)	2.76	1.84	1.8	1.7
GD1b (42:1)	18.0	11.9	16.0	15.5
GD1b (40:2)	1.2	0.9		
GD1b (40:1)	5.8	4.3		
Total	156.5	109.8	**Adherent > floating**	
Ratio		1.4		

Table 15 ***Mass spectrometry analysis of dialysed aqueous phase of cells collected in over-confluence.*** *BV-2 cells were seeded at $3x10^4/cm^2$. After 72 hours, samples were processed as described in Material and Methods. Similar amount of dialysed aqueous phase from adherent and floating cells were analysed trough ESI mass spectrometry. UNITECH OMICs (University of Milan, Italy) performed the analysis. and Peakview software was used for data processing. The results are presented in the form of a mass spectrum (arbitrary units). or the relative abundance of ions as a function of their mass/charge ratio. All gangliosides identified are distinguished as different molecular species differing in ceramide chain length.*

3. Sphingolipid turnover of BV-2 cells

Because BV-2 cells contain a limited number of sphingolipids, particularly ganglioside, we studied their sphingolipid turnover and identified the best experimental conditions using a tritiated precursor for sphingolipids, 1-[H^3] Sphingosine.

BV-2 cells were seeded at $1.5x10^4/cm^2$. At the conclusion of each time of chase the cells had reached 80-90% confluence, regardless of the chase period, and samples were processed as described in Materials and Methods.

The organic and aqueous phases obtained were measured for radioactivity and analysed by TLC using the solvent systems $CHCl_3$: CH_3OH: H_2O 110/40/6 (v/v/v) and $CHCl_3$: CH_3OH: $CaCl_2$ 0.2% 55/45/10 (v/v/v), respectively. The radioactive sphingolipids were subsequently evaluated by digital autoradiography (^{T}Racer Beta-Imager) and quantified using M3Vison software (Biospace, Paris, FR).

At different chase times, each SLs from the most hydrophobic in the organic phase, to the most hydrophilic in the aqueous phase, were analysed in both sub-populations.

TLC analysis and digital autoradiography evaluation of the hydrophobic lipids in the organic phase, revealed the presence of the same lipids, at all times considered, in both sub-populations (**Figure 22**).

In addition, when gangliosides are analysed in the aqueous phase, the presence of identical lipids at different chase times is observed in both sup-populations (**Figure 23**).

Although the nCi/mg concentrations of the different lipids analysed varies between the different times of chase, all of the different lipid species were identified at each time point of the examination.

In addition, the amount of certain lipids is lower at 24 hours of chase, as it occurs for 48 hours, than at 12 hours of chase. One of the many indicators of a biosynthetic or catabolic pathway is the amount of PE, a phospholipid that, despite not being formed by a sphingoid backbone, is tritiated and can be followed through digital autoradiography. This occurs because one of the final steps of the catabolism of the SLs is the irreversible activity of sphingosine-1-posphate lyase (S1P lyase) on sphingosine-1-phosphate (S1P), which leads to the formation of ethanolamine-phosphate and a long chain aldehyde (Hannun and Obeid, 2008, Giussani et al., 2014).

Nevertheless, considering that all lipids are identical at the time observed, we focused on this phospholipid, and the lower amount in both sub-populations has been evaluated at 12 hours of chase considering its percentage of the whole (**Figure 24**).

This analysis of kinetics with different chase times has therefore revealed that BV-2 cells have a rapid sphingolipid turnover and that 12 hours of chase is the optimal setting for a steady-state metabolic labelling experiment.

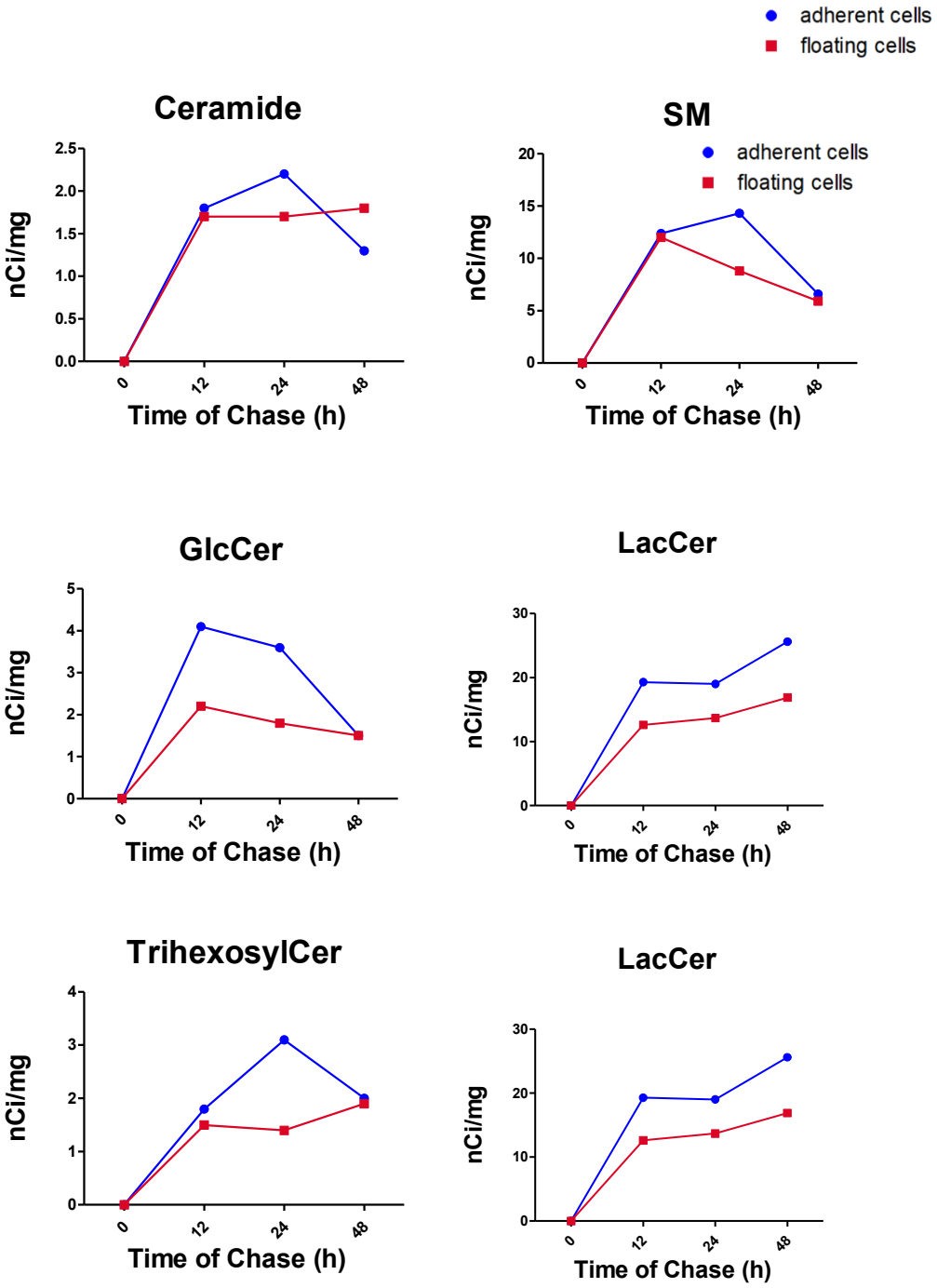

Figure 21 ***Sphingolipids turnover*** **analysis on organic phase in** ***BV-2 cells.*** *BV-2 cells were seeded at 1.5x10^4/cm^2.* At the conclusion of each time of chase *samples were processed as described in Materials and Methods. Lipids of organic phases were separated by HPTLC using $CHCl_3$: CH_3OH: H_2O 110/40/6 (v/v/v) as solvent systems and then analysed by digital autoradiography.*

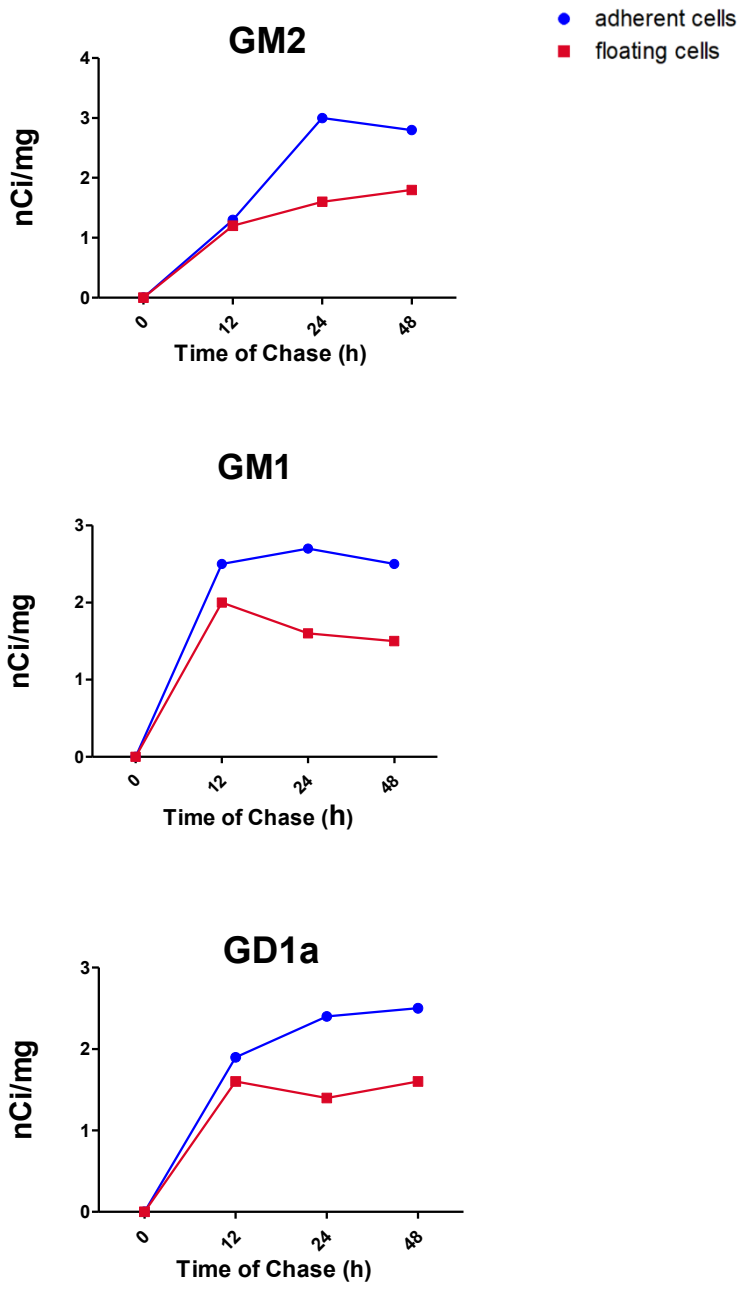

Figure 22 ***Sphingolipids turnover analysis on aqueous phase in BV-2 cells.*** *BV-2 cells were seeded at 1.5x10^4/cm^2. At the conclusion of each time of chase* samples were processed as described in Materials and Methods. *Lipids of aqueous phases were separated by HPTLC using $CHCl_3$: CH_3OH: 0.2%$CaCl_2$ in H_2O 55:45:10 as solvent systems and then analyzed by digital autoradiography.*

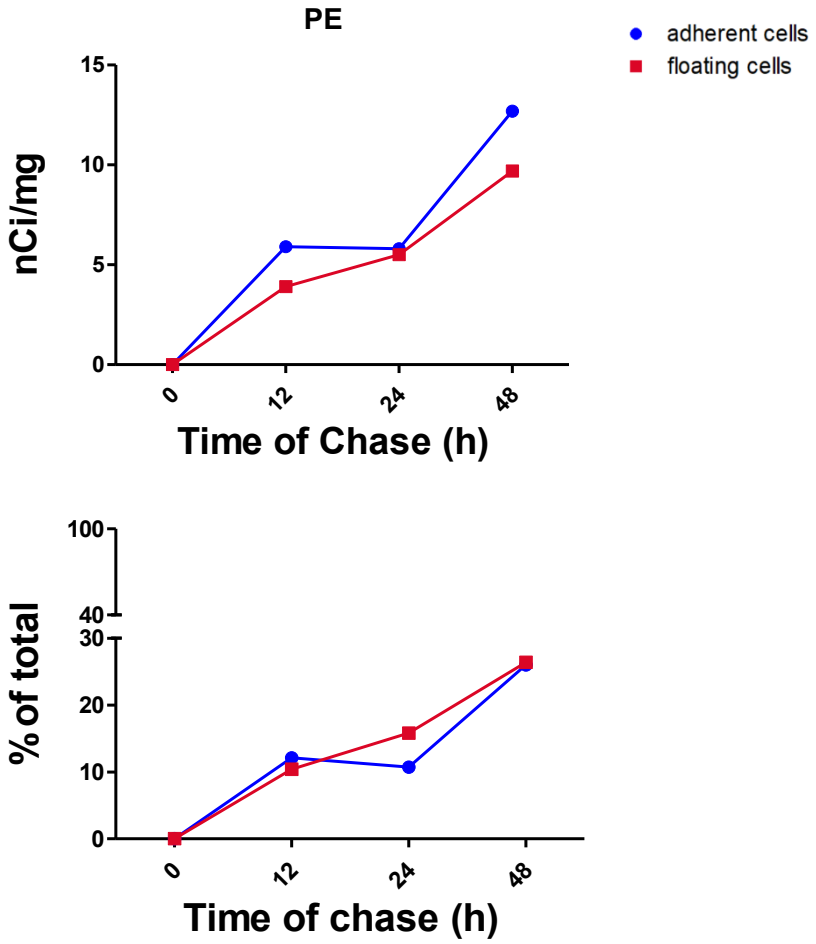

Figure 23 ***Phosphatidylethanolamine turnover in organic phase in BV-2 cells.*** *BV-2 cells were seeded at 1.5x10^4/cm^2.* At the conclusion of each time of chase *samples were processed as described in Materials and Methods.* *Lipids of organic phases were separated by HPTLC using $CHCl_3$: CH_3OH: H_2O 110/40/6 (v/v/v) as solvent systems and then analysed by digital autoradiography.*

4. Effects of rHIgM22 on the sphingolipid patter of BV-2 cells

Data obtained in our laboratory shows that different glycosphingolipids were implicated in the binding of rHIgM22 to the cell surface, suggesting that reorganisation of the lipid membrane microenvironment may be relevant to its biological activity (Grassi et al., 2023). In addition, it has been shown that rHIgM22 induces modifications in the sphingolipid pattern in other glial populations, such as OPCs and OLs, by significantly increasing some gangliosides (S. Grassi et al. , 2021).

Based on this information, we decided to look at how rHIgM22 affects the pattern of sphingolipids in BV-2 cells. The analysis of the effects of rHIgM22 on the lipid pattern of BV-2 cells has been conducted under two different experimental conditions, since we assessed that the lipid pattern is modified based on the confluence state of the culture but also because BV-2 cells have a rapid sphingolipid turnover.

4.1 Effects of rHIgM22 on the sphingolipid patter of BV-2 cells (2h pulse - 48h chase)

The first condition involved analysing cells during a metabolic labelling experiment (2 h pulse and 48 h chase) as well as seeding cells, which resulted in over confluence when collected.

Briefly, cells were seeded at $3x10^4/cm^2$ and during 48 hrs of chase cells were treated for 24 hours with either 10 µg/mL of rHIgM22 or a non-immunogenic human IgM (used as a negative control).At the conclusion of the time of chase the cells had reached over confluence, and samples were processed as described in Materials and Methods.

The radioactivity of the organic and aqueous phases was measured, and samples were analysed by TLC using the solvent systems $CHCl_3$:CH_3OH:H_2O 110/40/6 (v/v/v) and $CHCl_3$:CH_3OH:$CaCl_2$ 0.2% 55/45/10 (v/v/v), respectively. Subsequently, the radioactive SLs were detected by digital autoradiography (^{T}Racer Beta-Imager) and quantified with M3Vison software (Biospace. Paris. FR).

By analysing the most hydrophobic lipids in the organic phase (**Figure 25**), including Cer, PE, neutral GLs, and PE, it was determined that the two antibodies have opposing effects on the lipids examined in both sub-populations. Specifically, adherent cells treated with rHIgM22 showed a significant decrease in GlcCer, SM, and PE compared to the control IgM, whereas in floating cells the opposite occurs: an increase in all lipids examined after treatment with rHIgM22, with only GlcCer showing a significant effect. In terms of PE, there is also a significant decrease in adherent cells that were treated with rHIgM22 in comparison to both other conditions investigated, namely, the untreated and treated with control IgM conditions.

Even among gangliosides analysed in the aqueous phases, a similar phenomenon has been identified. However, what is identified is a significant decrease in GM1 ganglioside in rHIgM22-treated adherent cells *vs.* the control IgM, and a significant increase in GD1a ganglioside in rHIgM22 -treated floating cells if compared to the control IgM (**Figure 26**).

Considering this, it could be possible to imply that the function of the antibody rHIgM22 is to restore cells to a healthier state in order to exert its biological activity through alterations of lipid-dependent membrane organisation and/or signalling.

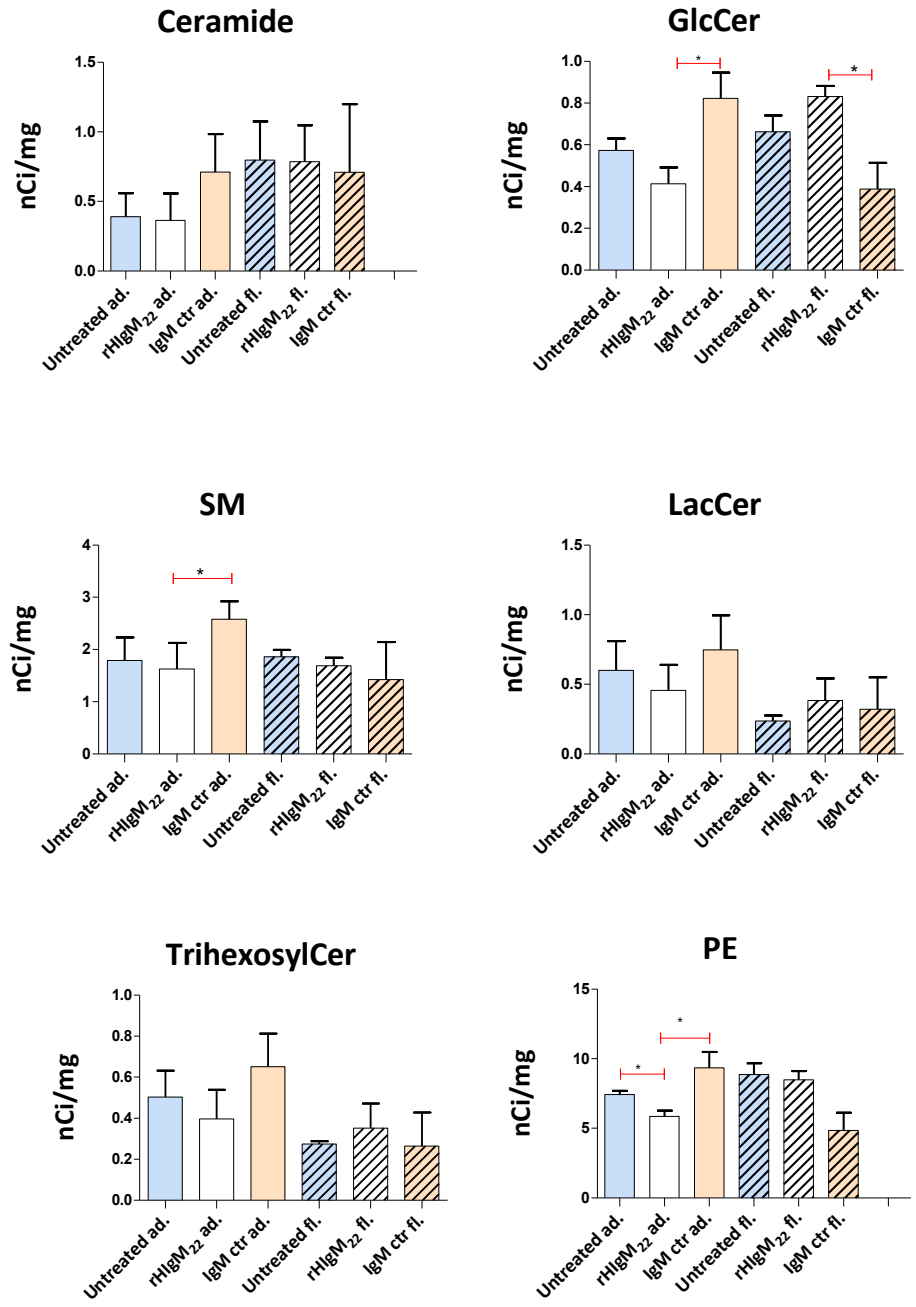

Figure 24 ***Effect of rHIgM22 on hydrophobic lipids of BV-2 cells collected in over-confluence.*** *BV-2 cells were seeded at density of 3x10^4 cells/cm^2.Metabolic labelling with [1-^{3}H] sphingosine (2h pulse-48h chase)was performed. 10µg/mL of either rHIgM22 or Human IgM 24 hrs treatment was carried out.* . At the conclusion *samples were processed as described in Materials and Methods. Lipids of organic phases were separated by HPTLC employing $CHCl_3$: CH_3OH: H_2O 110/40/6 (v/v/v) as solvent systems, respectively, and analysed by digital autoradiography. Data derive from three biological replicate of the same experiments conducted with cells collected in over-confluence The quantification of each separated lipids was performed using M3 vision software, and the values displayed are normalized nCi/mg of protein ±SD determined using an unpaired t-test. * p<0.05.*

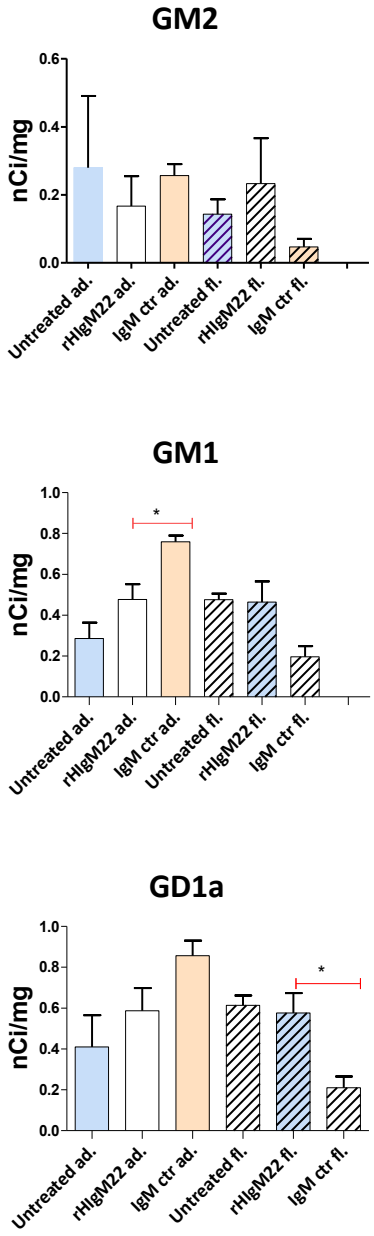

Figure 25 ***Effect of rHIgM22 on hydrophilic lipids of BV-2 cells collected in over-confluence*** *BV-2 cells were seeded at density of $3x10^4$ cells/cm^2.Metabolic labelling with [1-^{3}H] sphingosine (2h pulse-48h chase)was performed. 10µg/mL of either rHIgM22 or Human IgM 24 hrs treatment was carried out.* . At the conclusion *samples were processed as described in Materials and Methods. Lipids of organic and aqueous phases were separated by HPTLC employing $CHCl_3$:CH_3OH: $CaCl_2$ 0.2% in H_2O 55:45:10 as solvent systems and analysed by digital autoradiography. Data derive from three biological replicate of the same experiments conducted with cells collected in over-confluence. The quantification of each separated lipids was performed using M3 vision software, and the values displayed are normalized nCi/mg of protein ±SD determined using an unpaired t-test. * p<0.05.*

4.2 Effects of rHIgM22 on the sphingolipid patter of BV-2 cells (2h pulse - 12 h chase)

The other experiment, instead, was conducted under steady-state metabolic conditions identified by the analysis of sphingolipid turnover. Briefly, cells were seeded at $1.5x10^4/cm^2$, and during 12 hrs of chase cells were treated for 12 hrs with either 10 μg/mL of rHIgM22 or a non-immunogenic human IgM (used as a negative control).At the conclusion of the time of chase the cells had reached 80-90% confluence, and samples were processed as described in Materials and Methods.

The radioactivity of the organic and aqueous phases was measured, and samples were analysed by TLC using the solvent systems $CHCl_3$:CH_3OH:H_2O 110/40/6 (v/v/v) and $CHCl_3$:CH_3OH:$CaCl_2$ 0.2% 55/45/10 (v/v/v), respectively. Subsequently, all the radiolabelled SLs were evaluated with digital autoradiography (^{T}Racer Beta-Imager) and quantified with M3Vison software (Biospace. Paris. FR). This experiment was conducted only once.

From the analysis of the most hydrophobic lipids in the organic phase, Cer, SM, neutral GLs, and PE, it was determined, in terms of nCi/mg of protein, that rHIgM22 induces a decrease in all the lipids examined in comparison to the control IgM, in both sub-populations, with the exception of LacCer and TrihexosylCer which are increased only in adherent cells (**Figure 27**). Instead, the effect of rHIgM22 on gangliosides varies depending on the ganglioside considered. In adherent and floating cells, rHIgM22 induces an increase of GM2 in respect of the control IgM, whereas it induces a decrease of GM1 and GD1a in both adherent and floating cells in respect of the control IgM (**Figure 28**).

Considering this new condition, it is clear that the two antibodies have different effects when compared to one another, and if we consider the effect of rHIgM22, we observe a trend similar to that observed in the previous experiment, conducted under different metabolic labelling conditions: rHIgM22 appears to bring the amount of lipids closer to the untreated conditions, as it may be the optimum for correct membrane lipids reorganization.

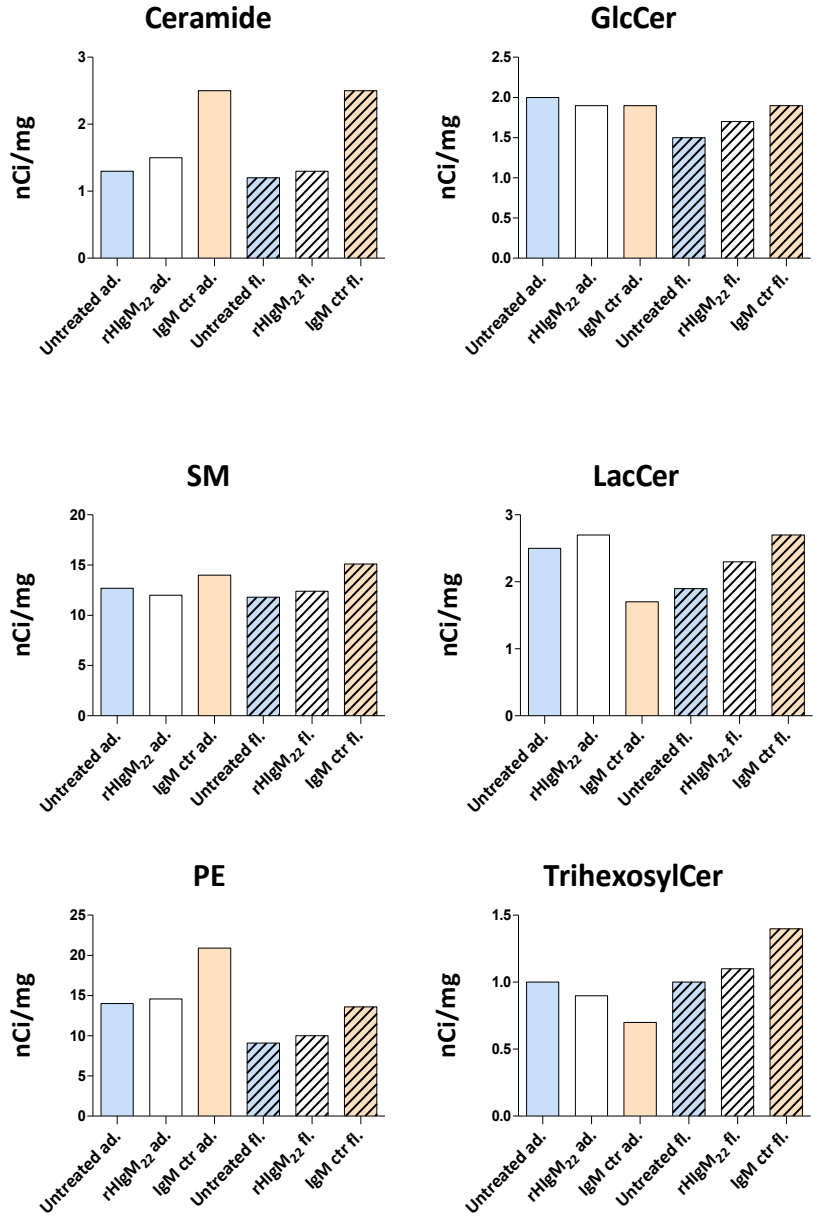

<u>Figure 26</u> Effect of rHIgM22 on hydrophobic lipids of BV-2 cells collected at optimal confluence. *BV-2 cells were seeded at a density of 1.5x10^4 cells/cm^2. Metabolic labelling with [1-^{3}H] sphingosine (2h pulse-48h chase)was performed. 10µg/mL of either rHIgM22 or Human IgM 24 hrs treatment was carried out.* At the conclusion, *samples were processed as described in Materials and Methods. Lipids of organic phases were separated by HPTLC employing $CHCl_3$: CH_3OH: H_2O 110/40/6 (v/v/v) as solvent systems, respectively, and analysed by digital autoradiography. The quantification of each separated lipids was performed using M3 vision software, and the values displayed are normalized nCi/mg of protein.*

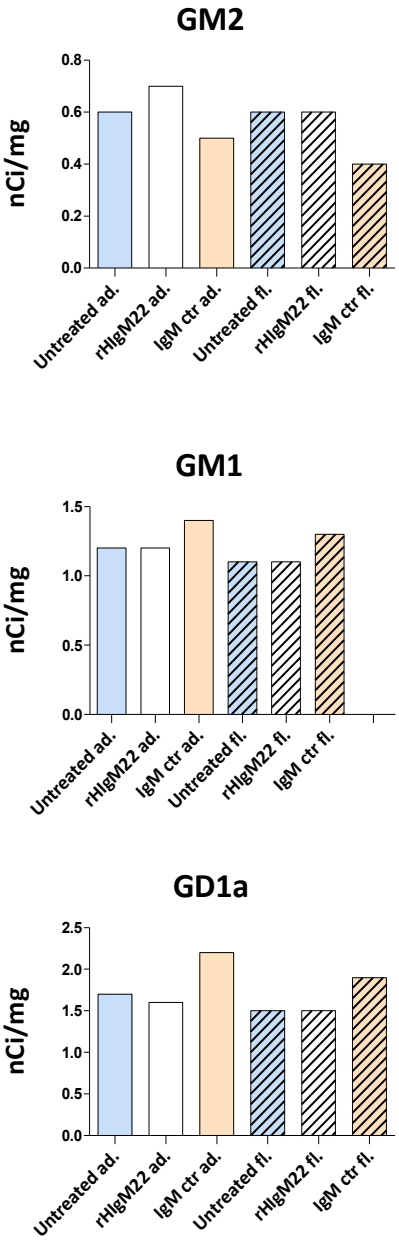

Figure 27 ***Effect of rHIgM22 on hydrophilic lipids of BV-2 cells collected at optimal confluence.*** *BV-2 cells were seeded at a density of $1.5x10^4$ cells/cm^2. Metabolic labelling with [1-^{3}H] sphingosine (2h pulse-48h chase)was performed. 10µg/mL of either rHIgM22 or Human IgM 24 hrs treatment was carried out.* . At the conclusion s*amples were processed as described in Materials and Methods. Lipids of organic and aqueous phases were separated by TLC employing $CHCl_3$:CH_3OH: $CaCl_2$ 0.2% in H_2O 55:45:10 as solvent systems and analysed by digital autoradiography. The quantification of each separated lipids was performed using M3 vision software, and the values displayed are normalized nCi/mg of protein.*

DISCUSSION

The Central Nervous System (CNS) is equipped with microglia, which are specialised resident immune cells (Colonna and Butovsky, 2017).

During development, microglia migrate from the yolk sac to the CNS, where they perform numerous functions, including the elimination of non-functional synapses, maintaining brain homeostasis, and protecting the CNS by acting as a sensory cell against any intrusion or insult (Aguzzi et al., 2013, Plastini et al., 2020, Domingues et al., 2016, Barres, 2008).

In addition to their physiological roles, microglia play important roles under several pathological conditions. In particular in demyelinating diseases such as multiple sclerosis they are transformed into phagocytes able to remove myelin debris thus creating an environment favourable to myelin repair (Neumann et al., 2009, Domingues et al., 2016).

Microglia can be both beneficial and harmful during diseases is quite a delicate question of proportion depending on when microglia are activated, and on the high or low inflammatory environment into which microglia is stimulated to act. Indeed, they secrete various soluble factors and cytokines (*e.g.,* TNF-α, IGF-1 and tissue inhibitor of metalloproteinases-1 (timp-1)) that can stimulate the recruitment and/or differentiation of OPCs, thereby promoting remyelination, but they also play a detrimental role by secreting the same factor (*e.g.,* TNF-α) and other factors (*e.g.,* IL-1β) that can induce astrogliosis, foment neuroinflammation and thus stimulates the resulting demyelination (Baaklini et al., 2019, Jha et al., 2019, Sen et al., 2022).

Multiple sclerosis is a chronic, demyelinating disease that causes axon loss with physical and sensory impairment, afflicts young adults, and is incredibly prevalent worldwide (Thompson et al., 2018). Although it has been known for a very long time, very little is known about its causes; however, it is hypothesised that an autoimmune attack (Lubetzki and Stankoff, 2014) first determines myelin damage and a consequent higher neuroinflammation into which all glial cells are involved. At the onset of pathology, endogenous mechanisms leading to the partial repair of damaged myelin are triggered, however these mechanism are not efficient and do not allow a definitive repair (Barres, 2008, Lassmann, 2014, Domingues et al., 2016, Thompson et al., 2018, Podbielska et al., 2013, Hanafy and Sloane, 2011, Ferrer, 2018).

Nevertheless, the existence of these endogenous mechanisms suggests that treatments able to stimulate and potentiate these mechanisms might represent valuable therapeutical

approaches aimed not only at alleviating symptoms but also at halting the progression of the disease. Among therapies promoting remyelination, the recombinant human antibody IgM22 (rHIgM22) is very promising. rHIgM22 is the recombinant form of a naturally occurring antibody isolated from a patient with Waldenström macroglobulinemia; it is able to bind selectively to myelin in vitro and to the surface of cultured oligodendrocytes (Warrington et al., 2000). It was shown to promote remyelination in mouse models of chronical demyelination (Mullin et al., 2017, Warrington et al., 2000, Bieber et al., 2002).

The mechanism of action of rHIgM22 is complex and still not totally understood, but apparently the main cellular target is represented by cells belonging to the oligodendrocyte lineage. On the other hand, it has been shown that rHIgM22 stimulates microglia to proliferate and phagocytize myelin debris through the antibody FC domain bound to myelin being recognised by complement receptor three of microglia [1]. In addition, data from our lab (article under revision) demonstrated that rHIgM22 was able to bind to various lipids *in vitro*, and that rHIgM22 binding to OPCs and OLs in culture was able to elicit significant changes in the expression of some glycolipids, in particular gangliosides, suggesting that reorganisation of the lipid membrane microenvironment may be relevant to rHIgM22 its biological activity (Grassi et al., 2015). Indeed, these findings agree with the existing literature, that suggests that the binding target of rHIgM22 may be associated with lipid rafts and that the biological activity of rHIgM22 might be dependent on the organisation of lipid rafts (Wright et al., 2009, Howe et al., 2004).

Since microglia are important players in myelin repair and could be a target for the remyelinating-promoting antibody rHIgM22, which is thought to work through a certain mechanism, the microglial cell line BV-2 was used for all analyses instead of primary microglia because of the low yield of the latter.

BV-2 cells derive from the C57BL/6 mouse brain and are transformed by recombinant retrovirus (v-raf/v-myc). This cell line is a continuous culture, which grows semi-adherent, where adherent and floating cells may represent two different sub-populations. BV-2 cell line is widely used instead of primary microglia because it retains the morphological, phenotypical, and functional properties described for freshly isolated primary microglia (Blasi et al., 1990).

First, the viability of floating cells was assessed, since suspended cells are usually dead in adherent cell cultures. The trypan blue exclusion assay showed that 94% of the floating cells were alive.

After seeding the cells at two distinct densities and achieving two distinct confluence states within 72 hours, a growth curve was constructed to evaluate the number of cells and protein distribution of both cell sub-populations every 24 hours.

The numerical values of each sub-population for each seeding density were used to construct a growth curves (**Figure 1**) that illustrate the distribution of adherent and floating cells in relation to the seeding density. Both sub-populations grow exponentially for 72 hours, but in the case of cells seeded at $1.5x10^4$ cells/cm^2 (Figure 1_ panel a), this time corresponds to the optimal confluence in which the adherent cells have reached 80-90% confluence, whereas in the case of cells seeded at $3x10^4$ cells/cm^2 (Figure1_ panel b), this corresponds to over confluence.

Being a semi-adherent cell culture in which the floating cells are viable, the correct definition of confluence has been somewhat misleading. In fact, if the growth curve gives information on exponential growth that seems equal in both seeding density and cell density, it is the vision under the microscope in conjunction with the protein quantification that allowed the optimal confluence to be determined.

Indeed, the quantification of proteins after collection revealed the differences that were evaluated by looking at the cells in the plate; in fact, for cells seeded at the lower density and that have reached optimal confluence after 72 hours of culturing, adherent cells account for 79.7% and floating cells for 20.3%, whereas for cells seeded at the higher density, the proportions of adherent and floating cells are similar: 55.9% adherent cells and 44.1% floating cells. In the latter instance, however, the floating cells are not only floating cells but also adherent cells that have detached due to the lack of space on the support.

Furthermore, because it has been reported in the literature that the biological activity of rHIgM22, may require a multimolecular complex consisting of Lyn, integrin αvβ3 and PDGFαR which by triggering Lyn activation promotes OPCs proliferation while decreasing the activity of the Src kinase family protein c-Src and Fyn (Watzlawik et al., 2010, Watzlawik et al., 2013a),

the expression of all of these protein where evaluated in BV-2 cell under basal conditions, meaning a condition in which there are no external stimuli and the culture is maintained with a complete medium supplemented with 10% FBS.

Remarkably, the presence of PDGFαR could not be revealed by western blotting in both sub-populations (**Figure 2**), suggesting that the biological effects of rHIgM22 in microglia might involve a mechanism completely different than in OPCs.

Regarding other proteins known to be directly involved in the mechanism of action of rHIgM22, Lyn, Fyn, and integrin αV, the same expression is observed in both cell sub-populations (**Figure 2**); however, adherent cells express more of integrin β_3 and the non-receptor tyrosine kinase c-Src.

Furthermore, the expression of caveolin-1 (Cav-1) was examined; Cav-1 is normally enriched in caveolae, which are flask-shaped invaginations of the plasma membrane enriched in cholesterol and GSLs that have been linked to cell signalling (Hooper, 1999) Moreover, Cav1 is also functioning as a membrane adaptor protein enriched in lipid rafts, which has been identified as a structural and metabolic regulator of microglia (Niesman et al., 2013b).

Indeed, it was reported that the expression of the caveolins, both isoforms 1 and 3, changed in microglia when polarising from a resting-surveillant state to an active state. In the patrolling state, microglia express high levels of Cav-1 and low levels of Cav-3 while in the activated state the expression levels of the two isoforms are inverted (Niesman et al., 2013b). However, in a different paper that focused on raft markers in astrocytes and microglia after exposure to stressful events, the absence of caveolin-1 and caveolin-2 in microglia was affirmed (Yun et al., 2011).

Since the analysis was performed on cells in the absence of external stimuli, only the expression of isoform 1 was evaluated, and it was discovered that neither subpopulation of BV-2 contains this protein (**Figure 2**)

Moreover, the expression of PrP, a GPI anchored protein usually regarded as a lipid raft marker, involved in many cellular functions such as cell proliferation, cell signalling, and protection against stress (Legname, 2017, Linden, 2017), and AKT or protein kinase B, a non-

raft marker and a fine regulator of cells survival, proliferation and cell metabolism (Song et al., 2005), were evaluated. There are no significant differences between the two sub-populations in the expression of these last two antigens (**Figure 2**).

Thus, it is possible to hypothesise that there are no significant differences between the two sub-populations in terms of the evaluated antigens.

Since there was no information regarding the lipid composition of microglia in the literature, we analysed the lipid pattern of BV-2 in the absence of external stimuli, in a condition that we have termed basal, by maintaining the cells in complete culture medium with 10% FBS for 72 hours prior to collection.

It has been reported that cell confluence affects lipid composition (Frechin et al., 2015, Puliafito et al., 2012).

Therefore, the analyses were performed on the same lipid classes by thin-layer chromatography and, in some cases, ESI-mass spectrometry. The samples are derived from cells collected at two distinct confluence states 72 hours after seeding at two distinct densities, similar to those used for growth curves.

At both confluence situations, all lipid classes, including phospholipids, cholesterol, and sphingolipids, have been analysed in both sub-populations. These analyses revealed that the lipid compositions of the two sub-populations were clearly different.

Through TLC analysis, the first information that emerges independently of the sub-population examined or the type of confluence considered, is that BV-2 cells are void of galactosylceramide (**Figure 13**) and sulfatide (**Figure 15**). The absence of sulfatide, is particularly remarkable if we consider the lipid targets bound by rHIgM22; indeed, this lipid has been identified in our laboratory as the lipid to which rHIgM22 binds with the highest affinity *in vitro* (Grassi et al., 2015, Grassi et al., 2023). Moreover, literature indicates that significant binding of rHIgM22 in cultured cells was only observed in mature, sulfatide-expressing oligodendrocytes, and that the binding was absent in tissues from CST KO animals (Wright et al., 2009).

Moreover, it was assessed that there is no difference in phospholipid content between adherent and floating cells; however, the high amount of phosphatidylcholine (PC) relative to phosphatidylethanolamine (PE) in both sub-populations at both stages of confluence is noteworthy. Indeed, the higher content of PC is quite rare if compared to other glial cells, such as oligodendrocytes, which contain a greater amount of PE (Fressinaud et al., 1990).

Likewise, cholesterol content was evaluated through TLC analysis using standard of cholesterol at known concentration and no significant differences were found between the two sub-populations or the two confluence situations studied.

Considering other lipid classes, the state of collection at 80-90% confluence or over confluence distinguishes the two sub-populations. First, TLC analysis was used to obtain basic information, which was then supported with electrospray ionisation mass spectrometry analysis for lipid classes that were significantly different or difficult to identify via TLC analysis.

In cells plated at a density of $1.5x10^4$ cells per square centimetre, it was discovered that floating cells contain more ceramide, the simplest sphingolipid, than adherent cells (**Table 4**). Additionally, complementary ESI-MS revealed that ceramide has a distinct distribution in relation to sphingoid bases. Ceramide is mostly composed of 18:1 and other sphingoid backbone (**Figure 7**).

In this regard, the abnormal enrichment of very short sphingoid-based ceramides with 14 carbon atoms (tetradecasphinganine (Pruett et al., 2008)) with 14 to 24 carbon atom acyl chains was discovered. Although they have been identified in plants, animals, and humans, ceramides with such a short sphingoid backbone are uncommon, as are other sphingoid bases with an odd carbon atom number (Pruett et al., 2008, Farwanah et al., 2007, Shaner et al., 2009, Fyrst et al., 2004). *Drosophila melanogaster* possesses the largest amount of 14-carbon atom sphingoid bases identified to date (Fyrst et al., 2004). In fact, in mammals, the majority of sphingoid backbone is represented by 18:0 and 18:1, 16:0 and 16:1, which represent sphinganine and sphingosine with 16 and 18 carbon atoms (Merrill, 2011); this predominance in mammals is due to the preference of serine palmitoyl-transferase (SPT) for saturated fatty acyl-CoA with 16 or 18 carbon atom (Pruett et al., 2008).

Moreover, considering different acyl chains, some of which also appear to be rare, they have been identified in a variety of living being, and the different length is due to the preference of the six isoforms of ceramide desaturase (Mizutani et al., 2005, Ho et al., 2022).

Among SLs, in cells collected at 80-90% confluence, it was discovered that the adherent cells have a greater amount of sphingomyelin than floating cell (***Table 4***). The sphingoid bases and acyl chains have been characterised by specific mass spectrometry analysis, and the enrichment in adherent cells has been confirmed; however, even though sphingomyelins sphingoid base are numerous, the most prevalent sphingoid bases are 18:0 and 18:1 (**Figure 10**; **Figure 11**).

This may lead to hypothesise sphingomyelin cannot be formed from short-chain ceramides and that short-chain ceramides result from the cleavage of more complex sphingolipids. Thus, the enrichment of ceramide in floating cells, particularly ceramide 14:0, may support the notion that these cells are undergoing apoptosis.

In addition, neutral glycolipids were analysed with mass spectrometry due to the limited amount of these lipids in these cells, which prevented TLC from providing an exhaustive result for all. This analysis revealed that glucosylceramide is more prevalent in adherent cells; accordingly, the analysis was a confirmation of that obtained via TLC using a standard of known concentration (**Figure 12**). While lactosylceramide identified by TLC was just suggested due to its low amount, its abundance in the adherent cells was identified via ESI-MS analysis (**Table 8**). In the case of trihexosylceramide, which was impossible to identify by TLC, its enrichment, in respect of total amount of sample analysed, was detected in floating cells (**Table 9**).

Regarding the analysis of gangliosides, the sialic acid containing GLS, it is clear from the TLC analysis that this lipid class is among the lowest represented in BV-2; in fact, despite a quantitative enrichment in respect of total amount of sample analysed, of gangliosides in adherent cells, only two species of gangliosides, GM1 and GD1a, are present in both microglia sub-population (**Figure 16**). Moreover, with both techniques, gangliosides in adherent cells were enriched relative to the total amount of the sample analysed, and ganglioside GD1a alone was found in a greater percentage, in respect of total, in floating cells.

In cells seeded at $3x10^4/cm^2$ and collected in over-confluence, phosphatidylethanolamine (PE) is the only lipid which varies significantly between the two sub-populations; however, this difference was not confirmed by the specific analysis of phospholipids by TLC, since the TLC analysis was conducted in single.

A plausible explanation for the increase of PE in floating cells may be similar to that of the increase of ceramide in floating cells collected at 80-90% confluence, such as the possibility for this cell sub-population to be in close proximity to cell death; In this regard, the transfer of phospholipids such as PE from the inner to the outer leaflet in response to the "eat me" signal during apoptosis is a well-known occurrence (Farooqui et al., 2000) (Harayama and Riezman, 2018); and also, it has been seen that in hepatoma cells (HepG2 cells) that treatment with exogenous PE, induces apoptosis via the mitochondrial pathway (Yao et al., 2009), thus the increased PE amount could be a pro-apoptotic signals.

In addition, TLC has not identified any differences between several lipids among the more hydrophobic ones, so mass spectrometry analysis has not been performed on these samples.

In addition to the differences found, the comparison of the same lipids between the two different situations of confluence, has revealed an inversion in the ratio of ceramide to glucosylceramide, with glucosylceramide being more abundant than ceramide, in adherent cells collected at 80-90% confluence. This evidence could indicate a preference for the biosynthetic pathways in 80-90% confluent cells in respect of the other, similar result were obtained here (Frechin et al., 2015).

Concerning gangliosides in cells collected at over-confluence, the same lipid species are present in both sub-populations; however, TLC reveals a greater number of gangliosides species in cells collected at over-confluence (**Figure 21**). Gangliosides, GM2, GM1, GD1a, GalNacGD1a, and GD1b and their enrichment in adherent cells, in respect of the amount analysed, have been found and confirmed by mass spectrometry (**Table 15**).

Regarding gangliosides, there are great differences between the two confluences considered; however, it should be noted that the sensitivity of the TLC analysis depends on the amount of

sample analysed. In cells collected at 80-90% confluence, a very low amount of sample (equivalent to 1 mg of protein) for each subpopulation, was analysed by TLC and the same amount was analysed by mass spectrometry, whereas for over-confluent cells, since it resulted in a greater amount of sample due to the culture conditions (as identified by the growth curve), an higher amount of sample was analysed with TLC and mass spectrometry, resulting in a greater degree of accuracy.

Moreover, if we only consider the mass spectrometry data, we observe that the lipid species are identical, except for the presence of GalNacGD1a only in over-confluent cells. In both confluence conditions, adherent cells have higher ganglioside levels than floating cells. Furthermore, if each ganglioside is considered separately, GD1a is always enriched in the floating cells.

According to these analyses, the degree of confluence modifies the different lipid composition between adherent and floating cells. However, it can also be observed that there are no lipid species that are exclusive to one subpopulation. Instead, both sub-populations have the same lipids, that are distributed in different ways depending on the degree of confluence; Except for GalNacGD1a, which is present in very small quantities compared to the total sample only in over-confluent cells.

Given the scarcity of glycosphingolipids in this cell line, the analyses continued through metabolic labelling with a tritiated precursor, namely [1-^{3}H]sphingosine, that allowed to identify the correct experimental setting conditions of steady state, identifying in a situation of equilibrium between biosynthesis and catabolism characterised by a radiolabelled sphingolipid composition mirroring that of endogenous lipids.

This first experiment of metabolic labelling has allowed us to characterise the sphingolipid turnover of BV-2 cells. Setting the experiment with a feeding time of two hours for the tritiated precursor (2h pulse) and three different chase times, 12 hours, 24 hours, and 48 hours. The time of chase is the period during which cells metabolise and use the precursor to synthesise all sphingolipids.

This experiment allowed us to determine the optimal experimental conditions for accurately evaluating the potential effects of the rHIgM22 antibody on the sphingolipid pattern of these

cells, using the same methodology that allowed to determine the effect of rHIgM22 of the sphingolipid pattern cells of the oligodendroglial lineage (S. Grassi et al. , 2021).

After all of the radiolabelled lipids were analysed at each time of chase, it was discovered that each lipid is present throughout this kinetics analysis; what differs in both sub-populations is their proportional amount in relation to the total, expressed as nCi/mg. Some of the lipids evaluated have a peak at 12 h of chase, and then decrease, with a sharper decrease in floating cells: GlcCer, LacCer, SM, PE, GM1, and GD1b (**Figure 22**; ***Figure 23***). Since there is no sharp decrease in all lipids over 12 hours, we focused on PE, the only phospholipid visible during a metabolic labelling experiment that is more related to catabolism.

Despite the fact that it lacks a sphingoid base, this lipid is radiolabelled because it is the end product of an irreversible reaction catalysed by sphingosine lyase (S1P lyase), which cleaves sphingosine 1-phosphate in into ethanolamine-phosphate and a long chain aldehyde (hexadecenal) (Hannun and Obeid, 2008). This lipid was evaluated to be lower at 24 hours of chase in terms of nCi/mg of protein in adherent cells. Still PE was found to be equal in adherent cells and less in floating cells, in respect of all other lipids, only at 12 hours of chase, in comparison with the other time of chase. In consideration of this, we have identified the situation most representative of the balance between synthesis and catabolism in the first 12 hours of the chase.

rHIgM22 has been shown to change the lipid pattern of oligodendrocytes (S. Grassi et al. , 2021), and we have shown that the lipid pattern of BV-2 changes significantly depending on how close the cells are together, so we did two very different experiments to find out how the antibody affects the lipid pattern of these cells.

In a first experiment, cells seeded at $3x10^4/cm^2$ were collected in over-confluence. Following a metabolic labelling of 2 hours of pulse and 48 hours of chase, a 24-hour treatment with rHIgM22 antibody or a control IgM was performed.

In the second experiment, instead, cells were seeded at $1.5x10^4/cm^2$ and collected at 80-90% of confluence. Following a metabolic labelling of 2 hours of pulse and 12 hours of chase, a 12-hour treatment with rHIgM22 antibody or a control IgM was performed.

According to radiolabelled lipid analysis, the rHIgM22 antibody alters the lipid pattern of microglia cells.

rHIgM22 and the control IgM have different effects on the lipids studied in both sub-populations after 24 hours of treatment.

Specifically, it was evaluated that rHIgM22 induces in adherent cells a significant decrease of GlcCer, SM, and PE compared to the control IgM, whereas in floating cells only a GlcCer significant increase was assessed.

In addition, a significant decrease in PE in adherent cells treated with rHIgM22 was evaluated with respect to both the control IgM and the untreated cells; therefore, a protective effect by rHIgM22 could be assumed since an excessive amount of PE is possibly related to cell death (Farooqui et al., 2000, Nicolson, 2013, Vance, 2015, Harayama and Riezman, 2018).

Moreover, rHIgM22-treated adherent cells exhibited a significant decrease in GM1 ganglioside relative to the control IgM, while rHIgM22-treated floating cells exhibited a significant increase in GD1a ganglioside relative to the control IgM (**Figure 26**).

Despite being conducted in single, the 12-hour treatment experiment shows that rHIgM22 induces a decrease in Cer, SM, and PE in both sub-populations, a decrease of GlcCer, LacCer, and TrihexosylCer in floating cells, and an increase of LactosylCer and TrihexosylCer in adherent cells in respect of the control IgM (**Figure 27**). Instead, the effect of rHIgM22 on gangliosides varies depending on which ganglioside is considered. In comparison to control IgM, rHIgM22 increases ganglioside GM2 levels while decreasing GM1 and GD1a levels in both sub-populations (**Figure 28**).

Comparing both experimental conditions, it is clear that the effects of the two antibodies, rHIgM22 and the human IgM, used as the negative control, are distinct. However, comparison of rHIgM22 treated cells and untreated cells, in both experiments, reveals a similar pattern: rHIgM22 appears to bring the amount of lipids closer to that of untreated cells, laying the groundwork for a reorganisation of membrane lipids. Consequently, it is plausible to hypothesise that the effect of an increase in phagocytosis activity in microglia following

treatment with rHIgM22, as demonstrated by Zorina and colleagues (Zorina et al., 2018), is due to a reorganisation of membrane lipids to restore the membrane to an optimal condition.

CONCLUSIONS

Given the existing scientific background, regarding the hypothesised mechanism of action of the rHIgM22 antibody on other glial populations, *e.g.* oligodendrocytes (Grassi et al., 2023, Watzlawik et al., 2010, Watzlawik et al., 2013a, Watzlawik et al., 2013b) and its effect on microglia (Zorina et al., 2018) it has become necessary to characterize the lipid profile of this cell population, actively involved in the process of myelin repair.

For various reasons, such as ease of retrieval and the difficulty of using primary microglia due to low yield we used the immortalized microglial cell line BV-2 to perform all experiments.

Although it is a frequently used semi adherent cell line, many features remain unknown and therefore we characterized many aspects of these cells under no external stimuli, starting from the viability, the protein expression, and the lipid profile of both the adherent and the floating subpopulation, assuming they were to some extent representative of two different microglia phenotypes.

We identified the viability of floating cells equal to 94% (***Table 1***) and that of adherent cells around 98%. We tested, whether the re-seeding of floating cells, could influence their behaviour, and indeed we found that the floating cells change their characteristics becoming partially adherent.

To further characterize the two subpopulations, we performed protein expression and lipid analysis.

As regards of protein analysis, we focused on proteins involved in the activity of rHIgM22, without identifying any difference in their expression levels between the two subpopulations. Interestingly, we observed the overall absent expression of the PDGFα receptor. This is a very interesting result considering that PDGFα receptor is among the most involved receptors in the mechanism of action of rHIgM22 {Watzlawik, 2013 #42}.

For what concerns the lipid characterization, we performed lipid analysis harvesting cells at optimal confluence or when they were over- confluent since it has been previously reported that the lipid pattern of cells changes if they grow in a high- or low- crowding area (Frechin et al., 2015, Puliafito et al., 2012). We observed many differences between the two subpopulations and the two harvesting conditions. In particular, adherent and floating cells harvested at optimal confluence differ in ceramide (Cer) and sphingomyelin (SM) content and this could be attributed, in part, to the stage of cell viability. Adherent cells are enriched in SM, whereas the floating cells present a higher content of Cer, which is known for its pro-apoptotic properties. Indeed, by mass spectrometry analysis we discovered that floating cells

are particularly enriched in short-chain Cer species, which cannot be precursors of the most common and represented long-chain SM species (18: 0 and 18:1), leading to the conclusion that floating cells are more prone to face the apoptotic process.

Similarly in cells collected at over confluence, although SM and Cer are at comparable levels between the two sub-populations, it emerged that phosphatidylethanolamine (PE) is significantly abundant in floating cells compared to adherent cells. This lipid is involved in the apoptotic process. In particular, it has been demonstrated that administration of PE to cell cultures induces apoptosis (Yao et al., 2009). Thus, again, the abundance of PE in floating cells suggests that this sub-population is close to undergoing apoptosis.

Moreover, when lipids of the two-confluence state are compared, especially regarding adherent cells, the percentage ratio between Cer and GlcCer changes. Cells collected at optimal confluence have more GlcCer than Cer, while overconfluent cells have the opposite.

Thus, from all these overall analyses, we can hypothesize that the floating cells might be less active in the biosynthetic pathway than the adherent cells, and the condition of optimal confluence is the ideal one to obtain good results in the future

We have also thoroughly analysed the gangliosides pattern of BV- 2 cells, even if it is a very little represented class of sphingolipids in this cell line. No significant difference has emerged between the two sub-populations nor between the different stages of confluence, the only difference emerged is the presence of the GalNacGD1a in over-confluent cells, which however is in negligible quantity when compared to all the others. Thus, a general enrichment of gangliosides was observed in adherent cells with respect to floating ones.

To the side of everything, without considering any difference in culture conditions nor between sub-populations, it emerged that BV-2 cells are completely devoid of sulfatides and galactosylceramide. This result is very intriguing because it has been previously demonstrated that the remyelination promoting antibody rHIgM22 mainly targets sulfatide, in other glial populations, *e.g.* oligodendrocytes (Grassi et al., 2023). However, sulfatide is not the only targeted lipid, also some phospholipids such as Phosphatidic Acid (PA), Phosphatidylserine (PS), and Phosphatidylinositol (PI) can be recognized by rHIgM22 (Grassi et al., 2023).

Conveniently, in each sub-populations at both stages of confluence, PS and PI, are present, although in smaller amounts compared to other phospholipids, such as PC and PE (***Table 3***;***Table 12***).

Nevertheless, it is of note that rHIgM22 is an IgM, and therefore it has a wide binding site. Indeed, even if BV-2 cells lack sulfatide, they respond to rHIgM22 treatment by increasing their phagocytic activity as demonstrated by Zorina and colleagues (Zorina et al., 2018) and by the results presented in this PhD work. The preliminary data obtained show how the antibody alters the lipid microenvironment of these cells and acts differently on the two subpopulations. Specifically, although the effects of the antibody are multiple in comparison to the control IgM and untreated cells (see results section **Figure 25**, **Figure 26**, **Figure 27**, **Figure 28**) the most noticeable effect is the decrease of PE in adherent cells, collected at both confluence state, for which a protective effect of rHIgM22 could be assumed.

Comparing both experimental conditions, it is clear that the effects of the two antibodies, rHIgM22 and the human IgM, used as the negative control, are distinct. Moreover, the comparison of cells treated with rHIgM22, and untreated cells shows a similar pattern in both experiments: rHIgM22 seems to bring the amount of lipids closer to that of the untreated cells, thus providing the basis for a reorganisation of membrane lipids. It is therefore plausible to hypothesise that the effect of increased phagocytosis activity in microglia after treatment with rHIgM22 demonstrated by Zorina and colleagues (Zorina et al., 2018) is due to a reorganisation of membrane lipids to restore the membrane to an optimal state.

Considering all the obtained results, we can affirm that the BV-2 cell line, widely used worldwide as a microglial model, has a very peculiar lipid composition, which differs between the two sub-populations and varies depending on the confluence considered. Moreover, we have identified significant differences with respect to other glial cells mainly concerning the possible binding target and the protein complex possibly involved in the mechanism of action of the remyelination promoting antibody rHIgM22.

Given the importance of microglia in myelin repair processes in demyelinating diseases such as multiple sclerosis, having a good *in vitro* model is an essential step to further investigate rHIgM22 mechanism of action and effects, with the ultimate purpose to help finding the correct therapeutic strategy against one of the most common demyelinating pathologies.

REFERENCES

ABU-RUB, M. & MILLER, R. H. 2018. Emerging Cellular and Molecular Strategies for Enhancing Central Nervous System (CNS) Remyelination. *Brain Sci,* 8.
AGGARWAL, S., YURLOVA, L. & SIMONS, M. 2011a. Central nervous system myelin: structure, synthesis and assembly. *Trends in Cell Biology,* 21**,** 585-93.
AGGARWAL, S., YURLOVA, L. & SIMONS, M. 2011b. Central nervous system myelin: structure, synthesis and assembly. *Trends Cell Biol,* 21**,** 585-93.
AGUZZI, A., BARRES, B. A. & BENNETT, M. L. 2013. Microglia: scapegoat, saboteur, or something else? *Science,* 339**,** 156-61.
ALIZADEH, A., DYCK, S. M. & KARIMI-ABDOLREZAEE, S. 2015. Myelin damage and repair in pathologic CNS: challenges and prospects. *Front Mol Neurosci,* 8**,** 35.
ANDERSON, R. G. 1998. The caveolae membrane system. *Annu Rev Biochem,* 67**,** 199-225.
ANTONUCCI, F., TUROLA, E., RIGANTI, L., CALEO, M., GABRIELLI, M., PERROTTA, C., NOVELLINO, L., CLEMENTI, E., GIUSSANI, P., VIANI, P., MATTEOLI, M. & VERDERIO, C. 2012. Microvesicles released from microglia stimulate synaptic activity via enhanced sphingolipid metabolism. *EMBO Journal,* 31**,** 1231-40.
AURELI, M., GRASSI, S., PRIONI, S., SONNINO, S. & PRINETTI, A. 2015. Lipid membrane domains in the brain. *Biochim Biophys Acta,* 1851**,** 1006-16.
BAAKLINI, C. S., RAWJI, K. S., DUNCAN, G. J., HO, M. F. S. & PLEMEL, J. R. 2019. Central Nervous System Remyelination: Roles of Glia and Innate Immune Cells. *Front Mol Neurosci,* 12**,** 225.
BANSAL, A. S., ABDUL-KARIM, B., MALIK, R. A., GOULDING, P., PUMPHREY, R. S., BOULTON, A. J., HOLT, P. L. & WILSON, P. B. 1994. IgM ganglioside GM1 antibodies in patients with autoimmune disease or neuropathy, and controls. *Journal of Clinical Pathology,* 47**,** 300-2.
BARRES, B. A. 2008. The mystery and magic of glia: a perspective on their roles in health and disease. *Neuron,* 60**,** 430-40.
BARTKE, N. & HANNUN, Y. A. 2009. Bioactive sphingolipids: metabolism and function. *J Lipid Res,* 50 Suppl**,** S91-6.
BERGHOFF, S. A., SPIETH, L. & SAHER, G. 2022. Local cholesterol metabolism orchestrates remyelination. *Trends Neurosci,* 45**,** 272-283.
BERGHOFF, S. A., SPIETH, L., SUN, T., HOSANG, L., SCHLAPHOFF, L., DEPP, C., DUKING, T., WINCHENBACH, J., NEUBER, J., EWERS, D., SCHOLZ, P., VAN DER MEER, F., CANTUTI-CASTELVETRI, L., SASMITA, A. O., MESCHKAT, M., RUHWEDEL, T., MOBIUS, W., SANKOWSKI, R., PRINZ, M., HUITINGA, I., SEREDA, M. W., ODOARDI, F., ISCHEBECK, T., SIMONS, M., STADELMANN-NESSLER, C., EDGAR, J. M., NAVE, K. A. & SAHER, G. 2021. Microglia facilitate repair of demyelinated lesions via post-squalene sterol synthesis. *Nat Neurosci,* 24**,** 47-60.
BEVERS, E. M., COMFURIUS, P., DEKKERS, D. W. & ZWAAL, R. F. 1999. Lipid translocation across the plasma membrane of mammalian cells. *Biochim Biophys Acta,* 1439**,** 317-30.
BIEBER, A. J., WARRINGTON, A., ASAKURA, K., CIRIC, B., KAVERI, S. V., PEASE, L. R. & RODRIGUEZ, M. 2002. Human antibodies accelerate the rate of remyelination following lysolecithin-induced demyelination in mice. *Glia,* 37**,** 241-9.
BLASI, E., BARLUZZI, R., BOCCHINI, V., MAZZOLLA, R. & BISTONI, F. 1990. Immortalization of murine microglial cells by a v-raf/v-myc carrying retrovirus. *J Neuroimmunol,* 27**,** 229-37.
BLUNSOM, N. J. & COCKCROFT, S. 2020. CDP-Diacylglycerol Synthases (CDS): Gateway to Phosphatidylinositol and Cardiolipin Synthesis. *Front Cell Dev Biol,* 8**,** 63.
BOGIE, J. F., STINISSEN, P. & HENDRIKS, J. J. 2014. Macrophage subsets and microglia in multiple sclerosis. *Acta Neuropathol,* 128**,** 191-213.
BOSCHER, C. & NABI, I. R. 2012. Caveolin-1: role in cell signaling. *Adv Exp Med Biol,* 729**,** 29-50.
BRAVERMAN, N. E. & MOSER, A. B. 2012. Functions of plasmalogen lipids in health and disease. *Biochimica et Biophysica Acta,* 1822**,** 1442-52.
BREMER, E. G., SCHLESSINGER, J. & HAKOMORI, S. 1986. Ganglioside-mediated modulation of cell growth. Specific effects of GM3 on tyrosine phosphorylation of the epidermal growth factor receptor. *J Biol Chem,* 261**,** 2434-40.
BROWN, D. A. & ROSE, J. K. 1992. Sorting of GPI-anchored proteins to glycolipid-enriched membrane subdomains during transport to the apical cell surface. *Cell,* 68**,** 533-44.
BUTON, X., HERVE, P., KUBELT, J., TANNERT, A., BURGER, K. N., FELLMANN, P., MULLER, P., HERRMANN, A., SEIGNEURET, M. & DEVAUX, P. F. 2002. Transbilayer movement of monohexosylsphingolipids in endoplasmic reticulum and Golgi membranes. *Biochemistry,* 41**,** 13106-15.
BUTT, A. M., DUNCAN, A. & BERRY, M. 1994. Astrocyte associations with nodes of Ranvier: ultrastructural analysis of HRP-filled astrocytes in the mouse optic nerve. *Journal of Neurocytology,* 23**,** 486-99.

CARLIN, C., MURRAY, L., GRAHAM, D., DOYLE, D. & NICOLL, J. 2000. Involvement of apolipoprotein E in multiple sclerosis: absence of remyelination associated with possession of the APOE epsilon2 allele. *J Neuropathol Exp Neurol,* 59**,** 361-7.
CHALMIN, F., ROCHEMONT, V., LIPPENS, C., CLOTTU, A., SAILER, A. W., MERKLER, D., HUGUES, S. & POT, C. 2015. Oxysterols regulate encephalitogenic CD4(+) T cell trafficking during central nervous system autoimmunity. *J Autoimmun,* 56**,** 45-55.
CHOI, J., YIN, T., SHINOZAKI, K., LAMPE, J. W., STEVENS, J. F., BECKER, L. B. & KIM, J. 2018. Comprehensive analysis of phospholipids in the brain, heart, kidney, and liver: brain phospholipids are least enriched with polyunsaturated fatty acids. *Mol Cell Biochem,* 442**,** 187-201.
CHOI, J. Y., KIM, J. Y., KIM, J. Y., PARK, J., LEE, W. T. & LEE, J. E. 2017. M2 Phenotype Microglia-derived Cytokine Stimulates Proliferation and Neuronal Differentiation of Endogenous Stem Cells in Ischemic Brain. *Exp Neurobiol,* 26**,** 33-41.
CHRAST, R., SAHER, G., NAVE, K. A. & VERHEIJEN, M. H. 2011. Lipid metabolism in myelinating glial cells: lessons from human inherited disorders and mouse models. *J Lipid Res,* 52**,** 419-34.
COELHO, R. P., SAINI, H. S. & SATO-BIGBEE, C. 2010. Sphingosine-1-phosphate and oligodendrocytes: from cell development to the treatment of multiple sclerosis. *Prostaglandins Other Lipid Mediat,* 91**,** 139-44.
COLONNA, M. & BUTOVSKY, O. 2017. Microglia Function in the Central Nervous System During Health and Neurodegeneration. *Annu Rev Immunol,* 35**,** 441-468.
CUNNIFFE, N. & COLES, A. 2021. Promoting remyelination in multiple sclerosis. *J Neurol,* 268**,** 30-44.
DASGUPTA, S. & RAY, S. K. 2019. Ceramide and Sphingosine Regulation of Myelinogenesis: Targeting Serine Palmitoyltransferase Using microRNA in Multiple Sclerosis. *Int J Mol Sci,* 20.
DIMOPOULOS, M. A., KASTRITIS, E. & GHOBRIAL, I. M. 2016a. Waldenstrom's macroglobulinemia: a clinical perspective in the era of novel therapeutics. *Annals of Oncology,* 27**,** 233-40.
DIMOPOULOS, M. A., KASTRITIS, E. & GHOBRIAL, I. M. 2016b. Waldenstrom's macroglobulinemia: a clinical perspective in the era of novel therapeutics. *Ann Oncol,* 27**,** 233-40.
DOMINGUES, H. S., PORTUGAL, C. C., SOCODATO, R. & RELVAS, J. B. 2016. Oligodendrocyte, Astrocyte, and Microglia Crosstalk in Myelin Development, Damage, and Repair. *Front Cell Dev Biol,* 4**,** 71.
DULAMEA, A. O. 2017. Role of Oligodendrocyte Dysfunction in Demyelination, Remyelination and Neurodegeneration in Multiple Sclerosis. *Adv Exp Med Biol,* 958**,** 91-127.
DUNCAN, I. D., RADCLIFF, A. B., HEIDARI, M., KIDD, G., AUGUST, B. K. & WIERENGA, L. A. 2018. The adult oligodendrocyte can participate in remyelination. *Proc Natl Acad Sci U S A,* 115**,** E11807-E11816.
EBERT, S., WEIGELT, K., WALCZAK, Y., DROBNIK, W., MAUERER, R., HUME, D. A., WEBER, B. H. & LANGMANN, T. 2009. Docosahexaenoic acid attenuates microglial activation and delays early retinal degeneration. *Journal of Neurochemistry,* 110**,** 1863-75.
ECKHARDT, M. 2008. The role and metabolism of sulfatide in the nervous system. *Mol Neurobiol,* 37**,** 93-103.
EISEN, A., GREENBERG, B. M., BOWEN, J. D., ARNOLD, D. L. & CAGGIANO, A. O. 2017. A double-blind, placebo-controlled, single ascending-dose study of remyelinating antibody rHIgM22 in people with multiple sclerosis. *Mult Scler J Exp Transl Clin,* 3**,** 2055217317743097.
ELMORE, M. R., NAJAFI, A. R., KOIKE, M. A., DAGHER, N. N., SPANGENBERG, E. E., RICE, R. A., KITAZAWA, M., MATUSOW, B., NGUYEN, H., WEST, B. L. & GREEN, K. N. 2014. Colony-stimulating factor 1 receptor signaling is necessary for microglia viability, unmasking a microglia progenitor cell in the adult brain. *Neuron,* 82**,** 380-97.
ENDO, T., SCOTT, D. D., STEWART, S. S., KUNDU, S. K. & MARCUS, D. M. 1984. Antibodies to glycosphingolipids in patients with multiple sclerosis and SLE. *Adv Exp Med Biol,* 174**,** 455-61.
ENE, C.-D. & NICOLAE, I. 2015. Gangliosides and Antigangliosides in Malignant Melanoma. Melanoma – Current Clinical Management and Future Therapeutics.
FAROOQUI, A. A., HORROCKS, L. A. & FAROOQUI, T. 2000. Glycerophospholipids in brain: their metabolism, incorporation into membranes, functions, and involvement in neurological disorders. *Chem Phys Lipids,* 106**,** 1-29.
FARRELL, D. F. & MCKHANN, G. M. 1971. Characterization of cerebroside sulfotransferase from rat brain. *J Biol Chem,* 246**,** 4694-702.
FARWANAH, H., PIERSTORFF, B., SCHMELZER, C. E., RAITH, K., NEUBERT, R. H., KOLTER, T. & SANDHOFF, K. 2007. Separation and mass spectrometric characterization of covalently bound skin ceramides using LC/APCI-MS and Nano-ESI-MS/MS. *J Chromatogr B Analyt Technol Biomed Life Sci,* 852**,** 562-70.
FEIZI, T. 1985. Demonstration by monoclonal antibodies that carbohydrate structures of glycoproteins and glycolipids are onco-developmental antigens. *Nature,* 314**,** 53-7.

FERNANDEZ-MURRAY, J. P. & MCMASTER, C. R. 2007. Phosphatidylcholine synthesis and its catabolism by yeast neuropathy target esterase 1. *Biochim Biophys Acta,* 1771**,** 331-6.
FERRER, I. 2018. Oligodendrogliopathy in neurodegenerative diseases with abnormal protein aggregates: The forgotten partner. *Prog Neurobiol,* 169**,** 24-54.
FFRENCH-CONSTANT, C. & RAFF, M. C. 1986. The oligodendrocyte-type-2 astrocyte cell lineage is specialized for myelination. *Nature,* 323**,** 335-8.
FITZNER, D., BADER, J. M., PENKERT, H., BERGNER, C. G., SU, M., WEIL, M. T., SURMA, M. A., MANN, M., KLOSE, C. & SIMONS, M. 2020. Cell-Type- and Brain-Region-Resolved Mouse Brain Lipidome. *Cell Rep,* 32**,** 108132.
FRANKLIN, R. J. M. & FFRENCH-CONSTANT, C. 2017. Regenerating CNS myelin - from mechanisms to experimental medicines. *Nat Rev Neurosci,* 18**,** 753-769.
FRECHIN, M., STOEGER, T., DAETWYLER, S., GEHIN, C., BATTICH, N., DAMM, E. M., STERGIOU, L., RIEZMAN, H. & PELKMANS, L. 2015. Cell-intrinsic adaptation of lipid composition to local crowding drives social behaviour. *Nature,* 523**,** 88-91.
FRESSINAUD, C., VALLAT, J. M., RIGAUD, M., CASSAGNE, C., LABOURDETTE, G. & SARLIEVE, L. L. 1990. Investigation of myelination in vitro: polar lipid content and fatty acid composition of myelinating oligodendrocytes in rat oligodendrocyte cultures. *Neurochem Int,* 16**,** 27-39.
FUTERMAN, A. H. 2006. Intracellular trafficking of sphingolipids: relationship to biosynthesis. *Biochimica et Biophysica Acta,* 1758**,** 1885-92.
FUTERMAN, A. H. & RIEZMAN, H. 2005. The ins and outs of sphingolipid synthesis. *Trends in Cell Biology,* 15**,** 312-8.
FYRST, H., HERR, D. R., HARRIS, G. L. & SABA, J. D. 2004. Characterization of free endogenous C14 and C16 sphingoid bases from Drosophila melanogaster. *J Lipid Res,* 45**,** 54-62.
GARCIA-REVILLA, J., ALONSO-BELLIDO, I. M., BURGUILLOS, M. A., HERRERA, A. J., ESPINOSA-OLIVA, A. M., RUIZ, R., CRUZ-HERNANDEZ, L., GARCIA-DOMINGUEZ, I., ROCA-CEBALLOS, M. A., SANTIAGO, M., RODRIGUEZ-GOMEZ, J. A., SOTO, M. S., DE PABLOS, R. M. & VENERO, J. L. 2019. Reformulating Pro-Oxidant Microglia in Neurodegeneration. *J Clin Med,* 8.
GAULT, C. R., OBEID, L. M. & HANNUN, Y. A. 2010. An overview of sphingolipid metabolism: from synthesis to breakdown. *Adv Exp Med Biol,* 688**,** 1-23.
GIBSON, C. J., HOSSAIN, M. M., RICHARDSON, J. R. & ALEKSUNES, L. M. 2012. Inflammatory regulation of ATP binding cassette efflux transporter expression and function in microglia. *J Pharmacol Exp Ther,* 343**,** 650-60.
GIUSSANI, P., TRINGALI, C., RIBONI, L., VIANI, P. & VENERANDO, B. 2014. Sphingolipids: key regulators of apoptosis and pivotal players in cancer drug resistance. *Int J Mol Sci,* 15**,** 4356-92.
GLEZER, I., SIMARD, A. R. & RIVEST, S. 2007. Neuroprotective role of the innate immune system by microglia. *Neuroscience,* 147**,** 867-83.
GOLDMANN, T., WIEGHOFER, P., JORDAO, M. J., PRUTEK, F., HAGEMEYER, N., FRENZEL, K., AMANN, L., STASZEWSKI, O., KIERDORF, K., KRUEGER, M., LOCATELLI, G., HOCHGERNER, H., ZEISER, R., EPELMAN, S., GEISSMANN, F., PRILLER, J., ROSSI, F. M., BECHMANN, I., KERSCHENSTEINER, M., LINNARSSON, S., JUNG, S. & PRINZ, M. 2016. Origin, fate and dynamics of macrophages at central nervous system interfaces. *Nat Immunol,* 17**,** 797-805.
GOLUSZKO, P. & NOWICKI, B. 2005. Membrane cholesterol: a crucial molecule affecting interactions of microbial pathogens with mammalian cells. *Infect Immun,* 73**,** 7791-6.
GOODRUM, J. F. 1991. Cholesterol from degenerating nerve myelin becomes associated with lipoproteins containing apolipoprotein E. *J Neurochem,* 56**,** 2082-6.
GRASSI, S., CABITTA, L., PRIONI, S., MAURI, L., CIAMPA, M. G., YOKOYAMA, N., IWABUCHI, K., ZORINA, Y. & PRINETTI, A. 2023. Identification of the Lipid Antigens Recognized by rHIgM22, a Remyelination-Promoting Antibody. *Neurochem Res*.
GRASSI, S., GIUSSANI, P., MAURI, L., PRIONI, S., SONNINO, S. & PRINETTI, A. 2020. Lipid rafts and neurodegeneration: structural and functional roles in physiologic aging and neurodegenerative diseases. *J Lipid Res,* 61**,** 636-654.
GRASSI, S., GIUSSANI, P., PRIONI, S., BUTTON, D., CAO, J., HAKIMI, I., SARMIERE, P., SRINIVAS, M., CABITTA, L., SONNINO, S. & PRINETTI, A. 2019a. Human Remyelination Promoting Antibody Stimulates Astrocytes Proliferation Through Modulation of the Sphingolipid Rheostat in Primary Rat Mixed Glial Cultures. *Neurochem Res,* 44**,** 1460-1474.
GRASSI, S., MAURI, L., PRIONI, S., CABITTA, L., SONNINO, S., PRINETTI, A. & GIUSSANI, P. 2019b. Sphingosine 1-Phosphate Receptors and Metabolic Enzymes as Druggable Targets for Brain Diseases. *Front Pharmacol,* 10**,** 807.

GRASSI, S., PRIONI, S., CABITTA, L., AURELI, M., SONNINO, S. & PRINETTI, A. 2016. The Role of 3-O-Sulfogalactosylceramide, Sulfatide, in the Lateral Organization of Myelin Membrane. *Neurochem Res,* 41**,** 130-43.

GRASSI, S., PRIONI, S., ZORINA, Y., CABITTA, L., SONNINO, S. & PRINETTI, A. 2015. Identification of the antigen recognized by rHIgM22, a remyelination-promoting human monoclonal antibody. *SpringerPlus,* 4**,** P15.

HAGHIGHI, S., LEKMAN, A., NILSSON, S., BLOMQVIST, M. & ANDERSEN, O. 2013. Increased CSF sulfatide levels and serum glycosphingolipid antibody levels in healthy siblings of multiple sclerosis patients. *J Neurol Sci,* 326**,** 35-9.

HAKOMORI, S., HANDA, K., IWABUCHI, K., YAMAMURA, S. & PRINETTI, A. 1998. New insights in glycosphingolipid function: "glycosignaling domain," a cell surface assembly of glycosphingolipids with signal transducer molecules,involved in cell adhesion coupled with signaling. *Glycobiology,* 8**,** xi-xix.

HAKOMORI, S. I. 2000. Cell adhesion/recognition and signal transduction through glycosphingolipid microdomain. *Glycoconj J,* 17**,** 143-51.

HALMER, R., WALTER, S. & FASSBENDER, K. 2014. Sphingolipids: important players in multiple sclerosis. *Cell Physiol Biochem,* 34**,** 111-8.

HALTER, D., NEUMANN, S., VAN DIJK, S. M., WOLTHOORN, J., DE MAZIERE, A. M., VIEIRA, O. V., MATTJUS, P., KLUMPERMAN, J., VAN MEER, G. & SPRONG, H. 2007. Pre- and post-Golgi translocation of glucosylceramide in glycosphingolipid synthesis. *Journal of Cell Biology,* 179**,** 101-15.

HAMBY, M. E. & SOFRONIEW, M. V. 2010. Reactive astrocytes as therapeutic targets for CNS disorders. *Neurotherapeutics,* 7**,** 494-506.

HAN, X. L. & GROSS, R. W. 1990. Plasmenylcholine and phosphatidylcholine membrane bilayers possess distinct conformational motifs. *Biochemistry,* 29**,** 4992-6.

HANADA, K. 2006. Discovery of the molecular machinery CERT for endoplasmic reticulum-to-Golgi trafficking of ceramide. *Molecular and Cellular Biochemistry,* 286**,** 23-31.

HANADA, K., KUMAGAI, K., TOMISHIGE, N. & YAMAJI, T. 2009. CERT-mediated trafficking of ceramide. *Biochimica et Biophysica Acta,* 1791**,** 684-91.

HANAFY, K. A. & SLOANE, J. A. 2011. Regulation of remyelination in multiple sclerosis. *FEBS Lett,* 585**,** 3821-8.

HANNUN, Y. A. & OBEID, L. M. 2008. Principles of bioactive lipid signalling: lessons from sphingolipids. *Nat Rev Mol Cell Biol,* 9**,** 139-50.

HANNUN, Y. A. & OBEID, L. M. 2011. Many ceramides. *J Biol Chem,* 286**,** 27855-62.

HARAYAMA, T. & RIEZMAN, H. 2018. Understanding the diversity of membrane lipid composition. *Nat Rev Mol Cell Biol,* 19**,** 281-296.

HIRBEC, H., RASSENDREN, F. & AUDINAT, E. 2019. Microglia Reactivity: Heterogeneous Pathological Phenotypes. *Methods Mol Biol,* 2034**,** 41-55.

HO, Q. W. C., ZHENG, X. & ALI, Y. 2022. Ceramide Acyl Chain Length and Its Relevance to Intracellular Lipid Regulation. *Int J Mol Sci,* 23.

HOOPER, N. M. 1999. Detergent-insoluble glycosphingolipid/cholesterol-rich membrane domains, lipid rafts and caveolae (review). *Mol Membr Biol,* 16**,** 145-56.

HOWE, C. L., BIEBER, A. J., WARRINGTON, A. E., PEASE, L. R. & RODRIGUEZ, M. 2004. Antiapoptotic signaling by a remyelination-promoting human antimyelin antibody. *Neurobiol Dis,* 15**,** 120-31.

ILYAS, A. A., CHEN, Z. W. & COOK, S. D. 2003. Antibodies to sulfatide in cerebrospinal fluid of patients with multiple sclerosis. *Journal of Neuroimmunology,* 139**,** 76-80.

INDARAM, M., MA, W., ZHAO, L., FARISS, R. N., RODRIGUEZ, I. R. & WONG, W. T. 2015. 7-Ketocholesterol increases retinal microglial migration, activation, and angiogenicity: a potential pathogenic mechanism underlying age-related macular degeneration. *Sci Rep,* 5**,** 9144.

INGOLFSSON, H. I., MELO, M. N., VAN EERDEN, F. J., ARNAREZ, C., LOPEZ, C. A., WASSENAAR, T. A., PERIOLE, X., DE VRIES, A. H., TIELEMAN, D. P. & MARRINK, S. J. 2014. Lipid organization of the plasma membrane. *J Am Chem Soc,* 136**,** 14554-9.

JACKMAN, N., ISHII, A. & BANSAL, R. 2009. Oligodendrocyte development and myelin biogenesis: parsing out the roles of glycosphingolipids. *Physiology (Bethesda),* 24**,** 290-7.

JASKIEWICZ, E. 2004. [Epitopes on myelin proteins recognized by autoantibodies present in multiple sclerosis patients]. *Postepy Hig Med Dosw (Online),* 58**,** 472-82.

JHA, M. K., JO, M., KIM, J. H. & SUK, K. 2019. Microglia-Astrocyte Crosstalk: An Intimate Molecular Conversation. *Neuroscientist,* 25**,** 227-240.

KALINCIK, T. 2015. Multiple Sclerosis Relapses: Epidemiology, Outcomes and Management. A Systematic Review. *Neuroepidemiology,* 44**,** 199-214.

KAMINSKA, J., KOPER, O. M., PIECHAL, K. & KEMONA, H. 2017. Multiple sclerosis - etiology and diagnostic potential. *Postepy Hig Med Dosw (Online),* 71**,** 551-563.
KANTARCI, O. H., PIRKO, I. & RODRIGUEZ, M. 2014. Novel immunomodulatory approaches for the management of multiple sclerosis. *Clinical Pharmacology and Therapeutics,* 95**,** 32-44.
KANTER, J. L., NARAYANA, S., HO, P. P., CATZ, I., WARREN, K. G., SOBEL, R. A., STEINMAN, L. & ROBINSON, W. H. 2006. Lipid microarrays identify key mediators of autoimmune brain inflammation. *Nature Medicine,* 12**,** 138-43.
KARUSSIS, D. 2014. The diagnosis of multiple sclerosis and the various related demyelinating syndromes: a critical review. *J Autoimmun,* 48-49**,** 134-42.
KAWAI, H., ALLENDE, M. L., WADA, R., KONO, M., SANGO, K., DENG, C., MIYAKAWA, T., CRAWLEY, J. N., WERTH, N., BIERFREUND, U., SANDHOFF, K. & PROIA, R. L. 2001. Mice expressing only monosialoganglioside GM3 exhibit lethal audiogenic seizures. *Journal of Biological Chemistry,* 276**,** 6885-8.
KERLERO DE ROSBO, N., MILO, R., LEES, M. B., BURGER, D., BERNARD, C. C. & BEN-NUN, A. 1993. Reactivity to myelin antigens in multiple sclerosis. Peripheral blood lymphocytes respond predominantly to myelin oligodendrocyte glycoprotein. *Journal of Clinical Investigation,* 92**,** 2602-8.
KESSARIS, N., PRINGLE, N. & RICHARDSON, W. D. 2008. Specification of CNS glia from neural stem cells in the embryonic neuroepithelium. *Philosophical Transactions of the Royal Society of London. Series B: Biological Sciences,* 363**,** 71-85.
KIRAY, H., LINDSAY, S. L., HOSSEINZADEH, S. & BARNETT, S. C. 2016. The multifaceted role of astrocytes in regulating myelination. *Exp Neurol,* 283**,** 541-9.
KITATANI, K., IDKOWIAK-BALDYS, J. & HANNUN, Y. A. 2008. The sphingolipid salvage pathway in ceramide metabolism and signaling. *Cell Signal,* 20**,** 1010-8.
KOHLER, S., WINKLER, U. & HIRRLINGER, J. 2021. Heterogeneity of Astrocytes in Grey and White Matter. *Neurochem Res,* 46**,** 3-14.
KOLTER, T., PROIA, R. L. & SANDHOFF, K. 2002a. Combinatorial ganglioside biosynthesis. *J Biol Chem,* 277**,** 25859-62.
KOLTER, T., PROIA, R. L. & SANDHOFF, K. 2002b. Combinatorial ganglioside biosynthesis. *Journal of Biological Chemistry,* 277**,** 25859-62.
KONISHI, H., KOBAYASHI, M., KUNISAWA, T., IMAI, K., SAYO, A., MALISSEN, B., CROCKER, P. R., SATO, K. & KIYAMA, H. 2017. Siglec-H is a microglia-specific marker that discriminates microglia from CNS-associated macrophages and CNS-infiltrating monocytes. *Glia,* 65**,** 1927-1943.
KOTTER, M. R., LI, W. W., ZHAO, C. & FRANKLIN, R. J. 2006. Myelin impairs CNS remyelination by inhibiting oligodendrocyte precursor cell differentiation. *J Neurosci,* 26**,** 328-32.
KUMAR, D. R., ASLINIA, F., YALE, S. H. & MAZZA, J. J. 2011. Jean-Martin Charcot: the father of neurology. *Clin Med Res,* 9**,** 46-9.
LAHIRI, S. & FUTERMAN, A. H. 2007. The metabolism and function of sphingolipids and glycosphingolipids. *Cell Mol Life Sci,* 64**,** 2270-84.
LASSMANN, H. 2014. Mechanisms of white matter damage in multiple sclerosis. *Glia,* 62**,** 1816-30.
LAVRNJA, I., SMILJANIC, K., SAVIC, D., MLADENOVIC-DJORDJEVIC, A., TESOVIC, K., KANAZIR, S. & PEKOVIC, S. 2017. Expression profiles of cholesterol metabolism-related genes are altered during development of experimental autoimmune encephalomyelitis in the rat spinal cord. *Sci Rep,* 7**,** 2702.
LEDEEN, R. W. & WU, G. 2008. Nuclear sphingolipids: metabolism and signaling. *J Lipid Res,* 49**,** 1176-86.
LEGNAME, G. 2017. Elucidating the function of the prion protein. *PLoS Pathog,* 13**,** e1006458.
LEMUS, H. N., WARRINGTON, A. E. & RODRIGUEZ, M. 2018. Multiple Sclerosis: Mechanisms of Disease and Strategies for Myelin and Axonal Repair. *Neurol Clin,* 36**,** 1-11.
LINDEN, R. 2017. The Biological Function of the Prion Protein: A Cell Surface Scaffold of Signaling Modules. *Front Mol Neurosci,* 10**,** 77.
LLOYD, A. F. & MIRON, V. E. 2019. The pro-remyelination properties of microglia in the central nervous system. *Nat Rev Neurol,* 15**,** 447-458.
LU, F., ZHU, J., GUO, S., WONG, B. J., CHEHAB, F. F., FERRIERO, D. M. & JIANG, X. 2018. Upregulation of cholesterol 24-hydroxylase following hypoxia-ischemia in neonatal mouse brain. *Pediatr Res,* 83**,** 1218-1227.
LUBETZKI, C. & STANKOFF, B. 2014. Demyelination in multiple sclerosis. *Handb Clin Neurol,* 122**,** 89-99.
LUBETZKI, C., THUILLIER, Y., GALLI, A., LYON-CAEN, O., LHERMITTE, F. & ZALC, B. 1989. Galactosylceramide: a reliable serum index of demyelination in multiple sclerosis. *Annals of Neurology,* 26**,** 407-9.
LUTTON, J. D., WINSTON, R. & RODMAN, T. C. 2004. Multiple sclerosis: etiological mechanisms and future directions. *Exp Biol Med (Maywood),* 229**,** 12-20.

MAGISTRI, M., KHOURY, N., MAZZA, E. M., VELMESHEV, D., LEE, J. K., BICCIATO, S., TSOULFAS, P. & FAGHIHI, M. A. 2016. A comparative transcriptomic analysis of astrocytes differentiation from human neural progenitor cells. *Eur J Neurosci,* 44**,** 2858-2870.
MAHLEY, R. W. 2016. Central Nervous System Lipoproteins: ApoE and Regulation of Cholesterol Metabolism. *Arterioscler Thromb Vasc Biol,* 36**,** 1305-15.
MARANGON, D., BOCCAZZI, M., LECCA, D. & FUMAGALLI, M. 2020. Regulation of Oligodendrocyte Functions: Targeting Lipid Metabolism and Extracellular Matrix for Myelin Repair. *J Clin Med,* 9.
MARCONI, S., DE TONI, L., LOVATO, L., TEDESCHI, E., GAETTI, L., ACLER, M. & BONETTI, B. 2005. Expression of gangliosides on glial and neuronal cells in normal and pathological adult human brain. *Journal of Neuroimmunology,* 170**,** 115-21.
MARZA, E., SIMONSEN, K. T., FAERGEMAN, N. J. & LESA, G. M. 2009. Expression of ceramide glucosyltransferases, which are essential for glycosphingolipid synthesis, is only required in a small subset of C. elegans cells. *J Cell Sci,* 122**,** 822-33.
MATHEWS, E. S., MAWDSLEY, D. J., WALKER, M., HINES, J. H., POZZOLI, M. & APPEL, B. 2014. Mutation of 3-hydroxy-3-methylglutaryl CoA synthase I reveals requirements for isoprenoid and cholesterol synthesis in oligodendrocyte migration arrest, axon wrapping, and myelin gene expression. *J Neurosci,* 34**,** 3402-12.
MATYASH, V. & KETTENMANN, H. 2010. Heterogeneity in astrocyte morphology and physiology. *Brain Res Rev,* 63**,** 2-10.
MCCARTHY, K. D. & DE VELLIS, J. 1980. Preparation of separate astroglial and oligodendroglial cell cultures from rat cerebral tissue. *J Cell Biol,* 85**,** 890-902.
MCMAHON, H. T. & BOUCROT, E. 2015. Membrane curvature at a glance. *J Cell Sci,* 128**,** 1065-70.
MEINL, E. & HOHLFELD, R. 2002. Immunopathogenesis of multiple sclerosis: MBP and beyond. *Clinical and Experimental Immunology,* 128**,** 395-7.
MENCARELLI, C. & MARTINEZ-MARTINEZ, P. 2013. Ceramide function in the brain: when a slight tilt is enough. *Cell Mol Life Sci,* 70**,** 181-203.
MERRILL, A. H., JR. 2011. Sphingolipid and glycosphingolipid metabolic pathways in the era of sphingolipidomics. *Chem Rev,* 111**,** 6387-422.
MILLER, D. H., CHARD, D. T. & CICCARELLI, O. 2012. Clinically isolated syndromes. *Lancet Neurol,* 11**,** 157-69.
MIRON, V. E., BOYD, A., ZHAO, J. W., YUEN, T. J., RUCKH, J. M., SHADRACH, J. L., VAN WIJNGAARDEN, P., WAGERS, A. J., WILLIAMS, A., FRANKLIN, R. J. M. & FFRENCH-CONSTANT, C. 2013. M2 microglia and macrophages drive oligodendrocyte differentiation during CNS remyelination. *Nat Neurosci,* 16**,** 1211-1218.
MIRON, V. E., KUHLMANN, T. & ANTEL, J. P. 2011. Cells of the oligodendroglial lineage, myelination, and remyelination. *Biochim Biophys Acta,* 1812**,** 184-93.
MIRON, V. E., LUDWIN, S. K., DARLINGTON, P. J., JARJOUR, A. A., SOLIVEN, B., KENNEDY, T. E. & ANTEL, J. P. 2010. Fingolimod (FTY720) enhances remyelination following demyelination of organotypic cerebellar slices. *American Journal of Pathology,* 176**,** 2682-94.
MITSUNAGA, Y., CIRIC, B., VAN KEULEN, V., WARRINGTON, A. E., PAZ SOLDAN, M., BIEBER, A. J., RODRIGUEZ, M. & PEASE, L. R. 2002. Direct evidence that a human antibody derived from patient serum can promote myelin repair in a mouse model of chronic-progressive demyelinating disease. *FASEB Journal,* 16**,** 1325-7.
MIZUTANI, Y., KIHARA, A. & IGARASHI, Y. 2005. Mammalian Lass6 and its related family members regulate synthesis of specific ceramides. *Biochem J,* 390**,** 263-71.
MOUTINHO, M., NUNES, M. J. & RODRIGUES, E. 2016. Cholesterol 24-hydroxylase: Brain cholesterol metabolism and beyond. *Biochim Biophys Acta,* 1861**,** 1911-1920.
MOYANO, A. L., PITUCH, K., LI, G., VAN BREEMEN, R., MANSSON, J. E. & GIVOGRI, M. I. 2013. Levels of plasma sulfatides C18 : 0 and C24 : 1 correlate with disease status in relapsing-remitting multiple sclerosis. *Journal of Neurochemistry,* 127**,** 600-4.
MUELLER, A. M., PEDRE, X., STEMPFL, T., KLEITER, I., COUILLARD-DESPRES, S., AIGNER, L., GIEGERICH, G. & STEINBRECHER, A. 2008. Novel role for SLPI in MOG-induced EAE revealed by spinal cord expression analysis. *J Neuroinflammation,* 5**,** 20.
MULLIN, A. P., CUI, C., WANG, Y., WANG, J., TROY, E., CAGGIANO, A. O., PARRY, T. J., COLBURN, R. W. & PAVLOPOULOS, E. 2017. rHIgM22 enhances remyelination in the brain of the cuprizone mouse model of demyelination. *Neurobiol Dis,* 105**,** 142-155.
MUNZEL, E. J. & WILLIAMS, A. 2013. Promoting remyelination in multiple sclerosis-recent advances. *Drugs,* 73**,** 2017-29.
NAPOLI, I. & NEUMANN, H. 2009. Microglial clearance function in health and disease. *Neuroscience,* 158**,** 1030-8.

NASH, B., THOMSON, C. E., LININGTON, C., ARTHUR, A. T., MCCLURE, J. D., MCBRIDE, M. W. & BARNETT, S. C. 2011. Functional duality of astrocytes in myelination. *Journal of Neuroscience,* 31**,** 13028-38.

NEUMANN, H., KOTTER, M. R. & FRANKLIN, R. J. 2009. Debris clearance by microglia: an essential link between degeneration and regeneration. *Brain,* 132**,** 288-95.

NICOLSON, G. L. 2013. Update of the 1972 Singer-Nicolson Fluid-Mosaic Model of Membrane Structure. *Discoveries (Craiova),* 1**,** e3.

NIESMAN, I. R., ZEMKE, N., FRIDOLFSSON, H. N., HAUSHALTER, K. J., LEVY, K., GROVE, A., SCHNOOR, R., FINLEY, J. C., PATEL, P. M., ROTH, D. M., HEAD, B. P. & PATEL, H. H. 2013a. Caveolin isoform switching as a molecular, structural, and metabolic regulator of microglia. *Molecular and Cellular Neurosciences,* 56**,** 283-97.

NIESMAN, I. R., ZEMKE, N., FRIDOLFSSON, H. N., HAUSHALTER, K. J., LEVY, K., GROVE, A., SCHNOOR, R., FINLEY, J. C., PATEL, P. M., ROTH, D. M., HEAD, B. P. & PATEL, H. H. 2013b. Caveolin isoform switching as a molecular, structural, and metabolic regulator of microglia. *Mol Cell Neurosci,* 56**,** 283-97.

NIEWEG, K., SCHALLER, H. & PFRIEGER, F. W. 2009. Marked differences in cholesterol synthesis between neurons and glial cells from postnatal rats. *J Neurochem,* 109**,** 125-34.

NORTON, W. T. 1981. Biochemistry of myelin. *Advances in Neurology,* 31**,** 93-121.

O'BRIEN, J. S. 1965. Stability of the Myelin Membrane. *Science,* 147**,** 1099-107.

OHMI, Y., OHKAWA, Y., YAMAUCHI, Y., TAJIMA, O. & FURUKAWA, K. 2012. Essential roles of gangliosides in the formation and maintenance of membrane microdomains in brain tissues. *Neurochem Res,* 37**,** 1185-91.

ORIHUELA, R., MCPHERSON, C. A. & HARRY, G. J. 2016. Microglial M1/M2 polarization and metabolic states. *Br J Pharmacol,* 173**,** 649-65.

ORTH, M. & BELLOSTA, S. 2012. Cholesterol: its regulation and role in central nervous system disorders. *Cholesterol,* 2012**,** 292598.

OZGEN, H., BARON, W., HOEKSTRA, D. & KAHYA, N. 2016. Oligodendroglial membrane dynamics in relation to myelin biogenesis. *Cell Mol Life Sci,* 73**,** 3291-310.

OZGEN, H., SCHRIMPF, W., HENDRIX, J., DE JONGE, J. C., LAMB, D. C., HOEKSTRA, D., KAHYA, N. & BARON, W. 2014. The lateral membrane organization and dynamics of myelin proteins PLP and MBP are dictated by distinct galactolipids and the extracellular matrix. *PLoS One,* 9**,** e101834.

PALTAUF, F. 1994. Ether lipids in biomembranes. *Chemistry and Physics of Lipids,* 74**,** 101-39.

PAOLICELLI, R. A. S., AMANDA AND STEVENS, BETH AND TREMBLAY, MARIE-EVE AND AGUZZI, ADRIANO AND AJAMI, BAHAREH AND AMIT, IDO AND AUDINAT, ETIENNE AND BECHMANN, INGO AND BENNETT, MARIKO AND BENNETT, FREDERICK AND BESSIS, ALAIN AND BIBER, KNUT AND BILBO, STACI AND BLURTON-JONES, MATHEW AND BODDEKE, ERIK AND BRITES, DORA AND BRÔNE, BERT AND BROWN, GUY C. AND BUTOVSKY, OLEG AND CARSON, MONICA J. AND CASTELLANO, BERNARDO AND COLONNA, MARCO AND COWLEY, SALLY A. AND CUNNINGHAM, COLM AND DAVALOS, DIMITRIOS AND DE JAGER, PHILIP L. AND DE STROOPER, BART AND DÉNES, ÁDÁM AND EGGEN, BART J.L. AND EYO, UKPONG AND GALEA, ELENA AND GAREL, SONIA AND GINHOUX, FLORENT AND GLASS, CHRISTOPHER K. AND GOKCE, OZGUN AND GOMEZ-NICOLA, DIEGO AND GONZÁLEZ, BERTA AND GORDON, SIAMON AND GRAEBER, MANUEL B. AND GREENHALGH, ANDREW D. AND GRESSENS, PIERRE AND GRETER, MELANIE AND GUTMANN, DAVID H. AND HAASS, CHRISTIAN AND HENEKA, MICHAEL T. AND HEPPNER, FRANK AND HONG, SOYON AND JUNG, STEFFEN AND KETTENMANN, HELMUT AND KIPNIS, JONATHAN AND KOYAMA, RYUTA AND LEMKE, GREG AND LYNCH, MARINA AND MAJEWSKA, ANIA AND MALCANGIO, MARZIA AND MALM, TARJA AND MANCUSO, RENZO AND MATTEOLI, MICHELA AND MCCOLL, BARRY AND MIRON, VERONIQUE E. AND MOLOFSKY, ANNA VICTORIA AND MONJE, MICHELLE AND MRACSKO, EVA AND NADJAR, AGNES AND NEHER, JONAS J. AND NENISKYTE, URTE AND NEUMANN, HARALD AND NODA, MAMI AND PENG, BO AND PERI, FRANCESCA AND PERRY, V. HUGH AND POPOVICH, PHILLIP G. AND PRILLER, JOSEF AND RAGOZZINO, DAVIDE AND RANSOHOFF, RICHARD M. AND SALTER, MICHAEL W. AND SCHAEFER, ANNE AND SCHAFER, DOROTHY P. AND SCHWARTZ, MICHAL AND SIMONS, MIKAEL AND STREIT, WOLFGANG J. AND TAY, TUAN LENG AND TSAI, LI-HUEI AND VERKHRATSKY, ALEXEI AND VON BERNHARDI, ROMMY AND WAKE, HIROAKI AND WITTAMER, VALERIE AND WOLF, SUSANNE A. AND WU, LONG-JUN AND WYSS-CORAY, TONY 2022. Defining Microglial States and Nomenclature: A Roadmap to 2030. 44.

PARK, J. Y., KIM, K. S., LEE, S. B., RYU, J. S., CHUNG, K. C., CHOO, Y. K., JOU, I., KIM, J. & PARK, S. M. 2009. On the mechanism of internalization of alpha-synuclein into microglia: roles of ganglioside GM1 and lipid raft. *Journal of Neurochemistry,* 110**,** 400-11.

PAUKNER, K., KRALOVA LESNA, I. & POLEDNE, R. 2022. Cholesterol in the Cell Membrane-An Emerging Player in Atherogenesis. *Int J Mol Sci,* 23.

PAZ SOLDAN, M. M., WARRINGTON, A. E., BIEBER, A. J., CIRIC, B., VAN KEULEN, V., PEASE, L. R. & RODRIGUEZ, M. 2003. Remyelination-promoting antibodies activate distinct Ca2+ influx pathways in astrocytes and oligodendrocytes: relationship to the mechanism of myelin repair. *Molecular and Cellular Neurosciences,* 22**,** 14-24.

PEARCE, J. M. 2005. Historical descriptions of multiple sclerosis. *Eur Neurol,* 54**,** 49-53.

PEFEROEN, L. A., VOGEL, D. Y., UMMENTHUM, K., BREUR, M., HEIJNEN, P. D., GERRITSEN, W. H., PEFEROEN-BAERT, R. M., VAN DER VALK, P., DIJKSTRA, C. D. & AMOR, S. 2015. Activation status of human microglia is dependent on lesion formation stage and remyelination in multiple sclerosis. *J Neuropathol Exp Neurol,* 74**,** 48-63.

PFEIFFER, S. E., WARRINGTON, A. E. & BANSAL, R. 1993. The oligodendrocyte and its many cellular processes. *Trends in Cell Biology,* 3**,** 191-7.

PIRKO, I., CIRIC, B., GAMEZ, J., BIEBER, A. J., WARRINGTON, A. E., JOHNSON, A. J., HANSON, D. P., PEASE, L. R., MACURA, S. I. & RODRIGUEZ, M. 2004. A human antibody that promotes remyelination enters the CNS and decreases lesion load as detected by T2-weighted spinal cord MRI in a virus-induced murine model of MS. *FASEB J,* 18**,** 1577-9.

PLASTINI, M. J., DESU, H. L. & BRAMBILLA, R. 2020. Dynamic Responses of Microglia in Animal Models of Multiple Sclerosis. *Front Cell Neurosci,* 14**,** 269.

PODBIELSKA, M., BANIK, N. L., KUROWSKA, E. & HOGAN, E. L. 2013. Myelin recovery in multiple sclerosis: the challenge of remyelination. *Brain Sci,* 3**,** 1282-324.

PODUSLO, S. E. & MILLER, K. 1985. Levels of sulfatide synthesis distinguish oligodendroglia in different stages of maturation. *Neurochem Res,* 10**,** 1285-97.

POLIANI, P. L., WANG, Y., FONTANA, E., ROBINETTE, M. L., YAMANISHI, Y., GILFILLAN, S. & COLONNA, M. 2015. TREM2 sustains microglial expansion during aging and response to demyelination. *J Clin Invest,* 125**,** 2161-70.

PRINETTI, A., CHIGORNO, V., PRIONI, S., LOBERTO, N., MARANO, N., TETTAMANTI, G. & SONNINO, S. 2001. Changes in the lipid turnover, composition, and organization, as sphingolipid-enriched membrane domains, in rat cerebellar granule cells developing in vitro. *J Biol Chem,* 276**,** 21136-45.

PRUETT, S. T., BUSHNEV, A., HAGEDORN, K., ADIGA, M., HAYNES, C. A., SULLARDS, M. C., LIOTTA, D. C. & MERRILL, A. H., JR. 2008. Biodiversity of sphingoid bases ("sphingosines") and related amino alcohols. *J Lipid Res,* 49**,** 1621-39.

PULIAFITO, A., HUFNAGEL, L., NEVEU, P., STREICHAN, S., SIGAL, A., FYGENSON, D. K. & SHRAIMAN, B. I. 2012. Collective and single cell behavior in epithelial contact inhibition. *Proc Natl Acad Sci U S A,* 109**,** 739-44.

QIAN, L., CHAI, A. B., GELISSEN, I. C. & BROWN, A. J. 2022. Balancing cholesterol in the brain: from synthesis to disposal. *Exploration of Neuroprotective Therapy***,** 1-27.

QUINTANA, F. J., FAREZ, M. F., VIGLIETTA, V., IGLESIAS, A. H., MERBL, Y., IZQUIERDO, G., LUCAS, M., BASSO, A. S., KHOURY, S. J., LUCCHINETTI, C. F., COHEN, I. R. & WEINER, H. L. 2008. Antigen microarrays identify unique serum autoantibody signatures in clinical and pathologic subtypes of multiple sclerosis. *Proceedings of the National Academy of Sciences of the United States of America,* 105**,** 18889-94.

QUINVILLE, B. M., DESCHENES, N. M., RYCKMAN, A. E. & WALIA, J. S. 2021. A Comprehensive Review: Sphingolipid Metabolism and Implications of Disruption in Sphingolipid Homeostasis. *Int J Mol Sci,* 22.

RAGHU, P., JOSEPH, A., KRISHNAN, H., SINGH, P. & SAHA, S. 2019. Phosphoinositides: Regulators of Nervous System Function in Health and Disease. *Front Mol Neurosci,* 12**,** 208.

RANSOHOFF, R. M. 2016. A polarizing question: do M1 and M2 microglia exist? *Nat Neurosci,* 19**,** 987-91.

RANSOHOFF, R. M., HAFLER, D. A. & LUCCHINETTI, C. F. 2015. Multiple sclerosis-a quiet revolution. *Nat Rev Neurol,* 11**,** 134-42.

RIBONI, L., PRINETTI, A., BASSI, R. & TETTAMANTI, G. 1994. Formation of bioactive sphingoid molecules from exogenous sphingomyelin in primary cultures of neurons and astrocytes. *FEBS Lett,* 352**,** 323-6.

RODRIGUEZ, M., WARRINGTON, A. E. & PEASE, L. R. 2009. Invited article: human natural autoantibodies in the treatment of neurologic disease. *Neurology,* 72**,** 1269-76.

ROVARIS, M., CONFAVREUX, C., FURLAN, R., KAPPOS, L., COMI, G. & FILIPPI, M. 2006. Secondary progressive multiple sclerosis: current knowledge and future challenges. *Lancet Neurol,* 5**,** 343-54.
RUSSO, D., CAPOLUPO, L., LOOMBA, J. S., STICCO, L. & D'ANGELO, G. 2018. Glycosphingolipid metabolism in cell fate specification. *J Cell Sci,* 131.
S. GRASSI ET AL. , S. P., C. D'APRILE, L. CABITTA, P. GIUSSANI, L. MAURI, A. PRINETTI 2021. SPHINGOLIPID-DEPENDENT MEMBRANE ORGANIZATION AND SIGNALING ORCHESTRATING MYELIN REPAIR. *In:* JOURNAL, S. (ed.) *2021 ASN Virtual Meeting Abstracts.*
SAHER, G., BRUGGER, B., LAPPE-SIEFKE, C., MOBIUS, W., TOZAWA, R., WEHR, M. C., WIELAND, F., ISHIBASHI, S. & NAVE, K. A. 2005. High cholesterol level is essential for myelin membrane growth. *Nature Neuroscience,* 8**,** 468-75.
SAHER, G., QUINTES, S. & NAVE, K. A. 2011. Cholesterol: a novel regulatory role in myelin formation. *Neuroscientist,* 17**,** 79-93.
SALEHI, Z., HADIYAN, S. P. & NAVIDI, R. 2013. Ciliary neurotrophic factor role in myelin oligodendrocyte glycoprotein expression in Cuprizone-induced multiple sclerosis mice. *Cell Mol Neurobiol,* 33**,** 531-5.
SANDHOFF, K. & KOLTER, T. 2003. Biosynthesis and degradation of mammalian glycosphingolipids. *Philos Trans R Soc Lond B Biol Sci,* 358**,** 847-61.
SCHMITT, S., CASTELVETRI, L. C. & SIMONS, M. 2015. Metabolism and functions of lipids in myelin. *Biochim Biophys Acta,* 1851**,** 999-1005.
SCHNAAR, R. L. 2019. The Biology of Gangliosides. *Adv Carbohydr Chem Biochem,* 76**,** 113-148.
SCHNAAR, R. L. & KINOSHITA, T. 2015. Glycosphingolipids. *In:* RD, VARKI, A., CUMMINGS, R. D., ESKO, J. D., STANLEY, P., HART, G. W., AEBI, M., DARVILL, A. G., KINOSHITA, T., PACKER, N. H., PRESTEGARD, J. H., SCHNAAR, R. L. & SEEBERGER, P. H. (eds.) *Essentials of Glycobiology.* Cold Spring Harbor (NY).
SELA, B. A., KONAT, G. & OFFNER, H. 1982. Elevated ganglioside concentration in serum and peripheral blood lymphocytes from multiple sclerosis patients in remission. *Journal of the Neurological Sciences,* 54**,** 143-8.
SEN, M. K., MAHNS, D. A., COORSSEN, J. R. & SHORTLAND, P. J. 2022. The roles of microglia and astrocytes in phagocytosis and myelination: Insights from the cuprizone model of multiple sclerosis. *Glia,* 70**,** 1215-1250.
SHANER, R. L., ALLEGOOD, J. C., PARK, H., WANG, E., KELLY, S., HAYNES, C. A., SULLARDS, M. C. & MERRILL, A. H., JR. 2009. Quantitative analysis of sphingolipids for lipidomics using triple quadrupole and quadrupole linear ion trap mass spectrometers. *J Lipid Res,* 50**,** 1692-707.
SHERMAN, D. L. & BROPHY, P. J. 2005. Mechanisms of axon ensheathment and myelin growth. *Nat Rev Neurosci,* 6**,** 683-90.
SHI, Q., CHEN, J., ZOU, X. & TANG, X. 2022. Intracellular Cholesterol Synthesis and Transport. *Front Cell Dev Biol,* 10**,** 819281.
SIMONS, K. & TOOMRE, D. 2000. Lipid rafts and signal transduction. *Nat Rev Mol Cell Biol,* 1**,** 31-9.
SIMONS, K. & VAN MEER, G. 1988a. Lipid Sorting in Epithelial-Cells. *Biochemistry,* 27**,** 6197-6202.
SIMONS, K. & VAN MEER, G. 1988b. Lipid sorting in epithelial cells. *Biochemistry,* 27**,** 6197-202.
SINGER, S. J. & NICOLSON, G. L. 1972. The fluid mosaic model of the structure of cell membranes. *Science,* 175**,** 720-31.
SINHA, S., BOYDEN, A. W., ITANI, F. R., CRAWFORD, M. P. & KARANDIKAR, N. J. 2015. CD8(+) T-Cells as Immune Regulators of Multiple Sclerosis. *Front Immunol,* 6**,** 619.
SIPIONE, S., MONYROR, J., GALLEGUILLOS, D., STEINBERG, N. & KADAM, V. 2020. Gangliosides in the Brain: Physiology, Pathophysiology and Therapeutic Applications. *Front Neurosci,* 14**,** 572965.
SKRIPULETZ, T., HACKSTETTE, D., BAUER, K., GUDI, V., PUL, R., VOSS, E., BERGER, K., KIPP, M., BAUMGARTNER, W. & STANGEL, M. 2013. Astrocytes regulate myelin clearance through recruitment of microglia during cuprizone-induced demyelination. *Brain,* 136**,** 147-67.
SOFRONIEW, M. V. & VINTERS, H. V. 2010. Astrocytes: biology and pathology. *Acta Neuropathol,* 119**,** 7-35.
SONG, G., OUYANG, G. & BAO, S. 2005. The activation of Akt/PKB signaling pathway and cell survival. *J Cell Mol Med,* 9**,** 59-71.
SONNINO, S., AURELI, M., GRASSI, S., MAURI, L., PRIONI, S. & PRINETTI, A. 2014. Lipid rafts in neurodegeneration and neuroprotection. *Mol Neurobiol,* 50**,** 130-48.
SONNINO, S., CHIRICOZZI, E., GRASSI, S., MAURI, L., PRIONI, S. & PRINETTI, A. 2018. Gangliosides in Membrane Organization. *Prog Mol Biol Transl Sci,* 156**,** 83-120.
SONNINO, S. & PRINETTI, A. 2009. Sphingolipids and membrane environments for caveolin. *FEBS Lett,* 583**,** 597-606.
SONNINO, S. & PRINETTI, A. 2010. Gangliosides as regulators of cell membrane organization and functions. *Adv Exp Med Biol,* 688**,** 165-84.

SONNINO, S. & PRINETTI, A. 2013. Membrane domains and the "lipid raft" concept. *Curr Med Chem,* 20**,** 4-21.
SONNINO, S., PRINETTI, A., MAURI, L., CHIGORNO, V. & TETTAMANTI, G. 2006. Dynamic and structural properties of sphingolipids as driving forces for the formation of membrane domains. *Chem Rev,* 106**,** 2111-25.
SOULET, D. & RIVEST, S. 2008. Microglia. *Current Biology,* 18**,** R506-8.
SPRONG, H., KRUITHOF, B., LEIJENDEKKER, R., SLOT, J. W., VAN MEER, G. & VAN DER SLUIJS, P. 1998. UDP-galactose:ceramide galactosyltransferase is a class I integral membrane protein of the endoplasmic reticulum. *J Biol Chem,* 273**,** 25880-8.
STANSLEY, B., POST, J. & HENSLEY, K. 2012. A comparative review of cell culture systems for the study of microglial biology in Alzheimer's disease. *J Neuroinflammation,* 9**,** 115.
STEINMAN, L. 1993. Connections between the immune system and the nervous system. *Proceedings of the National Academy of Sciences of the United States of America,* 90**,** 7912-4.
STEINMAN, L. 1995. Multiple sclerosis. Presenting an odd autoantigen. *Nature,* 375**,** 739-40.
STEINMAN, L., LINDSEY, J. W., ALTERS, S. & HODGKINSON, S. 1993. From treatment of experimental allergic encephalomyelitis to clinical trials in multiple sclerosis. *Immunology Series,* 59**,** 253-60.
SVENNERHOLM, L. 1963. Chromatographic Separation of Human Brain Gangliosides. *J Neurochem,* 10**,** 613-23.
TAKAMIYA, K., YAMAMOTO, A., FURUKAWA, K., YAMASHIRO, S., SHIN, M., OKADA, M., FUKUMOTO, S., HARAGUCHI, M., TAKEDA, N., FUJIMURA, K., SAKAE, M., KISHIKAWA, M., SHIKU, H. & AIZAWA, S. 1996. Mice with disrupted GM2/GD2 synthase gene lack complex gangliosides but exhibit only subtle defects in their nervous system. *Proceedings of the National Academy of Sciences of the United States of America,* 93**,** 10662-7.
TERNES, P., FRANKE, S., ZAHRINGER, U., SPERLING, P. & HEINZ, E. 2002. Identification and characterization of a sphingolipid delta 4-desaturase family. *J Biol Chem,* 277**,** 25512-8.
TETTAMANTI, G. 2004. Ganglioside/glycosphingolipid turnover: new concepts. *Glycoconj J,* 20**,** 301-17.
THOMPSON, A. J., BARANZINI, S. E., GEURTS, J., HEMMER, B. & CICCARELLI, O. 2018. Multiple sclerosis. *Lancet,* 391**,** 1622-1636.
TILLACK, T. W., ALLIETTA, M., MORAN, R. E. & YOUNG, W. W., JR. 1983. Localization of globoside and Forssman glycolipids on erythrocyte membranes. *Biochim Biophys Acta,* 733**,** 15-24.
TIMMERMAN, R., BURM, S. M. & BAJRAMOVIC, J. J. 2018. An Overview of in vitro Methods to Study Microglia. *Front Cell Neurosci,* 12**,** 242.
TRAJKOVIC, K., VALDEZ, C., YSSELSTEIN, D. & KRAINC, D. 2019. Fluctuations in cell density alter protein markers of multiple cellular compartments, confounding experimental outcomes. *PLoS One,* 14**,** e0211727.
TYLER, A. F., MENDOZA, J. P., FIRAN, M. & KARANDIKAR, N. J. 2013. CD8(+) T Cells Are Required For Glatiramer Acetate Therapy in Autoimmune Demyelinating Disease. *PLoS One,* 8**,** e66772.
ULLIAN, E. M., SAPPERSTEIN, S. K., CHRISTOPHERSON, K. S. & BARRES, B. A. 2001. Control of synapse number by glia. *Science,* 291**,** 657-61.
VAN DE KRAATS, C., KILLESTEIN, J., POPESCU, V., RIJKERS, E., VRENKEN, H., LUTJOHANN, D., BARKHOF, F., POLMAN, C. H. & TEUNISSEN, C. E. 2014. Oxysterols and cholesterol precursors correlate to magnetic resonance imaging measures of neurodegeneration in multiple sclerosis. *Mult Scler,* 20**,** 412-7.
VANCE, J. E. 2015. Phospholipid synthesis and transport in mammalian cells. *Traffic,* 16**,** 1-18.
VANCE, J. E. & STEENBERGEN, R. 2005. Metabolism and functions of phosphatidylserine. *Prog Lipid Res,* 44**,** 207-34.
VASKOVSKY, V. E. & KOSTETSKY, E. Y. 1968. Modified spray for the detection of phospholipids on thin-layer chromatograms. *J Lipid Res,* 9**,** 396.
VOSS, E. V., SKULJEC, J., GUDI, V., SKRIPULETZ, T., PUL, R., TREBST, C. & STANGEL, M. 2012. Characterisation of microglia during de- and remyelination: can they create a repair promoting environment? *Neurobiol Dis,* 45**,** 519-28.
WAKELAM, M. J. 1998. Diacylglycerol--when is it an intracellular messenger? *Biochim Biophys Acta,* 1436**,** 117-26.
WALTON, C., KING, R., RECHTMAN, L., KAYE, W., LERAY, E., MARRIE, R. A., ROBERTSON, N., LA ROCCA, N., UITDEHAAG, B., VAN DER MEI, I., WALLIN, M., HELME, A., ANGOOD NAPIER, C., RIJKE, N. & BANEKE, P. 2020. Rising prevalence of multiple sclerosis worldwide: Insights from the Atlas of MS, third edition. *Mult Scler,* 26**,** 1816-1821.
WARRINGTON, A. E., ASAKURA, K., BIEBER, A. J., CIRIC, B., VAN KEULEN, V., KAVERI, S. V., KYLE, R. A., PEASE, L. R. & RODRIGUEZ, M. 2000. Human monoclonal antibodies reactive to

oligodendrocytes promote remyelination in a model of multiple sclerosis. *Proc Natl Acad Sci U S A,* 97**,** 6820-5.
WATZLAWIK, J., HOLICKY, E., EDBERG, D. D., MARKS, D. L., WARRINGTON, A. E., WRIGHT, B. R., PAGANO, R. E. & RODRIGUEZ, M. 2010. Human remyelination promoting antibody inhibits apoptotic signaling and differentiation through Lyn kinase in primary rat oligodendrocytes. *Glia,* 58**,** 1782-93.
WATZLAWIK, J. O., WARRINGTON, A. E. & RODRIGUEZ, M. 2013a. PDGF is required for remyelination-promoting IgM stimulation of oligodendrocyte progenitor cell proliferation. *PLoS One,* 8**,** e55149.
WATZLAWIK, J. O., WOOTLA, B., PAINTER, M. M., WARRINGTON, A. E. & RODRIGUEZ, M. 2013b. Cellular targets and mechanistic strategies of remyelination-promoting IgMs as part of the naturally occurring autoantibody repertoire. *Expert Rev Neurother,* 13**,** 1017-29.
WENNEKES, T., VAN DEN BERG, R. J., BOOT, R. G., VAN DER MAREL, G. A., OVERKLEEFT, H. S. & AERTS, J. M. 2009. Glycosphingolipids--nature, function, and pharmacological modulation. *Angew Chem Int Ed Engl,* 48**,** 8848-69.
WILLIAMS, E. E., COOPER, J. A., STILLWELL, W. & JENSKI, L. J. 2000. The curvature and cholesterol content of phospholipid bilayers alter the transbilayer distribution of specific molecular species of phosphatidylethanolamine. *Mol Membr Biol,* 17**,** 157-64.
WRIGHT, B. R., WARRINGTON, A. E., EDBERG, D. D. & RODRIGUEZ, M. 2009. Cellular mechanisms of central nervous system repair by natural autoreactive monoclonal antibodies. *Arch Neurol,* 66**,** 1456-9.
YAMAUCHI, Y., REID, P. C., SPERRY, J. B., FURUKAWA, K., TAKEYA, M., CHANG, C. C. & CHANG, T. Y. 2007. Plasma membrane rafts complete cholesterol synthesis by participating in retrograde movement of precursor sterols. *J Biol Chem,* 282**,** 34994-5004.
YANG, S. T., KREUTZBERGER, A. J. B., LEE, J., KIESSLING, V. & TAMM, L. K. 2016. The role of cholesterol in membrane fusion. *Chem Phys Lipids,* 199**,** 136-143.
YAO, Y., HUANG, C., LI, Z. F., WANG, A. Y., LIU, L. Y., ZHAO, X. G., LUO, Y., NI, L., ZHANG, W. G. & SONG, T. S. 2009. Exogenous phosphatidylethanolamine induces apoptosis of human hepatoma HepG2 cells via the bcl-2/Bax pathway. *World J Gastroenterol,* 15**,** 1751-8.
YORK, N. R., MENDOZA, J. P., ORTEGA, S. B., BENAGH, A., TYLER, A. F., FIRAN, M. & KARANDIKAR, N. J. 2010. Immune regulatory CNS-reactive CD8+T cells in experimental autoimmune encephalomyelitis. *J Autoimmun,* 35**,** 33-44.
YU, R. K., NAKATANI, Y. & YANAGISAWA, M. 2009. The role of glycosphingolipid metabolism in the developing brain. *J Lipid Res,* 50 Suppl**,** S440-5.
YU, R. K., TSAI, Y. T. & ARIGA, T. 2012. Functional roles of gangliosides in neurodevelopment: an overview of recent advances. *Neurochem Res,* 37**,** 1230-44.
YUN, J. H., PARK, S. J., JO, A., KANG, J. L., JOU, I., PARK, J. S. & CHOI, Y. H. 2011. Caveolin-1 is involved in reactive oxygen species-induced SHP-2 activation in astrocytes. *Exp Mol Med,* 43**,** 660-8.
ZABALA, A., VAZQUEZ-VILLOLDO, N., RISSIEK, B., GEJO, J., MARTIN, A., PALOMINO, A., PEREZ-SAMARTIN, A., PULAGAM, K. R., LUKOWIAK, M., CAPETILLO-ZARATE, E., LLOP, J., MAGNUS, T., KOCH-NOLTE, F., RASSENDREN, F., MATUTE, C. & DOMERCQ, M. 2018. P2X4 receptor controls microglia activation and favors remyelination in autoimmune encephalitis. *EMBO Mol Med,* 10.
ZALC, B. 2018. One hundred and fifty years ago Charcot reported multiple sclerosis as a new neurological disease. *Brain,* 141**,** 3482-3488.
ZAMVIL, S. S. & STEINMAN, L. 1990. The T lymphocyte in experimental allergic encephalomyelitis. *Annual Review of Immunology,* 8**,** 579-621.
ZHAN, J. S., GAO, K., CHAI, R. C., JIA, X. H., LUO, D. P., GE, G., JIANG, Y. W., FUNG, Y. W., LI, L. & YU, A. C. 2017. Astrocytes in Migration. *Neurochem Res,* 42**,** 272-282.
ZHANG, J. & LIU, Q. 2015. Cholesterol metabolism and homeostasis in the brain. *Protein Cell,* 6**,** 254-64.
ZHORNITSKY, S., MCKAY, K. A., METZ, L. M., TEUNISSEN, C. E. & RANGACHARI, M. 2016. Cholesterol and markers of cholesterol turnover in multiple sclerosis: relationship with disease outcomes. *Mult Scler Relat Disord,* 5**,** 53-65.
ZORINA, Y., STRICKER, J., CAGGIANO, A. O. & BUTTON, D. C. 2018. Human IgM antibody rHIgM22 promotes phagocytic clearance of myelin debris by microglia. *Sci Rep,* 8**,** 9392.